UNIVERSITY OF EASTERN PIEDMONT

Department of Translational Medicine

PhD in Medical Sciences and Biotechnology

XXXIII Cycle

Toll-like receptor 4-mediated inflammation triggered by extracellular IFI16 is enhanced by lipopolysaccharide binding

Coordinator

Prof. Marisa Gariglio

Tutor

Prof. Marisa Gariglio

Prof. Marco De Andrea

Candidate

Andrea Iannucci

Table of contents

Abstract

Since its discovery in the early 90s, a cornucopia of biological activities has been attributed to the IFI16 protein, including cell cycle regulation, tumor suppression, apoptosis, DNA damage signaling, virus sensing, and virus restriction. In addition, aberrant IFI16 expression and release in the extracellular space has been reported in a series of inflammatory conditions. The current hypothesis is that overexpression of the IFI16 protein occurs in tissue compartments where it is not physiologically expressed during inflammation. The ensuing release of the IFI16 protein into the extracellular space may allow it to behave like a damage-associated molecular pattern (DAMP) that signals through the Toll-like receptor 4 (TLR4) triggering inflammation by itself or through interaction with exogenous molecules, *e.g.,* lipopolysaccharide (LPS). Pull down assays and ELISA were used to characterize IFI16 binding activity to LPS. The human monocytic cell line THP-1 and the renal carcinoma cell line 786-O, and the murine macrophages RAW 264.7 were used as target cells to define IFI16-induced proinflammatory activity. Co-immunoprecipitation (co-IP), surface plasmon resonance (SPR), and silencing experiments were used to define IFI16 signaling. We show that the IFI16 HINB domain binds to the lipid A moiety of either high or weak TLR4 agonist LPS variants. Treatment of THP-1, 786-O, or RAW 264.7 cells with IFI16 led to increased production of proinflammatory cytokines, which was further enhanced when IFI16 was pre-complexed with sub-toxic doses of high TLR4 agonist LPS but not low agonists. Silencing of TLR4/MD-2 or MyD88 abolished cytokine production. These findings alongside with other *in vitro* binding experiments indicate that PYRIN domain of IFI16 interacts and signals through TLR4. Collectively, our data provide compelling evidence that: i) IFI16 is a DAMP that triggers inflammation through the TLR4/MD2-MyD88 pathway; and ii) its activity is strongly enhanced upon binding to LPS variants regarded as full TLR4 activators. These data strengthen the notion that extracellular IFI16 functions as DAMP and point to new pathogenic mechanisms involving the crosstalk between IFI16 and subtoxic doses of LPS.

1. Introduction

1.1. Interferons

Interferons (IFNs) are pleiotropic cytokines that are important regulators of immunity and inflammation. Interferons trigger transcription of diverse genes influencing protein synthesis (both cellular and viral), autophagy, apoptosis, angiogenesis and innate and adaptive immunity (Borden et al., 2007). There are three major types of IFN: type I IFN (such as IFN-α and IFN-β), type II IFN (IFN-γ) and type III IFN (IFN-λ). IFN families are distinguished by their sequence identity, the nature and distribution of cognate receptors and, to a lesser extent, their inducing stimulus and cell of origin (Ivashkiv, 2018; Ivashkiv and Donlin, 2014; Wack et al., 2015). IFN bind specific cell-surface receptors expressed on most cell types and signal via pathways using the Janus family of tyrosine kinases (Jaks) and signal transducers and activators of transcription (STATs) to activate gene expression (Fig 1). Elevated production of IFNs during infection and in autoimmune diseases results in increased expression of target genes, most typically canonical interferon-stimulated genes (ISGs), in diseased tissues and often in circulating blood cells, in a pattern of expression defined as an IFN signature (Barrat et al., 2019). Canonical ISGs are defined as genes transcriptionally activated by IFNs, as identified by transcriptomic analysis of IFN-stimulated cells, and they typically are directly activated by transcription factors of the STAT family. The presence of an IFN signature is often considered a hallmark of certain autoimmune diseases, and the "signature genes" are inferred to have roles in pathogenesis (Jiang et al., 2020).

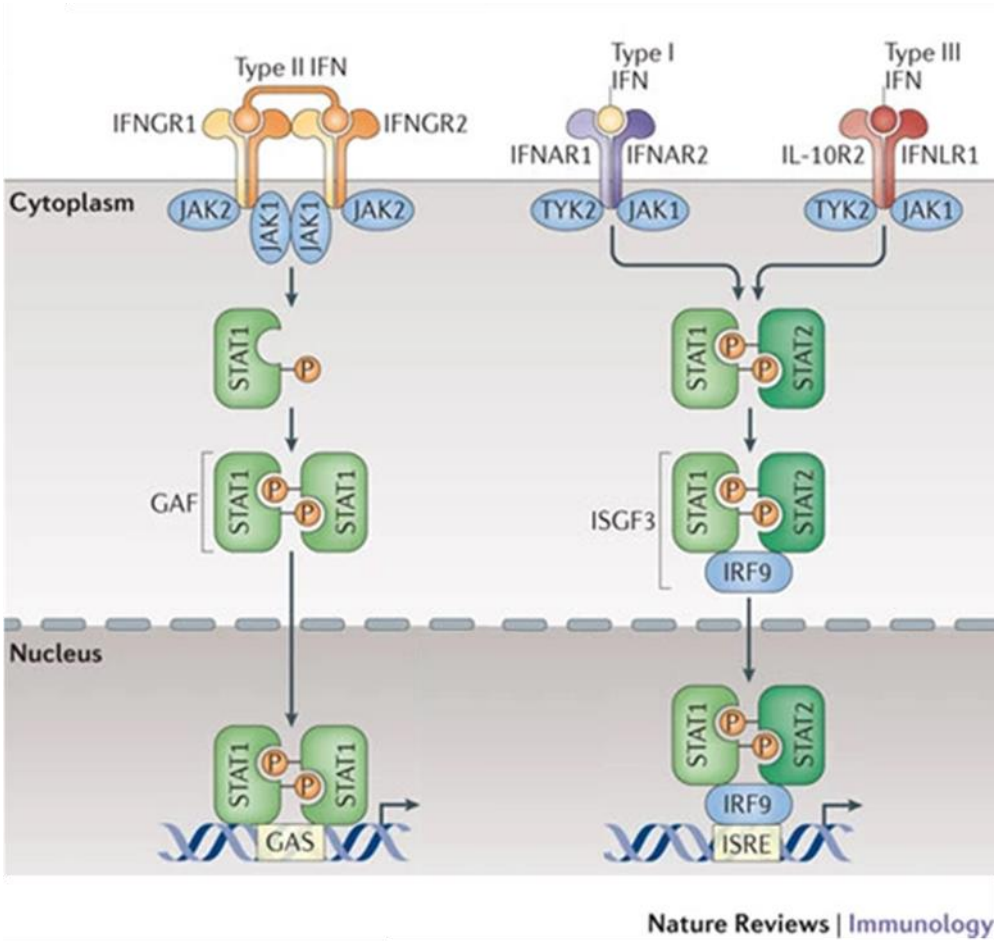

Fig 1. IFN signaling pathways. Interferons of different type engage different receptors. Type II interferon receptor is a tetramer while type I and III interferon receptor is a dimer. Adapted from MacMicking, 2012.

1.2. The PYHIN gene family

One family of the IFN-stimulated genes is the PYHIN gene family. The PYHIN genes were firstly identified as a cluster on syntenic genomic region of mouse and human chromosome 1 and were named mouse Ifi200 (interferon inducible) (Deschamps et al., 2003) and human HIN-200 (hematopoietic, interferon-inducible nuclear proteins with a 200 amino acid repeat) (Ludlow et al., 2005). Then, they have been annotated as the PYHIN family, acknowledging the defining features of an N-terminal PYRIN domain and C-terminal HIN domain. Four PYHIN protein have been identified in humans (IFI16, MNDA, AIM2, and IFIX), and seven in mouse (p202, p203,

p204, p205, p206, Aim2/p210, and Mndal), as well as a number of predicted proteins (Fig 2) (Cridland et al., 2012; Landolfo et al., 1998; Schattgen and Fitzgerald, 2011).

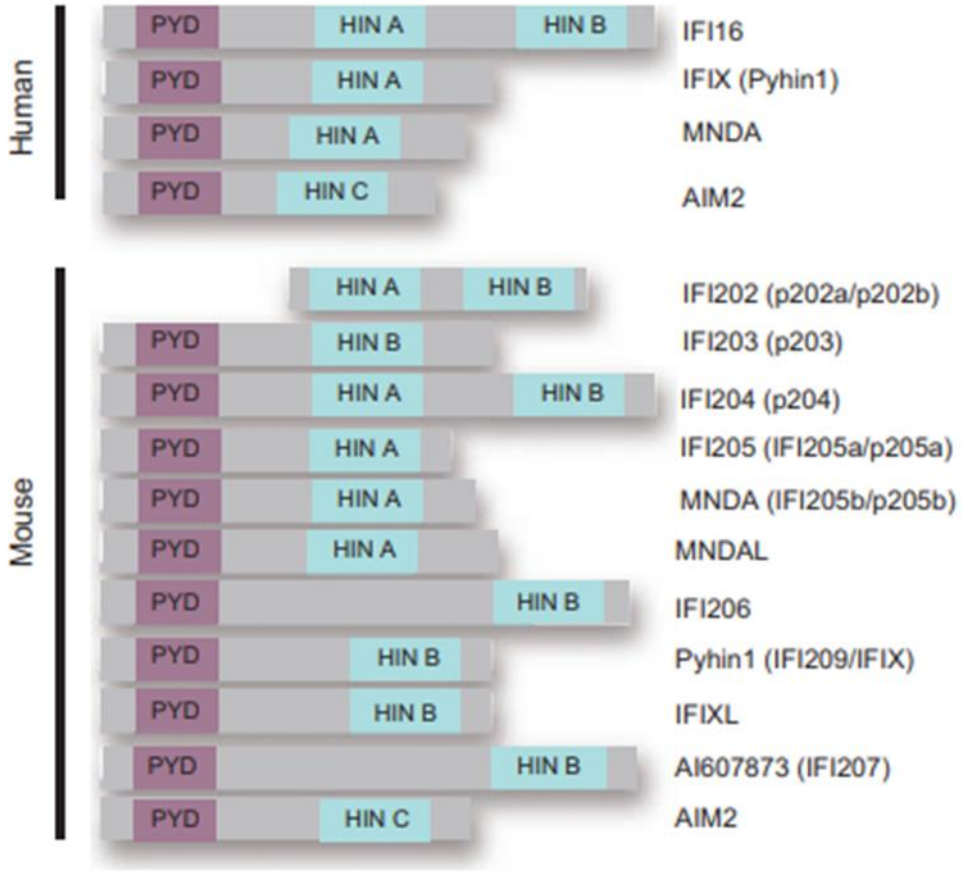

Fig 2. The human and murine PYHIN protein families. The PYHIN proteins consist of an N-terminal pyrin domain (PYD or PYRIN) and one or more HIN-200 domains, which can be one of 3 subtypes (HINA, HINB, or HINC) based on their sequence (Schattgen and Fitzgerald, 2011).

All the members of the PYHIN family contains one or two partially conserved repeats of 200-amino acid residues (HIN domains) at the C-terminus, which have been characterized into three subtypes termed A, B, and C according to consensus motifs (Ludlow et al., 2005). Within the HIN domains, there are at least two conserved motifs, the conserved MFHATVAT motif and the LxCxE pRb-binding motif, that have been shown to mediate protein-protein interactions. The high degree of conservation of this motifs may point to a functional role in mediating the

biological activities of the members of the PYHIN family (Asefa, 2004). MNDA, mndal, and IFIX contain a single HINA domain, whereas IFI16, p202, and p204 have a HINA and HINB domain. p203 has a single HINB domain, whereas AIM2 has a single HINC domain. The HIN domains are DNA-binding domains. The structural mechanism of DNA binding by HIN-200 domains was firstly described in 2005 by Albrecht and colleagues (Albrecht et al., 2005) using computational analysis which predicted the presence of two oligonucleotide/oligosaccharide (OB) folds, similar to that observed in the human replication protein A (RPA). This was later confirmed in the solved structure of the IFI16 HINA domain (Liao et al., 2011) (PDB: 2OQ0). Further biophysical analysis determined 2 OB folds in the IFI16 HINA domain, which had a higher affinity for single-stranded DNA (ssDNA) compared with double-stranded DNA (dsDNA), and could wrap, stretch and form oligomers with ssDNA (Yan et al., 2008). However, in subsequent studies the IFI16 HINB domain alone was demonstrated to be able to bind to dsDNA with relatively high affinity, which was further increased when both HIN domains were present (Ni et al., 2016; Unterholzner et al., 2010).

The N-terminus of the PYHIN proteins, with the exception of p202, contains a PYRIN domain. The PYRIN domain (also known as PYD, DAPIN or PAAD domain) is a death domain (DD) protein fold that forms homotypic interactions with other PYRIN-containing proteins to form higher complexes with known roles in inflammation, apoptosis, and the cell cycle (Chu et al., 2015). The most studied role of PYRIN domains relates to their ability to engage protein complexes referred to as “inflammasomes”. These are multiprotein oligomers that form upon PYRIN-PYRIN interaction with the adaptor molecule apoptosis-associated speck-like protein containing a CARD (ASC) which then which then recruits pro-caspase-1 via its caspase recruitment domain (CARD) domain and activates the effector caspase through proteolytic cleavage. The activation of the inflammasome promotes proteolytic cleavage, maturation, and secretion of pro-inflammatory cytokines interleukin 1β (IL-1β) and interleukin 18 (IL-18) (Broz and Dixit, 2016).

The PYHIN proteins have been shown to localize to the nucleus and with a few exceptions to the cytoplasm. IFI16, IFIX, MNDA, p204, and mndal have either a monopartite nuclear localization sequence (NLS), bipartite NLS, or both, and are primarily located within the nucleus (Ludlow et al., 2005). Relocalization of these proteins from the nucleus to the cytosol can occur following stimulation. In contrast, AIM2 and p202 lack an NLS and are predominantly if not exclusively localized to the cytoplasm.

The PYHIN proteins have been implicated in regulating growth and cell differentiation due to their tissue-specific inducibility by IFN treatment. The IFI16, p202, and p204 nuclear phosphoproteins are relatively well characterized with respect to their role in IFN action: these proteins are demonstrated to participate in the inhibition of cell cycle progression, modulation of differentiation, and cell survival. Generally, IFI-200 proteins are thought to act as scaffolds to assemble large protein complexes involved in the regulation of transcription (Ludlow et al., 2005). Another important role of some PYHIN proteins is to act as pattern recognition receptors (PRRs). PRRs serve as sensors for monitoring the extracellular and intracellular compartments for signs of infection or tissue injury. These PRRs, which are responsible for the detection of pathogen associated molecular patterns (PAMPs) which signal the presence of a pathogen, and damage associated molecular patterns (DAMPs) which signal tissue injury, include the Toll-like receptors (TLRs), the retinoic acid inducible gene-like receptors (RLRs), the nucleotide oligomerization domain-like receptors (NLRs), and the AIM2-like receptors (ALRs) (Kawai and Akira, 2009; Unterholzner et al., 2010). The ALRs are AIM2, p204 and IFI16.

1.3. The human interferon-inducible protein 16 – IFI16

IFI16 was originally identified by Trapani *et al.* as a gene that is constitutively expressed in human lymphoid cell lines and is inducible in myeloid cell lines after IFN-γ treatment or differentiating stimuli (Trapani et al., 1994). IFI16, as the other members of PYHIN family,

displays a PYRIN domain at its N-terminus, suggesting a role for this protein in the apoptotic pathway by regulating the activity of certain transcription factors in the nucleus, which are involved in the commitment to cell death. IFI16 also possesses both the HINA and HINB domains, which are separated by a 116 amino-acid spacer, a serine–threonine–proline (S/T/P)-rich spacer region. The size of the spacer region in IFI16 is regulated by mRNA splicing and can contain one, two, or three copies of the highly conserved 56-aa S/T/P/ domain (Fig 3). Three IFI16 isoforms (designated A, B, and C) arise due to alternative RNA splicing in the exons encoding the S/T/P domain, with the isoform B displaying the most abundant expression (Johnstone et al., 1998).

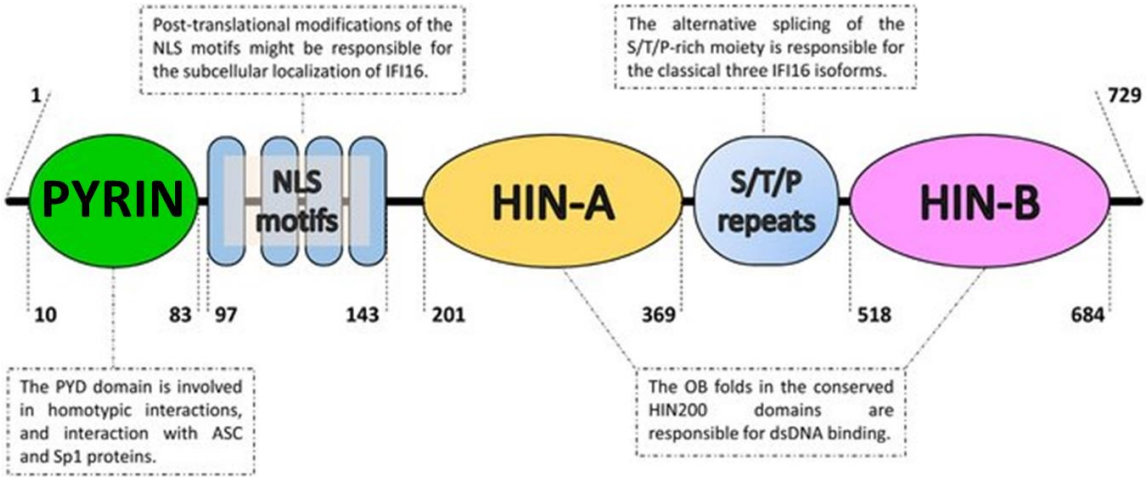

Fig 3. Domain organization of the IFI16 protein. The numbers represent the amino acid positions based on NCBI Reference Sequence NP_005522. From the N- to the C-terminal (left to right), IFI16 comprises a PYRIN domain involved in protein-protein interaction, and two hematopoietic interferon-inducible nuclear protein with 200-amino-acid repeats (HINA and HINB) domains, which are a hallmark of the absent in melanoma 2-like receptors (ALRs). S/T/P = serine/threonine/ proline-rich repeats, which are regulated by alternative mRNA splicing. Adapted from Caneparo et al., 2018.

IFI16 is expressed in CD34+ myeloid precursor cells and remains strongly expressed within monocyte precursors, peripheral blood monocytes, and throughout lymphoid development (Dawson et al., 1998). Following IFN-treatment, IFI16 localizes within the nucleolus and the

nucleoplasm of human cells. This nuclear import is mediated by a bipartite nuclear localization sequence (NLS) located at the N-terminus of the protein (Li et al., 2012). In addition to its expression in the hematopoietic system, immunohistochemical analysis of IFI16 expression in normal human tissues revealed that it is expressed in a highly restricted pattern in selected cells within certain organs (Gariglio et al., 2002; Wei et al., 2003). IFI16 was found in epithelial cells of the skin, gastrointestinal tract, urogenital tract, and glands and ducts of breast tissues. Prominent IFI16 expression was seen in stratified squamous epithelia, particularly intense in basal cells in the proliferating compartments, whereas it gradually decreases in a more differentiated suprabasal compartment. In the underlying dermis, staining of connective tissue was restricted to scattered fibroblasts. In addition, all vascular endothelial cells from both blood and lymph vessels strongly expressed IFI16.

IFI16 participates in the inhibition of cell cycle progression and in the regulation of apoptosis. IFI16 overexpression can result in decreased cell proliferation and a block in the cell cycle progression at the G1-S phase transition. IFI16-mediated growth arrest seems to be mediated by its interaction with p53 and pRb (Aglipay et al., 2003; Liao et al., 2011). Indeed, prostate cancer cell lines expressing functional p53 and pRb were significantly more sensitive to the antiproliferative activity of IFI16 (Xin et al., 2003). IFI16 has also been identified as an essential growth-specific effector of the cell extrinsic growth–inhibitory pathway of Ras/Raf signaling in medullary thyroid carcinoma cells (Kim et al., 2005). Finally, IFI16 expression has been found deregulated in several forms of human cancer (Azzimonti et al., 2004; Fujiuchi et al., 2004; Xin et al., 2003). Evaluation of some features of in vitro angiogenesis, namely chemotaxis, matrigel invasion, tube morphogenesis, and cell cycle progression, has demonstrated that IFI16 overexpression impairs tube morphogenesis and proliferation of human endothelial cells (Raffaella et al., 2004). Altogether, these results point to a role for IFI16 in the regulation of cell growth, differentiation, and angiogenesis.

IFI16 is also implicated in inflammation and immune response. Not only the IFN-γ but also other pro-inflammatory cytokines such us IL-1β and TNFα can significantly induce IFI16 expression (Mondini et al., 2007). Of note, anti-inflammatory cytokines (*e.g.,* IL-4, IL-10, IL-13, and IL-17) failed to induce IFI16 expression. In addition to that, Gugliesi *et al.,* reported that IFI16 is overexpressed in primary human umbilical vein endothelial cells (HUVEC) by oxidative stress (Gugliesi et al., 2005). Moreover, gene array analysis of IFI16 overexpressing HUVEC revealed an increased expression of genes involved in the regulation of the immune system (Caposio et al., 2007). IFI16 triggered the expression of adhesion molecules such as intercellular adhesion molecule-1 (ICAM-1) and E-selectin or chemokines such as IL-8 and monocyte chemoattractant protein-1 (MCP-1). Treatment of cells with short hairpin RNA targeting IFI16 significantly inhibited ICAM-1 induction by IFN-γ and TNFα, demonstrating that IFI16 is involved in proinflammatory gene stimulation by IFN-γ and TNFα. Finally, functional analysis of the ICAM-1 promoter demonstrated that NF-kB is the main mediator of IFI16-driven gene induction (Caposio et al., 2007; Sponza et al., 2009).

Regarding the role of IFI16 as a DNA sensor for intracellular DNA, many studies came out after it was firstly identified as an ALR (Unterholzner et al., 2010). IFI16 is unique, as it can shuttle between the cytoplasm and the nucleus, and can sense DNA derived from various pathogens, such as dsDNA from herpes simplex virus 1 (HSV-1), Kaposi sarcoma-associated herpesvirus (KSHV), human cytomegalovirus (HCMV), and ssDNA or dsDNA from bacteria, depending on the types of host cells and pathogens (Li et al., 2012; Veeranki and Choubey, 2012). Unlike AIM2, IFI16 predominantly localizes in the nucleus in most types of cells, acting as DNA sensor by detecting pathogenic DNA, and then triggering innate immune response against pathogen invasion by activation of cytoplasmic inflammasome and innate signaling pathways. Mechanistically, upon HSV-1 infection, IFI16 mainly detects HSV-1 genomic DNA in the nucleus and then translocates to the cytoplasm where cooperates with cyclic GMP-AMP synthase (cGAS) to activate the endoplasmic reticulum protein stimulator of interferon genes (STING) to

induce the expression of type I IFN through activating TBK1-IRF3 and NF-κB signaling pathways (Almine et al., 2017; Iqbal et al., 2016). In addition, during KSHV infection, nuclear IFI16 senses and binds to viral dsDNA, and then recruits the adaptor protein ASC, and procaspase-1 to form an activated inflammasome. Subsequently, the IFI16-inflammasome translocates to the cytoplasm where the proteolysis of inactivated procaspase-1 into activated caspase-1 and cleavage of IL-1β and IL-18 occur (Kerur et al., 2011; Singh et al., 2013). However, the detailed mechanisms for IFI16-mediated nuclear pathogenic DNA sensing and activation of STING and inflammasome in cytoplasm remain controversial. No defect in type I interferon production was found once knockout of IFI16 in human primary fibroblasts in response to HCMV infection (Gray et al., 2016). This may be due to specific cell types and species of virus used. Indeed, while similar activation of STING has been shown in macrophages and keratinocytes upon viral infection, IFI16 increases cyclic guanosine monophosphate-adenosine monophosphate (cGAMP) production by cGAS only in macrophages, indicating cell specific roles for IFI16 in cooperating with the cGAS pathway. In CD4+ T cells, HIV proviral DNA detection by IFI16 has a different outcome. Here IFI16 forms an inflammasome with ASC to activate caspase-1-dependent pyroptotic cell death, resulting in abortive infection of these cells, thus promoting clinical progression of the acquired immune deficiency syndrome (AIDS) (Monroe et al., 2014). Indeed, silencing of IFI16 or ASC by shRNA or caspase-1 inhibition rescued CD4+ T cells from death. This discovery may explain how CD4+ T cells die during HIV infection. IFI16 can also restrict viral genomic replication as a transcriptional regulator through epigenetic modifications. IFI16 promotes the loading of nucleosomes and the addition of heterochromatin marks on infected cell protein 0 (ICP0)-null HSV-1 chromatin by modulating repressive histone modifications to restrict viral replication (Johnson et al., 2014; Orzalli et al., 2013). Upon KSHV infection and latency, IFI16 recruits the H3K9 methyltransferase SUV39H1 and GLP to the KSHV genome for silencing of KSHV lytic genes (Roy et al., 2019). Similar to that, after human papilloma virus (HPV) infection, IFI16 promotes the addition of heterochromatin marks and the reduction of

euchromatin marks on viral chromatin at both early and late promoters, thus reducing both viral replication and transcription. Finally, acting as a restriction factor, IFI16 blocks the binding of transcription factor Sp1 to the promoter region of viral DNA polymerase gene (UL54), restricting viral genome replication during HCMV infection (Gariano et al., 2012). To summarize, IFI16 has four potentially distinct mechanisms to restrict viral infections, (1) activation of the cGAS-STING-IFN pathway, (2) formation of inflammasomes, (3) epigenetic silencing of viral promoters, (4) limiting access to host factors required for viral replication such as Sp1. This explains why IFI16 is such a frequent target of immune evasion by many different viruses (Chan and Gack, 2016). The protein pUL83 from HCMV binds IFI16 and blocks IFI16 oligomerization, thus preventing the activation of the STING-TBK1-IRF3 pathway (Li et al., 2013), while the protein pUL97 promotes IFI16 phosphorylation and delocalization to the cytoplasm of HCMV-infected cells (Dell'Oste et al., 2014). ICP0 from HSV targets IFI16 for degradation (Orzalli et al., 2012), while it was recently reported that the E7 protein from HPV recruits the E3 ligase TRIM21 to ubiquitinate and degrade IFI16 to inhibit IL-1 production and pyroptosis, both in Hela cells and HaCaT keratinocytes (Song et al., 2020).

1.4. IFI16 in autoimmune/autoinflammatory diseases

Several reports have indicated IFI16 in autoimmunity. Since the interferon system is considered as a key player in autoimmune and autoinflammatory disorders such as systemic lupus erythemathosus (SLE), systemic sclerosis (SSc), Sjögren's syndrome (SjS), and rheumatoid arthritis (RA), inflammatory bowel disease (IBD), it is conceivable to hypothesize an involvement of the IFN-inducible PYHIN proteins in the etiopathogenesis of autoimmune and autoinflammatory diseases (Jiang et al., 2020).

Aberrant IFI16 expression (*i.e.,* overexpression or *de novo* expression), at both mRNA and protein level, has been reported in colonic biopsies of patients with Crohn's disease (CD) and

ulcerative colitis (UC), collectively known as IBD, compared to healthy controls (Caneparo et al., 2016; Vanhove et al., 2015). IFI16 in the intestinal lamina propria is normally expressed in endothelial and inflammatory cells, whereas in IBD patients the colonic expression of IFI16 is substantially higher and well evident also in the epithelial cells.

Another disease in which aberrant IFI16 expression has been observed is systemic lupus erythematosus (Costa et al., 2011; Mondini et al., 2007). Indeed, IFI16 distribution pattern in the skin was substantially different in SLE patients compared to healthy donors. IFI16 expression in normal skin was restricted to the nuclei, with evident positive staining in the keratinocytes. Conversely, in SLE biopsies, IFI16 staining in keratinocytes was stronger and intense positive nuclei were also found in the upper epidermal layers, indicating a keratinocyte specific cytoplasmic translocation of IFI16 in pathological setting.

Finally, substantial evidence indicate that abnormal IFI16 expression can also be detected in the skin of patients affected by SSc (Mondini et al., 2006), or psoriasis (Cao et al., 2016; Chiliveru et al., 2014; Tervaniemi et al., 2016), as well as in salivary epithelial cells and infiltrating lymphocytes of individuals with SjS (Alunno et al., 2015; Antiochos et al., 2018).

All these data clearly indicate a possible role of IFI16 in autoimmune/autoinflammatory disease. Importantly, several groups have reported a IFI16 mislocalization from nucleus to cytoplasm and an eventual release under viral infection, stress stimuli or pathological conditions (Antiochos et al., 2018; Bawadekar et al., 2015a; Orvain et al., 2020). In particular, IFI16 has been shown to be released into the exosomes of Epstein-Barr virus (EBV) or KSHV infected cells (Ansari et al., 2013; Singh et al., 2013). Similarly, at the late phases of HCMV infection induces, IFI16 is hijacked and incorporated within newly assembled egressing virion particles and exits the host environment (Dell'Oste et al., 2014). In addition, IFI16 mislocalization and release has also been observed in experimental models of keratinocyte monolayers and human skin explants after ultraviolet-B (UVB) exposure (Costa et al., 2011). Finally, serum circulating IFI16 has also

been observed in various autoimmune diseases including SSc, RA, SLE, SjS, and psoriatic arthritis (PsA) (Alunno et al., 2015, 2016; De Andrea et al., 2020; Gugliesi et al., 2013).

The extracellular exposition of a protein usually expressed only in the nuclei of the cells causes the generation of specific autoantibodies. Indeed, IFI16 autoantibodies have been detected in a variety of autoimmune/autoinflammatory diseases. In 1994 Seelig *et al.* first detected anti-IFI16 antibodies in a serum positive for antinuclear antibodies (ANAs), anti-SSA/Ro, and anti-SSB/La autoantibodies. By immunoblotting analysis on recombinant IFI16 expressed as MS2-polymerase fusion protein, these investigators also reported the presence of anti-IFI16 antibodies in 29% of sera obtained from 374 SLE patients (Seelig et al., 1994). With a different technique, such as serological analysis of antigens by recombinant cDNA expression cloning (SEREX), Uchida *et al.* detected anti-IFI16 antibodies in 70% of patients suffering from both primary and secondary SjS (Uchida et al., 2005). Moreover, Mondini *et al*. identified anti-IFI16 antibodies in 21% of SSc patients by solid-phase enzyme-linked immunosorbent assay (ELISA), with a recombinant purified His-tagged IFI16 protein as antigen, and confirmed by ELISA that anti-IFI16 autoantibodies titers are significantly elevated in patients with SLE and SjS compared with controls (Mondini et al., 2006). By using the latter technique, anti-IFI16 autoantibodies have been then detected in IBD (Caneparo et al., 2016), SLE (Caneparo et al., 2013), SjS (Alunno et al., 2015; Baer et al., 2016), RA (Alunno et al., 2016), and PsA (De Andrea et al., 2020) patients. Overall, these data point to a pathogenic role of IFI16 in autoimmune/autoinflammatory diseases providing the rationale to investigate IFI16 extracellular activity.

1.5. The lipopolysaccharide and its recognition

The lipopolysaccharide (LPS) is the major component of the outer membrane of Gram-negative bacteria, and probably the best characterized pathogen-associated molecular pattern (PAMP). LPS consists of three genetically, biologically and chemically distinct domains (Miller

et al., 2005) (Fig 4): (1) the more or less acylated and phosphorylated lipid A anchored in the bacterial outer membrane, representing the most immunogenic portion, and also called endotoxin, (2) the core oligosaccharide linked by 3-deoxy-d-manno-oct-ulosonic acid (Kdo) with lipid A, and (3) the O-antigen, with the latter pointing to the aqueous environment. Lipopolysaccharides that comprise all three regions are called smooth (S)-form LPS, while LPS lacking the O-antigen are named rough (R)-form LPS. Over the last 30 years, several reports have contributed to mechanistically dissect how the host system recognizes LPS. What is now known is that the recognition of LPS is a multistep process involving different proteins that convey the LPS molecule, through its lipid A moiety, to its receptor named Toll-like receptor 4 (TLR4) (Ryu et al., 2017). The first identified player of this process was the lipopolysaccharide-binding protein (LBP), a molecule able to opsonize LPS-bearing particles and intact Gram-negative bacteria, mediating attachment of coated particles to macrophages, which then secrete tumor necrosis factor α (TNFα) (Schumann et al., 1990; Tobias et al., 1986). The extracellular LBP forms direct contacts with the bacterial outer membrane (or micelles of LPS) and alters the outer membrane thereby facilitating the extraction of a single molecule of LPS by the protein CD14 (Gioannini et al., 2004). CD14 can either exist as a soluble extracellular protein or a glycosylphosphatidylinositol (GPI)-anchored protein embedded in the outer layer of the cell plasma membrane (Frey et al., 1992; Lee et al., 1993; Tobias et al., 1986; Wright et al., 1990). Regardless of its soluble or membrane-bound positioning, CD14 acts to transfer a single molecule of LPS to the protein MD2 (Gioannini et al., 2004). MD2 is a small protein that stably interacts with the ectodomain of TLR4, forming TLR4/MD2 heterodimers that represent the functional LPS receptor (Nagai et al., 2002; Shimazu et al., 1999). Indeed, the real LPS-binding site resides into MD2 giving to this molecule a critical role for LPS-mediated TLR4 activation. Upon CD14-mediated transfer of LPS to MD2, TLR4-TLR4 dimerization occurs (Akashi et al., 2000). The lipid A moiety is the LPS portion that directly interacts with distinct regions of two TLR4/MD2 heterodimers. The general structure of most of bacteria lipid A resemble that of *Escherichia coli*

lipid A, which is a diglucosamine diphosphate headgroup and six acyl chains. An elegant study by Park et al. revealed the structural basis for lipid A recognition by the TLR4/MD2 receptor (Park et al., 2009). The structure showed LPS binding to two copies of TLR4 and MD2 arranged symmetrically. Five of the six acyl chains present in hexacylated lipid A are buried in the hydrophobic pocket present in the MD2 component of a TLR4-MD2 heterodimer. In order to the dimerization to occur, the sixth acyl chain does not interact with the TLR4 component of this heterodimer, but rather interacts with a different TLR4 molecule. Moreover, the binding of LPS causes structural changes in MD2, leading to hydrophilic interactions between MD2 and TLR4, further stabilizing the complex. Finally, the two phosphate groups of lipid A, also play an important role in dimerization by binding to a positively charged cluster of lysines and an arginines on both TLR4 molecules. Therefore, lipid A structures that contain less than six acyl chains, or less than two phosphate groups, have minimal ability to crosslink distinct sets of TLR4/MD2 heterodimers, thus explaining their weakened inflammatory activities. This aspect will be discussed in detail later.

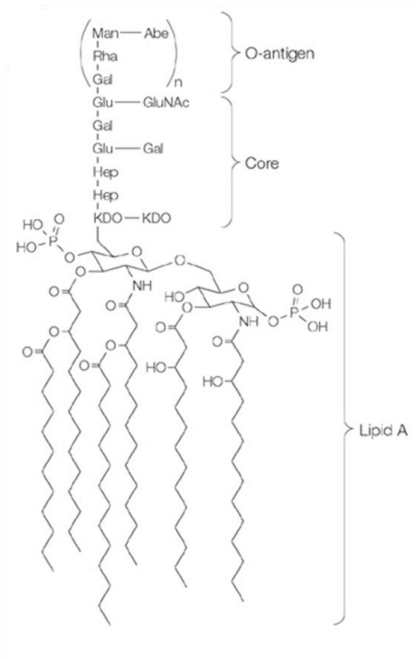

Fig 4. LPS structure. LPS is composed of lipid A (endotoxin), core oligosaccharide and O-antigen (Miller et al., 2005).

Upon TLR4-TLR4 dimerization, several intracellular pathways are activated, ultimately leading to inflammation (Fig 5, and Kieser and Kagan, 2017). TLR4 has a cytosolic Toll/IL-1R (TIR) domain that after the dimerization are detected by the protein TIR domain containing adaptor protein (TIRAP) (Horng et al., 2001), which is a phosphoinositide-binding protein, subsequently leading to the assembly of a supramolecular organizing center named myddosome (Kagan et al., 2014). The myddosome consist of TIRAP, the adaptor molecule MyD88 (from that the name myddosome), and several IRAK family kinases that initiate downstream signaling that ultimately results in the activation of the transcription factors nuclear factor-kB (NF-kB) and activator protein1 (AP-1).

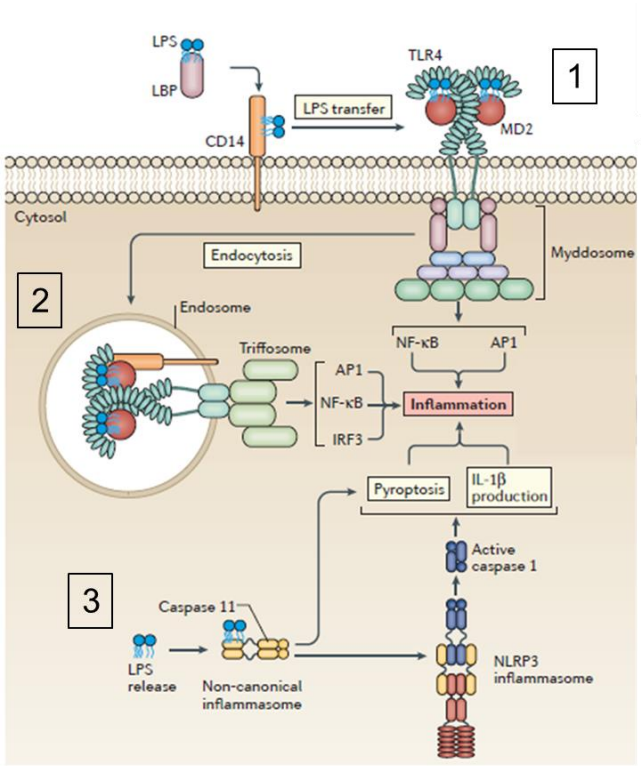

Figure 5. LPS-induced pathways leading to inflammation. LPS is delivered in a LBP-CD14-dependent manner to the TLR4-MD2 receptor, prompting the dimerization and activation of TLR4, a process that leads to myddosome assembly (1). CD14 then promote the endocytosis of the dimerized TLR4 to promote triffosome assembly (2). Both pathways result in inflammation. LPS can reach the cytoplasm where can be sensed by caspase 11 (or caspase 4/5 in humans) leading to the non-canonical inflammasome activation, which in turn promotes pyroptosis and IL-1β release (3). Adapted from Kieser and Kagan, 2017.

Concomitantly, CD14 mediates the LPS-TLR4/MD2 internalization from the plasma membranes into endosomes (Zanoni et al., 2011). This process is independent of TLR4-TIR domains, but it is strictly dependent on CD14 and MD2 (Tan et al., 2015), even if CD14 can also promotes an LPS endocytosis without TLR4 (Dunzendorfer et al., 2004). When TLR4 is located in the endosome, there is the assembly of the so called triffosome with the adaptor molecules translocating chain-associated membrane protein (TRAM) and TIR-domain-containing adapter-inducing interferon-β (TRIF) which are thought to only engage endosome-localized TLR4 (Yamamoto et al., 2003). The formation of this complex ultimately leads to a second wave of NF-kB and AP-1 activation and most importantly to the activation of the transcription factor IRF3 which acts along with NF-kB and AP-1 to drive the expression of type I interferon (IFN) genes.

Lastly, there is a recently discovered way in which LPS can be sensed directly into the cytoplasm of the host cell, independently of CD14-TLR4-MD2. LPS delivery into the cytoplasm induces a potent pyroptotic cell death response thanks to the activation of a non-canonical inflammasome (Hagar et al., 2013; Kayagaki et al., 2011, 2013). This response is important to prevent mammalian cells from being used as a growth substrate by intracellular bacteria (Jorgensen et al., 2017). LPS-induced pyroptosis is mediated by the cytosolic LPS receptor caspase-11 (or caspase-4 and caspase-5 in humans, Shi et al., 2014). LPS binding to the N-terminal caspase activation and recruitment domain (CARD) of caspase-11, that can be mediated by the interferon-induced guanylate-binding proteins (GBPs, Santos et al., 2020), promotes the oligomerization of this protein, and the activation of its intrinsic protease activity. Active caspase-11 then cleaves its cytosolic substrate gasdermin D (Kayagaki et al., 2015; Shi et al., 2015), releasing its N-terminal domain to oligomerize into a ring-shaped pore that disrupts the osmotic balance in the cell and ultimately causes swelling and disruption of the plasma membrane. Activated caspase-11 subsequently promotes NLRP3 activation dependent on potassium efflux (Rühl and Broz, 2015), probably because of GSDMD-mediated membrane perturbation, a known

activator of the NLRP3 inflammasome (Broz and Dixit, 2016), which ultimately leads to the processing and release of pro-IL1β and pro-IL18.

Already in the early ‘80s it was observed that several natural and synthetic partial lipid A structures lacking one or both of the phosphate residues, or having less than six acyl chains display reduced or even no stimulatory activities in endotoxin-responsive human cells (Alexander and Rietschel, 2001). It know known that this reduced capacity its due to a reduced interaction with the TLR4/MD2, or with the CD14 (Tan et al., 2015), or to a reduced capacity to induce TLR4-TLR4 dimerization (Park et al., 2009). Indeed, this is a common strategy evolved by bacteria (both pathogenic and commensal) to not be sensed by the host organism (d’Hennezel et al., 2017; Tan and Kagan, 2014). *Yersinia pestis, Francisella tularensis,* and *Shigella flexneri,* provide examples of how bacteria can modify their lipid A structures. *Y. pestis*, the bacterium causing plague, exhibits different lipid A depending on the temperature. Indeed, *Y. pesti*s mainly produces hexa-acylated lipid A at 25°C, whereas it synthesizes tetra-acylated lipid A at 37°C (*i.e.,* human body temperature), thus facilitating immune evasion by this bacterium (Kawahara et al., 2002). *F. tularensis*, the etiological agent of tularemia, is capable of synthesizing mono-phosphorylated and tetra-acylated lipid A (Vinogradov et al., 2002). Finally, *S. flexneri* can remodel its lipid A structure specifically during its intracellular growth phase (Paciello et al., 2013). Indeed, the majority of *S. flexneri* LPS purified from infected epithelial cells contained tri- or tetra-acylated lipid A. Conversely, bacteria grown in broth produced hexa-acylated lipid A. Therefore, *S. flexneri* LPS triggers significantly lower amount of cytokine production via the TLR4 signaling pathway and dampens inflammasome activation in macrophages, as indicated by the reduced release of IL-1β. An interesting example is that of the LPS from *Rhodobacter sphaeroides*. Its lipid A is penta-acylated and can antagonize *E. coli* LPS binding to the TLR4/MD2 (Anwar et al., 2015). This is due because *R. sphaeroides* lipid A fully accommodate into the MD2 binding pocket, thereby preventing other LPS to bind, but lacking the sixth acyl chain it cannot induce TLR4-TLR4 dimerization, thereby not activating TLR4 signaling pathway.

1.6. Damage-associated molecular patterns

One of the fundamental properties of the immune system is to initiate immune responses against invasive pathogens, based on the discrimination of "self" from "non-self". However, innate immune response can also be activated without any infection. Therefore, in 1994 Polly Matzinger proposed the so called "danger theory" postulating that danger signals released by stressed or damaged cells can initiate immune responses (Matzinger, 1994). This theory led to the discovery of a number of endogenous molecules that are released during tissue damage, that were named damage-associated molecular patterns (DAMPs) (Land, 2003). It is now known that DAMPs are endogenous molecules that are normally sequestered intracellularly and are therefore hidden from recognition by the immune system under normal physiological conditions. However, under conditions of cellular stress or injury, these molecules can then be released into the extracellular environment by dying cells and trigger sterile inflammation (Chen and Nuñez, 2010). Prototypical intracellular DAMPs are the chromatin-associated protein high-mobility group box 1 (HMGB1, Scaffidi et al., 2002), heat shock proteins (HSPs, Quintana and Cohen, 2005), Ca^{2+}-binding S100 proteins (Xia et al., 2018), nicotinate phosphoribosyltransferase (NAPRT, Managò et al., 2019), oxidized phospholipids (oxPAPC, Zanoni et al., 2017), and purine metabolites, such as ATP (Bours et al., 2006) and uric acid (Kono et al., 2010). In addition, there are also extracellularly located DAMPs. These are typically released by extracellular matrix degradation during tissue injury and include hyaluronan (Frey et al., 2013), heparan sulphate (Brennan et al., 2012), biglycan (Schaefer et al., 2005), fibronectin-EDA (Malara et al., 2019), and tenascin-C (Midwood et al., 2009).

Over the past 20 years, numerous new DAMP-receptor axes have been discovered in various injury scenarios, with both PRR and non-PRR playing a key role in DAMP-mediated innate immunity activation (Gong et al., 2020). Nucleic acids released from damaged cells can activate TLR3, TLR7 and TLR9, and intracellular proteins released by damaged cells and extracellular

matrix components cleaved following tissue injury can activate TLR2 and TLR4. Of particular interest is the TLR4, as it can be bound and activated from the majority of DAMPs. Indeed, many therapeutic strategies are ongoing in order to block TLR4 activation in several diseases (Garcia et al., 2020; Romerio and Peri, 2020). Tenascin-C, an extracellular matrix glycoprotein associated with tissue injury and repair, was shown to induce pro-inflammatory cytokines synthesis in macrophages, through its fibrinogen-like globe (FBG). This activity was mediated by the binding and the activation of the TLR4, in a MyD88-dependent manner, as neutralizing antibodies to TLR4, genetic deletion of TLR4 or expression of a dominant negative MyD88 mutant completely abrogates Tenascin-C proinflammatory activity (Midwood et al., 2009). Subsequential analyses have also identified tenascin-C specific sites that directly and cooperatively interact with TLR4 (Zuliani-Alvarez et al., 2017). HMGB1, maybe the most studied DAMP, has been shown to bind and activate TLR4/MD2 to produce proinflammatory cytokines (Yang et al., 2010, 2015a). Interestingly, HMGB1 proinflammatory activity was also confirmed using necrotic wild-type (WT) or HMGB1-knockout (HMGB1-KO) cells, proving that TLR4 activation was not due to bacterial contaminants in the recombinant protein. Surface plasmon resonance (SPR) analysis has revealed that HMGB1-TLR4-MD2 interaction is initiated by HMGB1-TLR4 binding via HMGB-1 A-box domain (high affinity and slow off-rate) and, once in close proximity, the HMGB1 B-box domain binds to MD2 (low affinity but extremely slow off-rate) (He et al., 2018). However, HMGB-1 is a pleiotropic DAMP since it can also bind and activate different receptors, such as TLR2 or receptor for advanced glycation endproducts (RAGE, Yang et al., 2015b). The latter, in particular, is a non-PRR demonstrating that, differently from PAMPs, DAMPs can be recognized by a variety of receptors to induce inflammation, promoting the idea that continue exposition of these molecules to the extracellular environment can lead to unresolve chronic inflammation. The reason why DAMPs can activate the innate immune response is that, after an injury, they are key players in promoting tissue repair and regeneration (Pandolfi et al., 2016; Vénéreau et al., 2015). However, unresolved chronic inflammation is detrimental to the host and can lead to sterile

inflammatory diseases, including metabolic disorders, neurodegenerative diseases, autoimmune diseases and cancer (Roh and Sohn, 2018). Accordingly, high levels of DAMPs occur locally and/or systemically in many of these conditions. For example, a wide range of endogenous TLR activators, including heat shock proteins, HMGB1, and tenascin-C, has been observed in synovia of RA patients but not in synovia from normal joints or non-inflamed synovia from osteoarthritis (OA) patients (Baillet et al., 2010; Goldstein et al., 2007; Midwood et al., 2009). Tenascin-C levels are also elevated in SSc skin biopsy samples and serum, and in fibrotic skin tissues from mice (Bhattacharyya et al., 2016, 2018). Indeed, tenascin-C stimulates collagen gene expression and myofibroblast transformation via TLR4 signaling. High levels of HMGB1, NAPRT, and tenascin-C circulate in the serum of septic patients (Schenk et al., 1995; Wang et al., 1999), and high serum concentrations of DNA-containing immune complexes are associated with SLE (Tian et al., 2007). In many cases levels of endogenous TLR activators are indicative of disease activity; elevated levels of extracellular HMGB1 localize specifically to active lesions of multiple sclerosis (MS) patients and correlate with active inflammation (Andersson et al., 2008). Further support of a role for endogenous TLR activators in driving disease has also been derived from *in vivo* studies using experimental models of inflammatory disease, where not high levels of serum DAMPs were found, but also the administration of exogenous DAMPs were sufficient to initiate inflammation. As an example intra-articular injection of the TLR4 activators fibronectin-EDA or tenascin-C has been shown to induce joint inflammation in wild type but not in TLR4 null mice (Gondokaryono et al., 2007; Midwood et al., 2009). Interestingly, inhibition of DAMP function through neutralizing antibodies, small molecules and genetic deletion can ameliorate disease *in vivo*, further supporting a key role of DAMP in driving persistent inflammation and point to their inhibition as a needed therapeutic intervention.

1.7. DAMPs and PAMPs interaction: HMGB-1 as an example

As PAMPs and DAMPs can be recognized by the same receptors, it is conceivable that both molecules can synergize to amplify and sustain proinflammatory response. Indeed, it is known that DAMPs extracellular released can be promoted by PAMPs such as LPS, viruses, fungi by promoting cellular damage. In addition, these molecules can physically associate to result in a more prominent innate immune activation. In 2008, HMGB-1 was found to facilitate the transfer of LPS to CD14 thereby enhancing its proinflammatory activity (Youn et al., 2008). By means of a series of enzyme-linked immunosorbent assays (ELISAs) and SPR experiments, the authors showed that a physical interaction occurs between HMGB1 and LPS. Interestingly, this interaction was responsible for a significant enhancement of the LPS-mediate immune activation. Accordingly, the blockade of HMGB-1-LPS interaction through the use of synthetic peptides, completely abrogated HMGB-1-LPS synergism (Youn et al., 2011). Moreover, it was also shown that HMGB-1 synergizes with both endogenous and exogenous molecules, such as the synthetic derivate of triacylated bacterial lipoproteins Pam3CSK4, or the microbial CpG-DNA, in inducing a strong immune response. Finally, in 2018 Deng et al. demonstrated that hepatocyte-released HMGB1 binds to LPS and targets its internalization into the lysosomes of macrophages and endothelial cells via RAGE. Subsequently, HMGB1 permeabilizes the phospholipid bilayer in the acidic environment of lysosomes, resulting in LPS leakage into the cytosol and caspase-11 activation and cell death for pyroptosis (Deng et al., 2018). Altogether, these results suggest that PAMPs and DAMPs orchestrate innate immune activation, providing the rationale to investigate this crosstalk potentially involved in many human diseases (Tang et al., 2012).

2. Aim of the study

Briefly, the autoinflammatory/autoimmune activity of IFI16 can be summarized through the following steps: 1) IFI16 expression is enhanced in damaged tissues of patients affected by autoimmune/autoinflammatory diseases as a result of abnormal type I IFN production and/or other proinflammatory stimuli, including UVB; 2) IFI16 is then released as a consequence of increased cell damage/stress; 3) the released IFI16 protein leads to a breakdown in tolerance to self-antigens; 4) this loss of tolerance favors the generation of specific anti-IFI16 autoantibodies; 5) IFI16 freely circulating may act as a DAMP, amplifying the injury of target cells.

In an attempt to investigate IFI16 extracellular activity, Gugliesi *et al.* treated HUVEC with different concentrations of recombinant IFI16 (Gugliesi et al., 2013). By using several techniques, they demonstrated that extracellular IFI16 did not affect HUVEC cell viability, but severely limits their tubulogenesis and transwell migration activities, through a direct binding on HUVEC plasma membranes. Interestingly, these inhibitory effects were fully reversed in the presence of anti-IFI16 N-terminal antibodies, suggesting that its extracellular activity resides within its N-terminal domain. These results were further corroborated by Bawadekar *et al.,* who expanded on HUVEC treatment with extracellular IFI16 demonstrating that recombinant IFI16 caused dose/time-dependent mRNA upregulation of pro-inflammatory cytokines such as IL-6, IL-8, CCL2, CCL5, CCL20, ICAM1, and VCAM1 (Bawadekar et al., 2015b). Interestingly, the IFI16-mediated release of IL-6 and IL-8 was enhanced when a combinatorial IFI16-LPS treatment was performed.

Altogether, these results clearly pointed out to a role of extracellular IFI16 as a DAMP. Moreover, they suggested an interaction between IFI16 and LPS.

Therefore, this PhD project aimed to:

1) Mechanistically dissect the interaction between LPS and IFI16, using not only the canonical TLR4-activator LPS (*e.g.,* LPS form *E. coli*), but also TLR4-weak activator or TLR4-antagonist LPS (*e.g.,* LPS from *P. gingivalis*, and LPS from *R. sphaeroides*);
2) Corroborate the role of IFI16 as a novel DAMP using other target cells, and explore the biological impact of the IFI16-LPS complex;
3) Characterize the membrane-bound receptor responsible for IFI16 (-LPS)-mediated pro-inflammatory activity;
4) Dissect the IFI16-receptor molecular platform.

3. Materials and methods

3.1. Reagents, antibodies, and recombinant proteins

LPS from *Escherichia coli* O111:B4 (LPS-EB), *Porphyromonas gingivalis* (LPS-PG) or *Rhodobacter sphaeroides* (LPS-RS), biotin-labeled LPS from *Escherichia coli* O111:B4 (biotin-labeled LPS-EB), detoxified LPS from *Escherichia coli* O111:B4 (detoxLPS) and polimixin B (PMB) were all purchased from InvivoGen. LPS from *Escherichia coli* F583 (LPS-F583), monophosphoryl lipid A from *Escherichia coli* F583 (MPLA), diphosphoryl lipid A from *Escherichia coli* F583 (DPLA) were purchased from Sigma-Aldrich. Bovine serum albumin Fraction V pH 7 (BSA) was purchased from Euroclone.

The following antibodies were used: mAb anti-human TLR4 (sc-293072, Santa Cruz Biotechnologies), mAb anti-human TLR4 (sc-13593, Santa Cruz Biotechnologies), mAb anti-human TLR4 (mabg-htlr4, InvivoGen), rabbit polyclonal anti-MD2 (AHP1717T, Bio-Rad), rabbit monoclonal anti-MyD88 (4283, Cell Signaling Technology), mAb anti-NF-κB p65 (sc-8008 X, Santa Cruz Biotechnologies), PE mouse anti-human CD14 (555398, BD Pharmingen), mAb anti-β-actin (A1978, Sigma-Aldrich), rabbit IgG-HRP (A6154, Sigma-Aldrich,), mouse IgG-HRP (NA931V, GE Healthcare), streptavidin-HRP (E2886, Sigma-Aldrich,), mouse IgG-Alexa Flour 488 (A11001, Thermo Fisher Scientific), normal mouse IgG2a isotype control (sc-3878, Santa Cruz Biotechnologies). Rabbit polyclonal anti-IFI16 N-term and C-term were produced as described previously (Gariglio et al., 2002). Briefly, N-terminus or C-terminus IFI16 cDNA from pBKS-IFI16 (kindly provided by J. Trapani, The Peter MacCallum Cancer Institute, Victoria, Australia) were cloned into a pGEX-4T-2 vector (Pharmacia, Uppsala, Sweden) to create an in-frame fusion protein with the GST coding region. The expression of N-terminus or C-terminus GST-IFI16 fusion protein in the Escherichia coli host AD202 was induced by treatment with 0.1 mM isopropyl-b-D-thiogalactopyranoside (IPTG) for 3 h. The bacterial cells were harvested by centrifugation, resuspended in cold lysis buffer (0.5 mg/ml lysozyme, 25 mM

Tris-HCl, pH 7.9, 150 mM NaCl, 1 mM EDTA, 1 mM DTT, 10% glycerol, 0.2% Triton X-100 containing 2 mM PMSF, 50 mM pepstatin A, and 50 mM leupeptin as protease inhibitors) and lysed by sonication. Fusion proteins were purified from the cleared lysate by glutathione-Sepharose affinity chromatography. Antisera against IFI16 were raised by injecting rabbits with the purified GST-IFI16 fusion proteins. The sera obtained after bleeding at 1 week after the fourth immunization were precipitated with ammonium sulfate at 45% saturation. The precipitate was then resuspended in phosphate-buffered saline (PBS) and purified on a protein A affinity column (Pharmacia) according to the specification of the supplier.

Human recombinant IFI16, IFI16 domains (*i.e.*, PYRIN, HINA and HINB), and IFI16 variants lacking the HINB domain (*i.e.*, IFI16ΔHINB) or the PYRIN domain (*i.e.*, IFI16ΔPYRIN) were produced as previously described (Bawadekar et al., 2015b). Briefly, the different coding regions were amplified from the full-length human IFI16 cDNA (isoform b) and cloned in a pET30a expression vector (Novagen) containing an N-terminal histidine tag. The expression of the proteins in the ClearColi® BL21(DE3) host (to ensure no endotoxin contamination) and the lysis of the bacteria, were performed as described above. Recombinant proteins were purified from the cleared lysate by nickel-affinity purification and stored at - 80°C in endotoxin-free vials.
GST recombinant protein was expressed using pGEX-4T2 vector and purified according to standard procedures. The purity of the proteins was assessed by 12% SDS-polyacrylamide gel electrophoresis. Recombinant TLR4 protein and TLR4/MD2 complex (478-TR-050 and 3146-TM-050/CF, respectively) were purchased from R&D Systems.

3.2. Pull-down assay, ELISA and competitive ELISA

Biotin-labeled LPS-EB (10 µg) was incubated with 30 µl of streptavidin sepharose high performance beads (GE Healthcare) for 3 h at 4°C. After a washing step, 3 µg of recombinant IFI16, PYRIN, HINA, HINB, IFI16ΔHINB, or GST were added and incubated O/N at 4°C. After

five washes with 1X PBS with 0.25% Triton X-100 (Sigma-Aldrich), samples were boiled in sample buffer containing SDS and β-mercaptoethanol and centrifuged. Supernatants were separated on a 7.5% or 12% SDS-polyacrylamide gel (Bio-Rad). Gels were stained with Coomassie brilliant blue (Serva Electrophoresis GmbH) for protein visualization.

For saturation binding experiments, microtiter plates (Nunc-Immuno MaxiSorp, Thermo Fischer Scientific) were coated with 2 µg/ml of recombinant IFI16 or 10 µg/ml of BSA or GST in 1X PBS O/N at 4°C. After a washing step with 1X PBS and 0.25% Tween 20 (v/v, Sigma-Aldrich) and blocking step with 1X PBS with 3% BSA and 0.05% Tween 20 for 1 h, increasing concentrations of biotin-labeled LPS-EB, preincubated with 10 µg/ml of polymyxin B (PMB) when specified, were added to the wells and incubated for 1 h at room temperature (RT). Bound proteins were then detected using HRP-conjugated streptavidin. TMB solution (Thermo Fischer Scientific) was used for color development, and OD was measured at 450 nm. Alternatively, microtiter plates were coated with 10 µg/ml of LPS-EB, LPS-PG, LPS-RS, LPS-F583, MPLA, DPLA, or detoxLPS in 1X PBS for 24 h at RT. After washing and blocking for 2 h, increasing concentrations of IFI16, PYRIN, HINA, or HINB were added to the wells, preincubated with 10 µg/ml of PMB when specified, for 2 h. Anti-IFI16 antibodies against the N- or the C-terminus of the protein and HRP-labeled anti-rabbit IgG were then added as primary and secondary antibodies, respectively. The binding was detected as described above.

For whole-cell ELISA, different strains of bacteria (*i.e.,* gram-positive: Staphylococcus aureus, Staphylococcus epidermidis and Streptococcus pyogenes; gram-negative: Escherichia coli and Klebsiella pneumonia) were grown in LB medium without antibiotics and, after washing with 1X PBS, fixed in 0.5% formalin O/N at 4°C. Subsequently, the bacteria were diluted to an OD600 of 0.5 and were used to coat microtiter plates O/N at 37°C. After blocking, increasing concentrations of IFI16 were added to the wells and incubated for 2 h at RT. Anti-IFI16 antibodies

against the N-terminus of the protein and HRP-labelled anti-rabbit IgG were then added as primary and secondary antibody, respectively, and binding was detected as described above.

For competitive ELISA, microtiter plates were coated with 1 µg/ml LPS-EB in 1X PBS O/N at RT. Successively, a constant amount of 2 µg/ml IFI16 was added to the wells in the presence of increasing concentration of LPS-EB, MPLA or detoxLPS. After incubation for 4 h at RT under gentle agitation, plates were incubated with an anti-IFI16 N-terminal primary antibody and an HRP-conjugated anti-rabbit IgG secondary antibody. The binding was detected as described above. To determine KD constants, saturation binding experiments were performed, and data were fitted to the Langmuir isotherm equation, which describes the equilibrium binding of the ligands (Hulme and Trevethick, 2010). Data are reported as sigmoid concentration-response curves plotted against log concentrations.

3.3. Cell cultures, treatments and transfection

Human kidney adenocarcinoma cells 786-O, human leukemia monocytes THP-1, and mouse macrophages RAW 264.7 were obtained from ATCC and grown in RPMI 1640 Medium (Sigma-Aldrich) containing 10% of fetal bovine serum (FBS, Immunological Sciences) and 1% of penicillin/streptomycin/glutamine solution (PSG, Gibco) at 37°C and 5% CO_2. Wild-type and IFI16-knockout (U2OS-IFI16$^{-/-}$) human osteosarcoma cells U2OS were kindly gifted by Dr. Bala Chandran (University of South Florida, FL, USA; (Cigno et al., 2015) and grown in Dulbecco's modified Eagle's medium (Sigma-Aldrich) containing 10% of FBS and 1% of PSG at 37°C and 5% CO_2. UVB irradiations were performed as previously described (Costa et al., 2011). Briefly, UV irradiation were performed in PBS and provided by a UVB lamp (HD 9021; Delta Ohm S.r.l., Padova, Italy), which emits most energy within the UVB range (280–315 nm), with an emission peak at 312 nm. Irradiation intensity was monitored by a UVB irradiance meter cosine corrector with spectral range of 280–319 nm (LP 9021 RAD; Delta Ohm). Following irradiation with the

required UVB dose, cells were incubated in complete medium for 16h at 37 °C in a humidified 5% CO2 atmosphere. The resulting cell culture supernatants were centrifuged to remove any cellular pellet and stored at -80°C for the following experiments.

For treatments, cells were stimulated in complete medium with IFI16, PYRIN, HINA, HINB, IFI16ΔHINB, IFI16ΔPYRIN, MPLA, DPLA, LPS-F583, LPS-EB, LPS-RS, alone or pre-complexed by O/N incubation at 4°C, unless specified otherwise. Additionally, cells were stimulated with supernatants of untreated or UVB-treated U2OS or U2OS-IFI16$^{-/-}$ cells alone or preincubated O/N at 4°C with LPS-EB, or LPS-RS. LPS variants or lipid A moieties were used at a concentration of 10 ng/ml. All treatments were carried out at 37°C and 5% CO_2.

For TLR4 neutralization, THP-1 cells were pretreated with 10 µg/ml of anti-TLR4 antibodies for 1 h before treatments. For treatments with anti-IFI16 antibodies, IFI16 was incubated with rabbit polyclonal anti-IFI16 N-term or C-term for 1 h at RT before treatments.

For TLR4, MD2 or Myd88 gene silencing, cells were transfected with specific human TLR4, MD2, Myd88 or control siRNAs (Dharmacon, siGENOME smart pool) using DharmaFect1 transfection reagent (Dharmacon). The efficiency of knockdown was confirmed by FACS analysis and immunoblotting at 48 h after transfection.

3.4. FACS analysis

Single cell suspensions were incubated for 30 min on ice with anti-TLR4 (sc-13593), PE-conjugated anti-CD14 (555398) or with isotype control diluted in staining buffer (PBS 1% FBS 0.1% NaN_3). To detect TLR4 staining, cells were further washed and incubated for 30 min on ice with Alexa Fluor 488-conjugated secondary antibody. Cell counts and fluorescence intensity measurements were calculated by Attune NxT Flow Cytometer (Thermo Fisher Scientific). Background fluorescence was subtracted using unlabeled cells, and channel compensation was

performed using Attune performance tracking beads (Thermo Fisher Scientific). A total of 10,000 events were recorded. Data were analyzed by FlowJo cell analysis software (BD Life Sciences).

3.5. Western blot and immunoprecipitation

Whole-cell extracts were prepared using RIPA lysis and extraction buffer (Pierce) with halt protease and phosphatase inhibitor (Thermo Fisher Scientific) on ice, and total protein concentration was quantified by Bradford Reagent (Sigma-Aldrich) measuring absorbance at 595 nm. Twenty μg of cell extracts, or 30 μl of U2OS culture supernatants were separated by electrophoresis on 7.5% or 12% SDS-polyacrylamide gels (Bio-Rad), transferred to nitrocellulose membranes, blocked with 10% non-fat milk in tris-buffered saline-tween (TBST), and probed with specific primary antibodies O/N at 4°C. After being washed with TBST, membranes were incubated with specific HRP-conjugated secondary antibodies, and binding was detected by ECL (Thermo Fisher Scientific, Super Signal West Pico). Expression of β-actin was used as protein loading control.

Co-immunoprecipitation of TLR4 with interacting proteins was performed using the Dynabeads Protein G Immunoprecipitation Kit (ThermoFisher), according to the manufacturer's instructions with minor modifications. Briefly, after lysis of treated cells, 20 μg of total cell extracts were kept as the input control, while 90 μg of total cell extracts were incubated for 1 h at RT with 2.5 μg of anti-TLR4 antibody previously conjugated with magnetic beads. The resulting complexes were then washed, eluted, denatured, and subjected to Western blotting as described above. For DNase-treated cell extracts, DNase I (Sigma Aldrich) was added at a 1:10 dilution and incubated for 15 min at RT. Images were acquired, and densitometry of the bands was performed using Quantity One software (version 4.6.9, Bio-Rad). Densitometry values were normalized using the corresponding loading controls.

3.6. Quantitative real time PCR

Quantitative real-time PCR (qRT-PCR) was performed on a CFX96 Real-Time PCR Detection System (Bio-Rad) as previously described (Albertini et al., 2018). Briefly, total RNA was extracted using TRI Reagent (Sigma-Aldrich), and 1 μg was retrotranscribed using an iScript cDNA Synthesis Kit (Bio-Rad). Reverse-transcribed cDNAs were amplified in duplicate using SsoAdvanced Universal SYBR Green Supermix (Bio-Rad), up to 40 cycles of PCR. The human glyceraldehyde 3-phosphate dehydrogenase (GAPDH) gene, or the murine actin gene, were used as housekeeping gene to normalize for variations in cDNA levels. The relative normalized expression after stimulation as compared to control was calculated as fold change = $2^{-\Delta(\Delta CT)}$ where $\Delta CT = CT_{target} - CT_{GADPH}$ and $\Delta(\Delta CT) = \Delta CT_{stimulated} - \Delta CT_{control}$. Primer sequences are summarized in Table 1.

Table 1. List of primers used for qRT-PCR (h: human; m: mouse).

Gene	*Forward (5' to 3')*	*Reverse (5' to 3')*
hIL-6	ACCGGGAACGAAAGAGAAGC	CTGGCAGTTCCAGGGCTAAG
hIL-8	ATGACTTCCAAGCTGGCCGTGGCT	TCTCAGCCCTCTTCAAAAACTTCTC
hTNF-α	GCCAGAGGGCTGATTAGAGA	TCAGCCTCTTCTCCTTCCTG
hIL-1β	TCCCCAGCCCTTTTGTTGA	TTAGAACCAAATGTGGCCGTG
hGAPDH	AACGTGTCAGTGGTGGACCTG	AGTGGGTGTCGCTGTTGAAGT
mACTIN	CCCAAGGCCAACCGCGAGAAGAT	GTCCCGGCCAGCCAGGTCCAG
mIL-6	GGATACCACTCCCAACAGACCT	GCCATTGCACAACTCTTTTCTC
mIL-1β	AAGTTGACGGACCCCAAAAGA	TGTTGATGTGCTGCTGCGA

3.7. Cytokines measurement by ELISA

Cytokines secreted in culture supernatants after treatments were analyzed using human IL-6 DuoSet ELISA and human IL-8 DuoSet ELISA (all from R&D Systems), human TNF-α Uncoated ELISA and human IL-1β Uncoated ELISA (Thermo Fisher Scientific) according to the manufacturer's instructions. Absorbance was measured using a Spark multimode microplate reader (Tecan).

3.8. Transcription factor assay

Nuclear extracts were prepared using NE-PER Nuclear and Cytoplasmic Extraction Reagents (Thermo Fisher Scientific), according to the manufacturer's instructions. NF-κB binding activity to a DNA probe containing its binding consensus sequence was measured by Universal Transcription Factor Assay Colorimetric kit (Merck Millipore). The binding of NF-κB to the DNA probe was revealed using a specific primary antibody, with an HRP-conjugated secondary antibody used for detection with TMB substrate. The intensity of the reaction was measured at 450 nm. The following biotinylated oligonucleotides were used: sense (biotin): 5'-ATGACATAGGAAAACTGAAAGGGAGAAGTGAAAGTGGGAAATTCCTCTG-3'; antisense: 5'-CAGAGGAATTTCCCACTTTCACTTCTCCCTTTCAGTTTTCCTATGTCAT-3'.

3.9. Surface plasmon resonance analysis

The Biacore X100 (GE Healthcare) instrument was used for real-time binding interaction experiments. Recombinant TLR4 or TLR4/MD2 complex was covalently immobilized onto the surface of sensor CM5 (cat # BR100012, GE Healthcare) chips *via* amine coupling. TLR4 was diluted to a concentration of 10 μg/ml in 10 mM sodium acetate at pH 4.0, while TLR4/MD2

complex was diluted to a concentration of 20 µg/ml in the same buffer. Both proteins were injected on CM5 chips at a flow rate of 10 µl/min, upon activation of the carboxyl groups on the sensor surface with 7-min injection of a mixture of 0.2 M EDC and 0.05 M NHS. The remaining esters were blocked with 7-min injection of ethanolamine. Taking into account the ligands (TLR4 or TLR4/MD2) and analytes (IFI16, LPS-EB or IFI16/LPS-EB) molecular weights (MW) of 70 or 90 kDa, and 90, 10 or 100 kDa respectively, the appropriate ligand density (RL) on the chip was calculated according to the following equation: RL = (ligand MW/analyte MW) × Rmax × (1/Sm), where Rmax is the maximum binding signal and Sm corresponds to the binding stoichiometry. The target capture level of the TLR4 or TLR4/MD2 was of 596.0 or 1223.9 response units (RUs), respectively. The other flow cell was used as a reference and was immediately blocked after the activation. Increasing concentrations of endotoxin-free IFI16, LPS-EB or IFI16/LPS-EB complex were flowed over the CM5 sensor chip coated with TLR4 or TLR4/MD2 at a flow rate of 30 µl/min at 25°C with an association time of 120 s for IFI16 alone and the IFI16/LPS-EB complex, and 180 s for LPS-EB, and a dissociation phase of 180 s for IFI16 and IFI16/LPS-EB complex or 600 s for LPS-EB. A single regeneration step with 50 mM NaOH was performed following each analytic cycle. All the analytes tested were diluted in the HBS-EP+ buffer (GE Healthcare).

Recombinant IFI16 was covalently immobilized onto the surface of sensor CM5 chips via amine coupling as done for TLR4 and TLR4/MD2 complex. IFI16 was diluted to a concentration of 25 µg/ml in 10 mM sodium acetate at pH 4.0. The target capture level of IFI16 was of 1926.6 response units (RUs). Increasing concentrations of LPS-EB, diluted in HBS-EP+ buffer, were flowed over the CM5 sensor chip coated with IFI16 at a flow rate of 30 µl/min at 25°C with an association time of 180 s and a dissociation phase of 600 s. A single regeneration step with 50 mM NaOH was performed following each analytic cycle. The K_Ds were evaluated using the BIAcore evaluation software (GE Healthcare) and the reliability of the kinetic constants calculated by assuming a 1:1 binding model supported by the quality assessment indicators values.

For the binding inhibition experiments, a fixed concentration of IFI16 (500 nM) was incubated with increasing concentrations of rabbit polyclonal anti-IFI16 N-term or C-term for 1 h at RT, diluted in HBS-EP+ buffer. IFI16–antibody complexes were injected over the TLR4/MD2 sensor chip surface for 120 s and allowed to dissociate for 180s. A single regeneration step with 50 mM NaOH was performed following each analytic cycle. Data were background-subtracted using the adjacent control flow cell and buffer-alone injections. The reported RUs were calculated using the BIAcore evaluation software.

3.10. Statistical analysis

All statistical analyses were performed using GraphPad Prism version 6.00 for Windows (GraphPad Software, La Jolla California USA, www.graphpad.com). The data are expressed as mean ± SD. For comparisons between two groups, means were compared using a two-tailed Student's t test. For comparisons among three groups, means were compared using one-way or two-way ANOVA followed by Dunnett's test. Differences were considered statistically significant at a P value < 0.05.

4. Results

4.1. IFI16 binds to LPS of different bacterial origin and inflammatory activity

To investigate the occurrence of a direct association between IFI16 and LPS, we performed an *in vitro* pull-down assay using biotin-labeled LPS from *E. coli* O111:B4 (biotin-LPS-EB) and human recombinant IFI16 protein. As shown in Fig 6A, we could readily detect a highly reproducible ~100-kDa band corresponding to biotin-LPS-bound IFI16. To rule out that this binding was due to bacterial contaminants, we next performed a pull-down assay using a recombinant glutathione-S transferase (GST) protein prepared with the same procedure as that employed to obtain recombinant IFI16. As shown in Fig 6B, we failed to isolate any GST-containing band following incubation of GST with biotin-LPS-EB and streptavidin beads, demonstrating the specificity of the IFI16/LPS interaction. Furthermore, saturation binding experiments using IFI16-coated microtiter plates challenged with increasing amounts of biotin-LPS-EB revealed biotin-labeled LPS bound to solid-phase IFI16 in a concentration-dependent manner, reaching saturation at 100,000 ng/ml of biotin-LPS-EB (Fig 6C). When recombinant GST or BSA were coated onto the microtiter plates, no binding occurred in the presence of biotin-LPS-EB (Fig 6C). To assess binding specificity, we asked whether polymyxin B (PMB), an LPS-sequestering agent able to bind to negatively charged phosphate groups of lipid A (Velkov et al., 2013), would disrupt IFI16/LPS interaction. As shown in Fig 6C, when PMB was pre-incubated with biotin-LPS-EB and then added to the IFI16-coated wells, it completely prevented IFI16 from binding to LPS. Next, IFI16/LPS-EB interaction was confirmed by surface plasmon resonance (SPR) analysis flowing increasing amounts of LPS-EB over a CM5 IFI16-coated chip. As shown in Fig 6D, LPS interacted with IFI16 in a concentration-dependent manner, with a kinetic association constant (K_a) of $1.13*10^4$ 1/Ms and a kinetic dissociation constant (K_d) of $1.94*10^{-3}$ 1/s, respectively.

Altogether, these results indicate that IFI16 binds to LPS-EB with high affinity and that such interaction is inhibited by PMB, presumably by masking the negatively charged groups of the LPS lipid A moiety.

We next sought to determine whether IFI16 could bind to LPS in its natural setting, such as the outer membrane of fixed gram-negative bacteria. To this end, a panel of gram-negative bacteria, including a laboratory strain of *E. coli* and a clinical isolate of *Klebsiella pneumoniae*, were assessed as solid phase antigens by whole cell ELISA. Gram-positive clinical isolates of *Staphylococcus aureus*, *Staphylococcus epidermidis* and *Streptococcus pyogenes* were used as negative controls. As shown in Fig 6E, IFI16 strongly associated with the surface of both gram-negative bacteria species. By contrast, no IFI16 binding could be detected when gram-positive bacteria were used as solid phase antigens (Fig 6E). Thus, IFI16-LPS binding can also occur in the natural setting where LPS is anchored to the bacterial outer membrane by its lipid A moiety.

We next asked whether IFI16 would bind with the same affinity to LPS variants derived from different gram-negative strains with highly variable structure and broad-spectrum activity. For this purpose, microtiter plates were coated with the following LPS variants: 1) the two full TLR4 agonists *E. coli* O111:B4 (LPS-EB) and *E. coli* F583 (LPS-F583), with the latter harboring a similar lipid A moiety but a shorter polysaccharide chain length compared to that of the O111:B4 strain; 2) the weak TLR4 agonist *P. gingivalis* (LPS-PG), carrying a mixture of di-, mono- and de-phosphorylated penta- or tetra-acylated lipid A moieties; or 3) the TLR4 antagonist *R. sphaeroides* (LPS-RS), harboring a di-phosphorylated lipid A loaded with 3 long and 2 short acyl chains (Fig 6F). As shown in Fig 6G, IFI16 was able to bind to all the aforementioned solid-phase LPS variants in a concentration-dependent manner, although with slightly different kinetics. Specifically, we obtained similar K_Ds for the two *E. coli* LPS variants—*i.e.,* 4.2 nM and 4.3 nM for LPS-EB and LPS-F583, respectively—, while we observed slightly higher K_Ds for LPS-PG and LPS-RS—*i.e.,* 12.0 nM and 19.3 nM, respectively (Table 2). Consistently, treatment of immobilized LPS molecules with PMB prior to the addition of IFI16 completely abolished IFI16

binding. Thus, IFI16 binds to not only the canonical TLR4-activating LPS but also variants characterized by weaker triggering activity.

Table 2. Full-length IFI16 and IFI16 domains binding affinities to LPS

LPS variant	Equilibrium dissociation constant (KD), nM			
	IFI16	PYRIN	HINA	HINB
LPS *E. coli* O111:B4 (LPS-EB)	4.2	116.5	85.3	3.3
LPS *E. coli* F583 (LPS-F583)	4.3	-	-	-
LPS *P. gingivalis* (LPS-PG)	12.0	46.9	84.0	1.6
LPS *R. sphaeroides* (LPS-RS)	19.3	-	-	-
DPLA *E. coli* F583 (DPLA)	0.9	47.5	67.7	2.8
MPLA *E. coli* F583 (MPLA)	1.2	47.2	94.1	2.7
Detoxified LPS *E. coli* O111:B4 (detoxLPS)	> 20	-	-	-

K_D, equilibrium dissociation constant

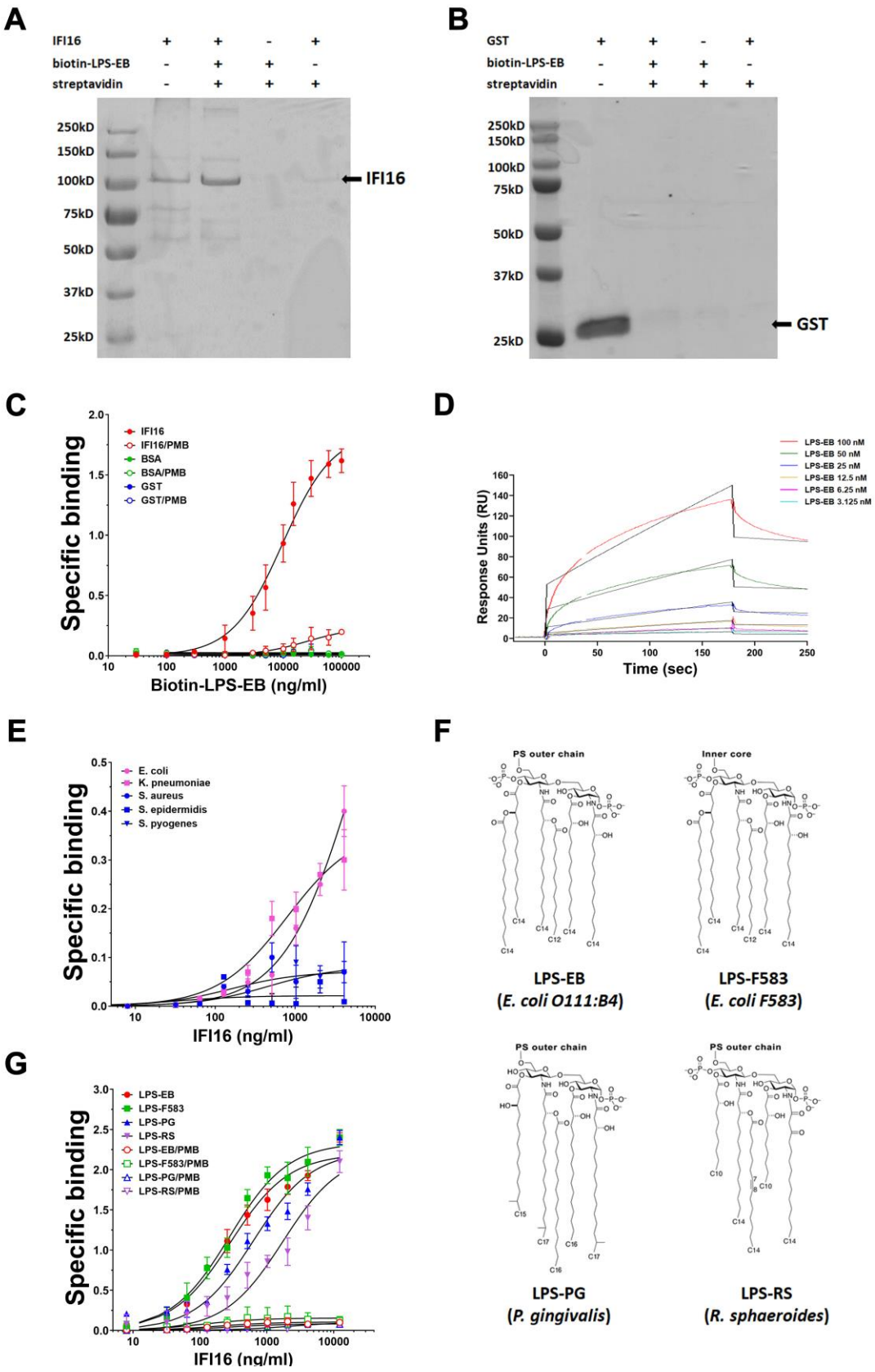

Fig 6. IFI16 binds to LPS of different bacterial origin and inflammatory activity. Coomassie brilliant blue staining of pull-down assays performed with 3 µg of recombinant IFI16 **(A)** or GST **(B)** in the presence or absence of biotin-labeled lipopolysaccharide (LPS) from *E. coli* O111:B4 (biotin-LPS-EB). **(C)** Saturation binding experiments performed

with 2 μg/ml of IFI16 (red circles) and increasing amount of biotin-LPS-EB. Binding was detected by ELISA using HRP-conjugated streptavidin. Optical density (OD) of samples was measured at 450 nm. An excess of recombinant GST (blue circles) or BSA (green circles) and pre-treatment of biotin-LPS-EB with polymyxin B (PMB, empty circles) were used as negative controls. Data are expressed as mean values ± SD of three independent experiments. **(D)** Surface plasmon resonance (SPR) analysis of LPS-EB binding to immobilized IFI16. After immobilization of IFI16 on the CM5 sensor chip surface, increasing concentration of LPS-EB (3.125-100 nM) diluted in running buffer were injected over immobilized IFI16. Data are representative of three independent experiments. **(E)** *Ex-vivo* interaction analysis between increasing amount of recombinant IFI16 and formalin-fixed gram-negative (*E. coli* and *K. pneumonia*; pink circles and pink squares, respectively) or gram-positive (*S. aureus*, *S. epidermidis*, *S. pyogenes*; blue circles, squares and triangles, respectively) bacteria. Data are expressed as mean values ± SD of three independent experiments. **(F)** Lipid A structures of LPS derived from *E. coli* O111:B4 or F583 LPS (LPS-EB and LPS-F583, respectively; strong TLR4 agonists), *P. gingivalis* (LPS-PG; weak TLR4 agonist) and *R. sphaeroides* (LPS-RS, TLR4 antagonist). For LPS-PG, which harbors a mixture of di-, mono- and de-phosphorylated penta- or tetra-acylated lipid A moieties, a single isoform is represented for simplicity. PS-outer chain = polysaccharide outer chain. **(G)** Saturation binding experiments with increasing amount of recombinant IFI16 (8 to 12,288 ng/ml) and 10 μg/ml of LPS-EB (red line), LPS-F583 (green line), LPS-PG (blue line) or LPS-RS (purple line). Anti-IFI16 antibodies against the N-terminus of the protein and HRP-labelled anti-rabbit IgG were added as primary and secondary antibody, respectively, and binding was detected by ELISA at 450 nm. Data are expressed as mean values ± SD of three independent experiments.

4.2. IFI16 binds to the lipid A moiety of LPS through its HINB domain

To identify which LPS moiety is involved in IFI16 binding, we performed saturation binding experiments using two different variants of lipid A derived from the *E. coli* F583 strain, namely diphosphorylated and monophosphorylated lipid A (DPLA and MPLA, respectively), alongside a detoxified LPS molecule derived from the *E. coli* strain O111:B4 (detoxLPS) (Fig 7A). The first two molecules lack the heteropolysaccharide outer chain and differ in the number of phosphate groups, with MPLA being a weaker agonist than DPLA (Casella and Mitchell, 2013). On the other hand, the detoxLPS lipid A moiety is partially delipidated by alkaline hydrolysis, resulting in only four primary acyl chains being directly esterified with the sugar moiety, in which the outer

chain is however preserved. DetoxLPS endotoxin levels are about 10,000 times lower than that of parental LPS (Wähämaa et al., 2011). As shown in Fig 7B, IFI16 readily bound to both forms of lipid A in a concentration-dependent fashion. The K_D values showed higher affinity for the lipid A moieties (either form) in comparison with LPS-F583—0.9 nM and 1.2 nM, respectively, *vs*. 4.3 nM (Table 2). Interestingly, the K_D value for IFI16 binding to detoxLPS (55.6 nM) was the highest among all LPS forms, indicating that the canonical acyl chain is required for IFI16 binding to LPS. When lipid A was pre-treated with PMB, no signal was detected. Thus, LPS binds to IFI16 through its lipid A moiety. To corroborate these data, a competition ELISA was performed by immobilizing LPS from the *E. coli* strain O111:B4 (LPS-EB) onto the microtiter plates followed by the addition of a mixture of a constant amount of IFI16 and increasing concentrations of LPS-EB, MPLA or detoxLPS, in this case used as competitors. As expected, addition of LPS-EB reduced IFI16 binding to immobilized LPS in a concentration-dependent manner (Fig 7C, white bars). Interestingly, a concentration of 5 μg/ml of MPLA was sufficient enough to achieve a much stronger reduction in IFI16 binding to LPS compared to a similar dose of LPS-EB (Fig 7, grey bars). Binding inhibition was further enhanced at higher concentrations of MPLA, but the difference between the two variants was less evident. By contrast, detoxLPS did not interfere with the binding of IFI16 to the canonical agonist LPS, even at the highest concentrations used (25 μg/ml: LPS-*EB vs.* detoxLPS, $P = 0.0059$; MPLA *vs.* detoxLPS, $P < 0.0004$; LPS-EB *vs.* MPLA, ns; unpaired t-test) (Fig 7, black bars). Taken together, these findings indicate that lipid A is the LPS moiety involved in the binding to IFI16 and that the heteropolysaccharide outer chain, absent in MPLA, might constitute a steric hindrance for such interaction.

To identify the domain of IFI16 mediating binding to LPS, an *in vitro* pull-down assay was performed using three distinct recombinant domains of IFI16 spanning either the N-terminal portion containing the pyrin domain (PYRIN) or each of the 200 amino acid-long HIN domains (namely HINA or HINB) (Fig 7D). As shown in Fig 7E, a signal at ~35 kDa was only detected

when the HINB fragment was incubated with biotin-LPS-EB bound to streptavidin beads (lane 9), while neither the PYRIN nor the HINA fragment was co-precipitated in the presence of biotinylated LPS (lanes 3 and 6).

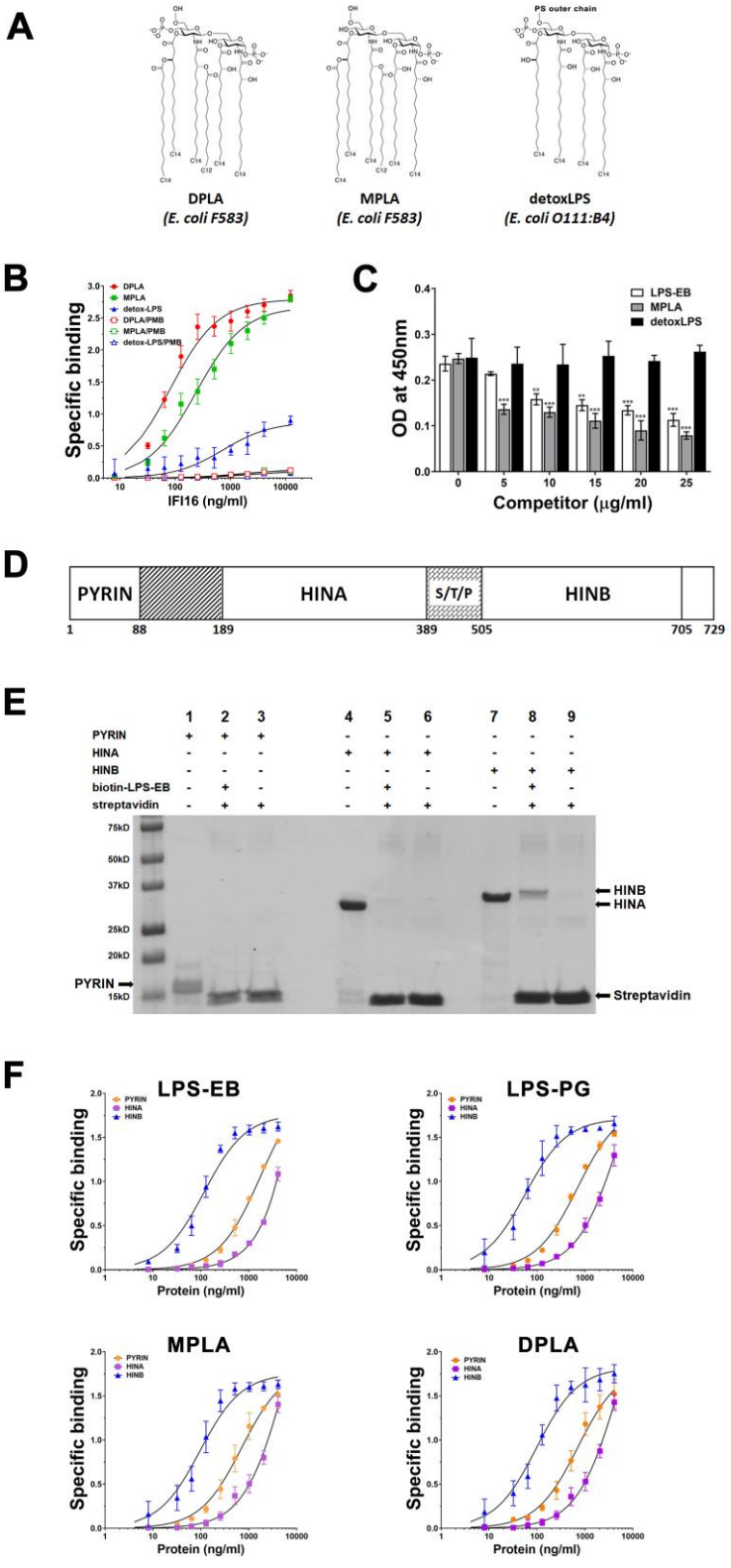

Fig 7. IFI16 binds to the lipid A moiety of LPS through its HINB domain. (A) Structures of di- or mono-phosphorylated lipid A from *E. coli* F583 (DPLA and MPLA, respectively) and detoxified LPS (detox-LPS) derived from *E. coli* O111:B4. PS-outer chain = polysaccharide outer chain. **(B)** Saturation binding experiments with increasing amount of recombinant IFI16 (from 8 to 12,288 ng/ml) and 10 μg/ml of MPLA (green line), DPLA (red line) or detox-LPS (purple line). Binding was detected by ELISA as described in the legend to Fig 7G. Data are expressed as mean values ± SD of three different experiments. **(C)** Competition ELISA assay for LPS-EB binding to IFI16 with increasing amount of LPS-EB, MPLA or detox-LPS as competitors. Briefly, microtiter plates were coated with 1 μg/ml LPS-EB, then 2 μg/ml of IFI16 were added to the wells in the presence of increasing concentration (5 to 25 μg/ml) of competitor. Binding was detected by ELISA as described in the legend to Fig 7F. Data are expressed as mean values ± SD of three independent experiments (***P<0.001, **P<0.01, Student's t test). **(D)** Domain organization of the IFI16 protein. The numbers represent the amino acid positions based on NCBI Reference Sequence NP_005522. From the N- to the C-terminal (left to right), IFI16 comprises a pyrin domain involved in protein-protein interaction, and two hematopoietic interferon-inducible nuclear protein with 200-amino-acid repeats (HINA and HINB) domains, which are a hallmark of the absent in melanoma 2-like receptors (ALRs). S/T/P = serine/threonine/proline-rich repeats, which are regulated by alternative mRNA splicing. **(E)** Coomassie brilliant blue staining of pull-down assays performed with 3 μg of recombinant PYRIN, HINA, and HINB domains, in presence or absence of biotin-labeled LPS from *E. coli* O111:B4 (biotin-LPS-EB). **(F)** Saturation binding experiments performed by using increasing amount (8 to 4096 ng/ml) of recombinant PYRIN, HINA or HINB domains (orange, purple and blue lines, respectively) and 10 μg/ml of LPS-EB, LPS-PG, MPLA or DPLA. Anti-IFI16 antibodies against the N- or C-terminus of the protein and HRP-labeled anti-rabbit IgG were added as primary and secondary antibody, respectively, and binding detected in ELISA at 450 nm. Data are expressed as mean values ± SD of three independent experiments**.**

To corroborate these data, an *in vitro* pull-down assay was performed using a truncated variant of IFI16 lacking the HINB domain (IFI16ΔHINB) (Fig 8A). As expected, no binding was observed when IFI16ΔHINB was incubated with biotin-LPS-EB and streptavidin beads (Fig 8B, lane 2), confirming that the HINB is required for LPS binding. To further support a role of the HINB domain in mediating the binding of IFI16 to LPS, we performed saturation binding experiments using increasing concentrations of the three IFI16 domains (*i.e.*, PYRIN, HINA, and HINB) with fixed amounts of different interactors. As shown in Fig 7F (blue lines), the HINB

domain was able to bind to both LPS variants, displaying either strong or weak TLR4 agonist activity, as well as to lipid A. The binding was not affected by the origin of bacterial LPS or by the number of phosphate groups, and displayed K_D values in a similar range to that obtained with the full-length recombinant IFI16 protein (Table 2). Conversely, the PYRIN (orange lines) and HINA (purple lines) domains displayed very low affinity for the immobilized molecules when compared to HINB, with K_D values indicative of unspecific binding (Table 2). Thus, the HINB domain displays the highest affinity for LPS, indicating that HINB may play a major role in the interaction between IFI16 and LPS.

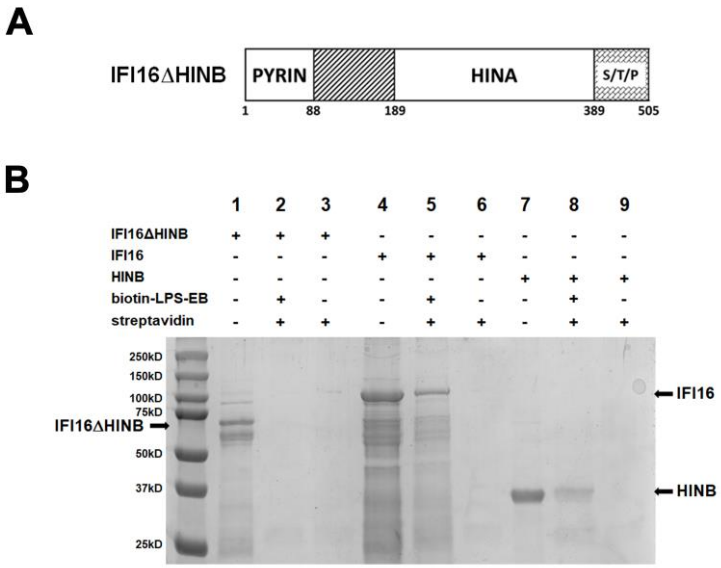

Fig 8. IFI16 variant lacking HINB domain does not bind to LPS. (A) Domain organization of the IFI16ΔHINB protein. The numbers represent the amino acid positions based on NCBI Reference Sequence NP_005522. From the N- to the C-terminal (left to right), IFI16ΔHINB comprises a pyrin domain, and only one hematopoietic interferon-inducible nuclear protein with 200-amino-acid repeats (HINA) domain. S/T/P = serine/threonine/proline-rich repeats. **(B)** Coomassie brilliant blue staining of pull-down assays performed with 3 μg of recombinant IFI16ΔHINB, full-length IFI16, or HINB domain in the presence or absence of biotin-labeled LPS from *E. coli* O111:B4 (biotin-LPS-EB).

4.3. Only potent TLR4-activating endotoxins can potentiate the proinflammatory activity of IFI16

The results so far obtained prompted us to investigate whether IFI16 binding to the strong agonist variant LPS-EB would modulate IFI16-mediated transcriptional activation of proinflammatory cytokines *in vitro*. For these experiments, in addition to the standard human monocytic cell line THP-1, we chose as a model the renal tubular carcinoma cell line 786-O. We first assessed protein expression levels of the main components of the LPS recognition complex (*i.e.,* TLR4, MD2, MyD88 and CD14) by Western blotting and/or flow cytometry (data not shown). While TLR4 and MD2 were expressed at similar levels in both cell lines, CD14 expression was 4-fold lower in THP-1 *vs.* 786-O cells, as judged by FACS analysis (data not shown), in good agreement with a previous report (Petes et al., 2018). The expression of the TLR4 canonical adaptor MyD88 was similar in both cell lines (data not shown).

Next, cells were stimulated with full-length IFI16 or the IFI16ΔHINB variant, alone or pre-incubated with LPS-EB, and then total RNA was extracted to assess mRNA levels of a panel of proinflammatory cytokines (Fig 9A). Consistent with IFI16 acting as a DAMP, IL-6, IL-8 and tumor necrosis factor-α (TNF-α) mRNA levels were strongly upregulated in cells treated with IFI16 alone when compared to mock- or LPS-treated cells in the presence of either low or high LPS concentration. Interestingly, we detected a further increase in mRNA expression levels of the aforementioned genes in cells treated with the IFI16/LPS-EB complex compared to IFI16 alone—*i.e.,* 1.8- and 1.6-fold induction for IL-6; 1.7- and 1.3-fold induction for IL-8; and 2.1- and 1.6-fold induction for TNF-α in 786-O and THP-1 cells, respectively. Likewise, IL-1β gene expression levels were also significantly induced by IFI16 alone or IFI16/LPS-EB complex treatment of THP-1 cells—*i.e.,* 72- and 83-fold induction, respectively—and, albeit to a lower extent, 786-O cells—*i.e.,* 13- and 27-fold induction, respectively. When IFI16ΔHINB alone or pre-incubated with LPS-EB was used to stimulate the cells, the degree of cytokine induction was

similar to that observed with the full-length protein, while it was not enhanced following pre-incubation with LPS-EB.

Altogether, these findings further strengthen the notion that the HINB moiety is necessary for the formation of the functional IFI16/LPS complex.

Consistent with the mRNA data, the amounts of IL-6, IL-8 and TNF-α secreted into the culture supernatants were significantly higher in cells treated with the IFI16/LPS-EB complex than those of cells treated with IFI16 alone, while they did not vary upon pre-incubation with LPS-EB in the case of the IFI16ΔHINB variant (Fig 9B). In contrast, neither IFI16 nor IFI16ΔHINB *per se* or after forming a complex with LPS induced IL-1β release in both cell lines, indicating lack of inflammasome-mediated IL-1β processing at 24 h post-treatment.

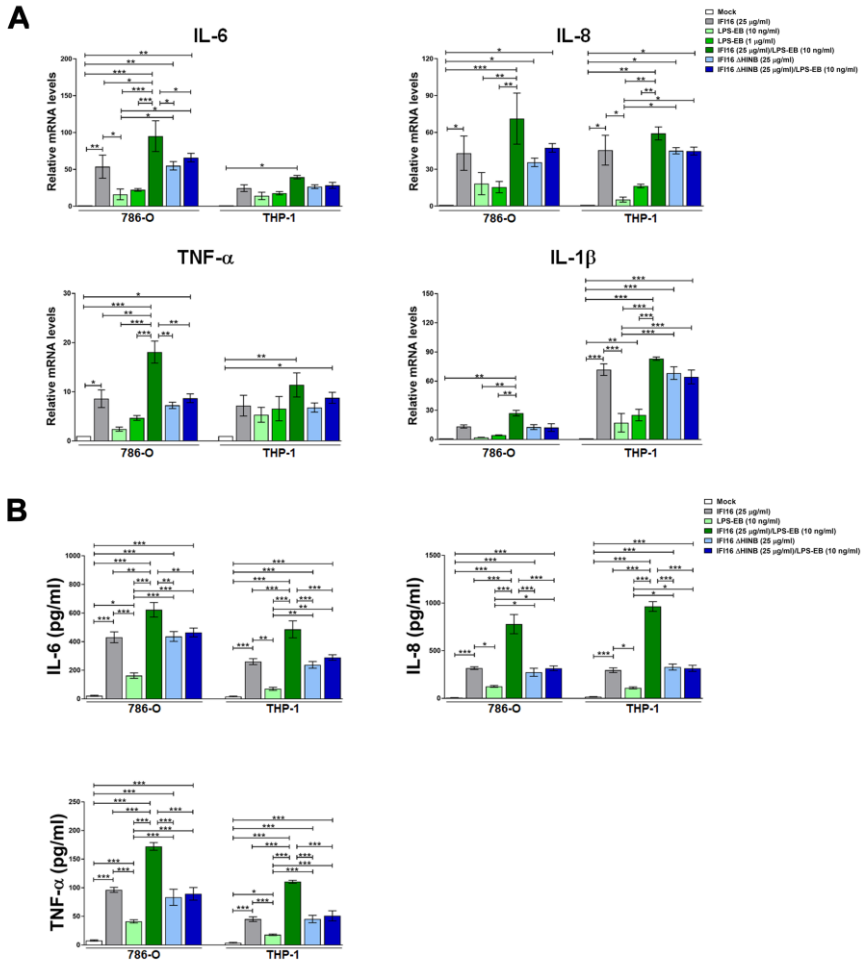

Fig 9. IFI16 proinflammatory activity is potentiated by the strong TLR4 activator LPS-EB. (A) qRT-PCR analysis of IL-6, IL-8, TNF-α and IL-1β mRNA expression levels in 786-O or THP-1 cells stimulated for 24 h with IFI16

(25 μg/ml), IFI16ΔHINB (25 μg/ml), LPS from *E. coli* O111:B4 (LPS-EB, 10 ng/ml or 1 μg/ml), IFI16/LPS-EB complex (preincubated O/N at 4°C), IFI16ΔHINB/LPS-EB (preincubated O/N at 4°C), or left untreated (mock). Values are normalized to GAPDH mRNA and plotted as fold induction over mock-treated cells. qRT-PCR data are presented as mean values of biological triplicates. Error bars indicate SD (**P* < 0.05, ***P* < 0.01, ****P* < 0.001; two-way ANOVA followed by Dunnett's test). **(B)** Protein concentration of IL-6, IL-8 and TNF-α evaluated by ELISA in supernatants derived from 786-O or THP-1 cells stimulated for 24 h as described in **A**. Data are expressed as mean values ±SD of three independent experiments (**P* < 0.05, ***P* < 0.01, ****P* < 0.001; two-way ANOVA followed by Dunnett's test).

Next, we asked whether the LPS derivatives DPLA and MPLA or the TLR4 antagonist LPS-RS would be equally able to modulate the biological activity of IFI16. The full agonist LPS-F583, from which DPLA and MPLA were derived, was included as positive control (full TLR4 activator). Cells were treated with the aforementioned compounds, alone or pre-complexed with IFI16 protein, and then total RNA and supernatants were collected to assess the mRNA expression and cytokine production profiles of IL-6, IL-8 and TNF-α. As expected, cells treated with the IFI16/LPS-F583 displayed a similar transcriptional activation pattern to that previously observed in IFI16/LPS-EB-treated cells (Fig 10A). On the other hand, when cells were treated with IFI16 complexed with LPS-RS, MPLA or DPLA, we failed to observe any transcriptional enhancement in comparison with IFI16 alone. A similar pattern was found when the same cytokines were measured in the culture supernatants by ELISA (Fig 10B), although a significant increase in IFI16-induced secretion of IL-6 and IL-8 was only observed when cells were treated with the IFI16-DPLA complex—*i.e.,* 1.4-fold induction for IL-6 in THP-1 cells, 1.3- and 1.8-fold induction for IL-8 in 786-O and THP-1, respectively.

Collectively, these data indicate that the proinflammatory activity of full-length IFI16 is potentiated when this protein is complexed with potent TLR4-activating LPS variants *via* the HINB moiety, while it is not affected when it forms a complex with the TLR4 antagonist LPS-RS or the weak agonists MPLA and DPLA.

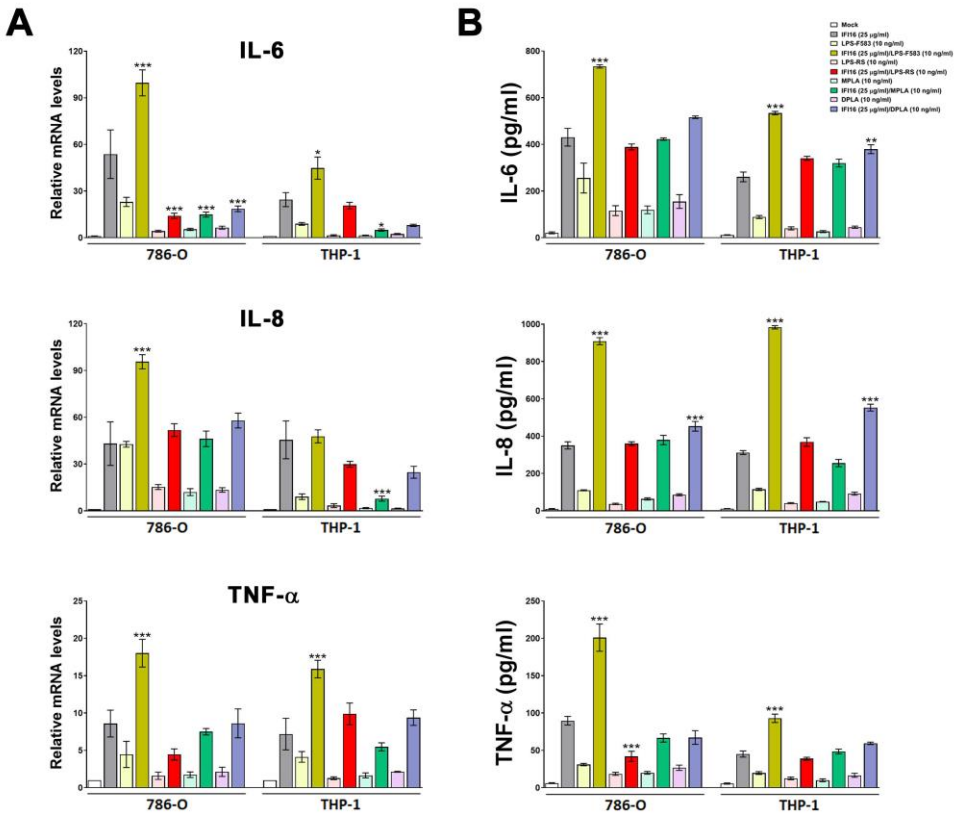

Fig 10. Weak TLR4-activating LPS variants and the TLR4 antagonist LPS-RS do not potentiate IFI16 proinflammatory activity. (A) qRT-PCR analysis of IL-6, IL-8 and TNF-α mRNA expression levels in 786-O or THP-1 cells stimulated for 24 h with or without IFI16 (25 μg/ml), LPS from *E. coli* F583 (LPS-F583, 10 ng/ml) or LPS from *R. sphaeroides* (LPS-RS, 10 ng/ml), MPLA (10 ng/ml), DPLA (10 ng/ml) or in the presence of one of the following complexes: IFI16/LPS-F583, IFI16/LPS-RS, IFI16/MPLA or IFI16/DPLA. Values are normalized to GAPDH mRNA and plotted as fold induction over mock-treated cells. qRT-PCR data are presented as mean values of biological triplicates. Error bars indicate SD, and the *P* values refer to comparisons between IFI16 *vs.* IFI16/LPS or IFI16/lipid A complex-treated cells (**P* < 0.05, ***P* < 0.01, ****P* < 0.001; two-way ANOVA followed by Dunnett's test). **(B)** Protein concentration of IL-6, IL-8 and TNF-α evaluated by ELISA in supernatants derived from 786-O or THP-1 cells stimulated for 24 h as described in the legend to panel **A**. Data are expressed as mean values ±SD of three independent experiments (**P* < 0.05, ***P* < 0.01, ****P* < 0.001; ns, not significant; two-way ANOVA followed by Dunnett's test). The *P* values are relative to comparisons between IFI16- and IFI16/LPS- or IFI16/lipid A-treated cells.

4.4. IFI16 exerts its proinflammatory activity in a TLR4/MyD88-dependent fashion

Since we had previously implicated TLR4 signaling in IFI16-mediated cytokine release in endothelial cells (Bawadekar et al., 2015b), we sought to determine whether ablation of the

TLR4/MD2 complex would affect IFI16/LPS proinflammatory activity. To this end, we performed gene silencing of TLR4 and MD2 genes in both 786-O and THP-1 cells, achieving complete knockdown of both genes, as judged by immunoblotting and flow cytometric analysis (data not shown). As shown in Fig 11, the transcriptional activation of IL-6, IL-8 and TNF-α genes (panels A and B) as well as the release of the same cytokines (Fig 12 A, B) in the culture supernatants upon exposure to both IFI16 or IFI16/LPS-EB was almost completely abolished in siTLR4- and siMD2-silenced cells when compared to siRNA control (siCTRL)-transfected cells. Similar results were obtained in both 786-O and THP-1 cells, indicating that IFI16 signaling through the TLR4-MD2 complex is not cell type-specific.

Upon LPS stimulation, TLR4 induces two independent signaling pathways regulated by either the TIRAP/MyD88 or TRAM/TRIF pair of adaptors, which promote the production of proinflammatory cytokines and type I interferons (IFN-I), respectively (Kagan, 2017; Takeda and Akira, 2004). As IFN-β could never be detected in IFI16- or IFI16/LPS-stimulated cells, we assumed that the TRAM-TRIF pathway would not play a role in our model. To address a potential role of the TIRAP-MyD88 complex, we performed siRNA-mediated knockdown of MyD88 in both 786-O and THP-1 cells (data not shown). In MyD88-silenced cells treated with IFI16 alone or IFI16/LPS-EB, transcription of IL-6, IL-8 and TNF-α genes (Fig 11C) and release of the corresponding cytokines (Fig 12C) were dramatically reduced in comparison with siCTRL-transfected cells, indicating that IFI16 or the IFI16/LPS complex signals through the TIRAP-MyD88 axis. Fittingly, ELISA-based transcription factor binding assay, performed using a probe containing the NF-κB binding site (Fig 12D), showed NF-κB binding activity to be significantly increased in cells challenged with IFI16 alone or pre-complexed with LPS-EB in comparison with untreated cells—*i.e.,* 2.2- and 3.9-fold induction in 786-O cells; 2.4- and 2.9-fold induction in THP-1 cells, respectively (Fig 12E). Overall, these results demonstrate that IFI16-mediated proinflammatory cytokine production requires the TLR4-MD2/TIRAP-MyD88 signaling pathway, which then promotes NF-κB nuclear binding activity to target DNA.

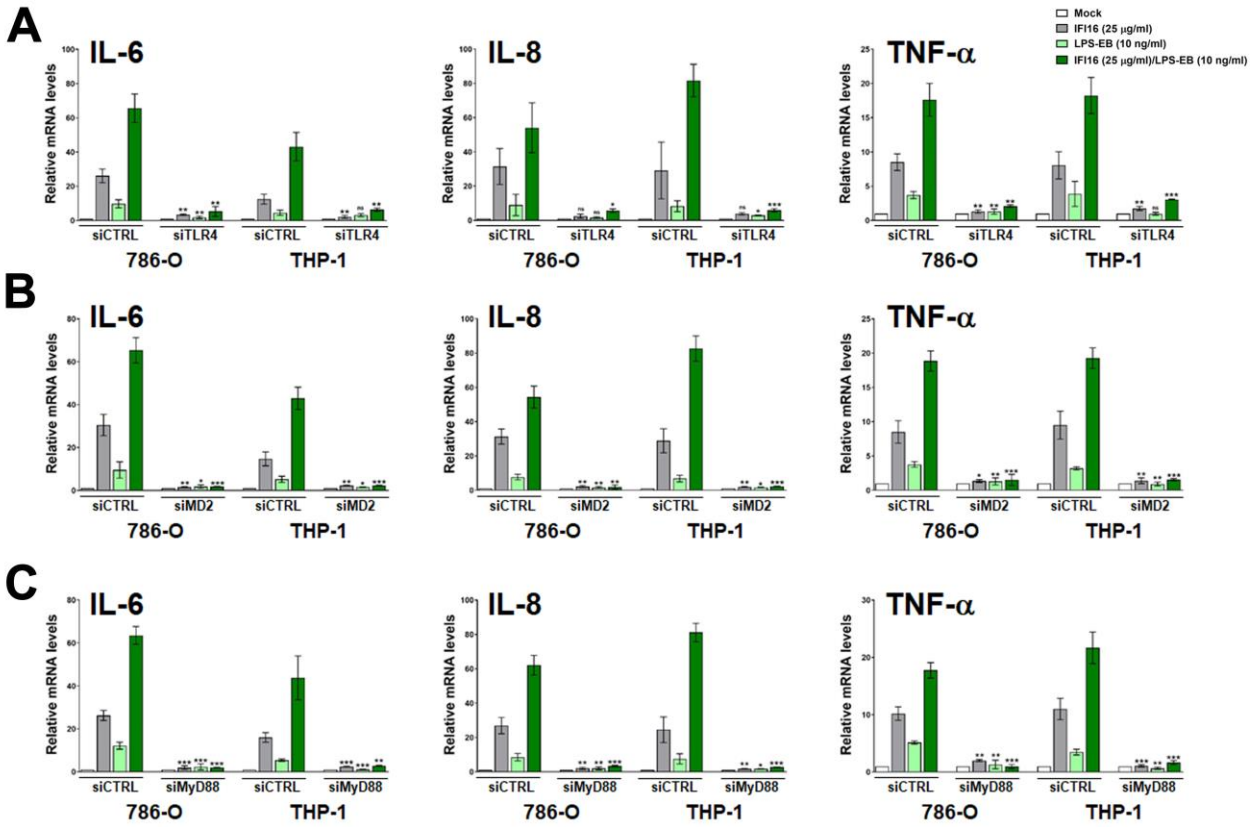

Fig 11. Quantitative RT-PCR analysis of proinflammatory cytokine expression in TLR4, MD2 and MyD88 knockdown cells. (A-C) qRT-PCR analysis of IL-6, IL-8 and TNF-α mRNA expression levels in 786-O or THP-1 cells transfected for 48 h with scramble control (siCTRL), or siRNAs against TLR4 (siTLR4) **(A)**, MD2 (siMD2) **(B)** or MyD88 (siMyD88) **(C)**. Cells were then stimulated for 24 h with IFI16 (25 µg/ml), LPS from *E. coli* O111:B4 (LPS-EB, 10 ng/ml) or IFI16/LPS-EB complex (preincubated O/N at 4°C), or left untreated (mock). Values were normalized to GAPDH mRNA and plotted as fold induction over mock-treated cells. qRT-PCR data are expressed as mean values of biological triplicates. Error bars indicate SD (*$P < 0.05$, **$P < 0.01$, ***$P < 0.001$, ns: not significant; unpaired Student's *t*-test for comparison of silenced cells *vs.* their relative control counterpart).

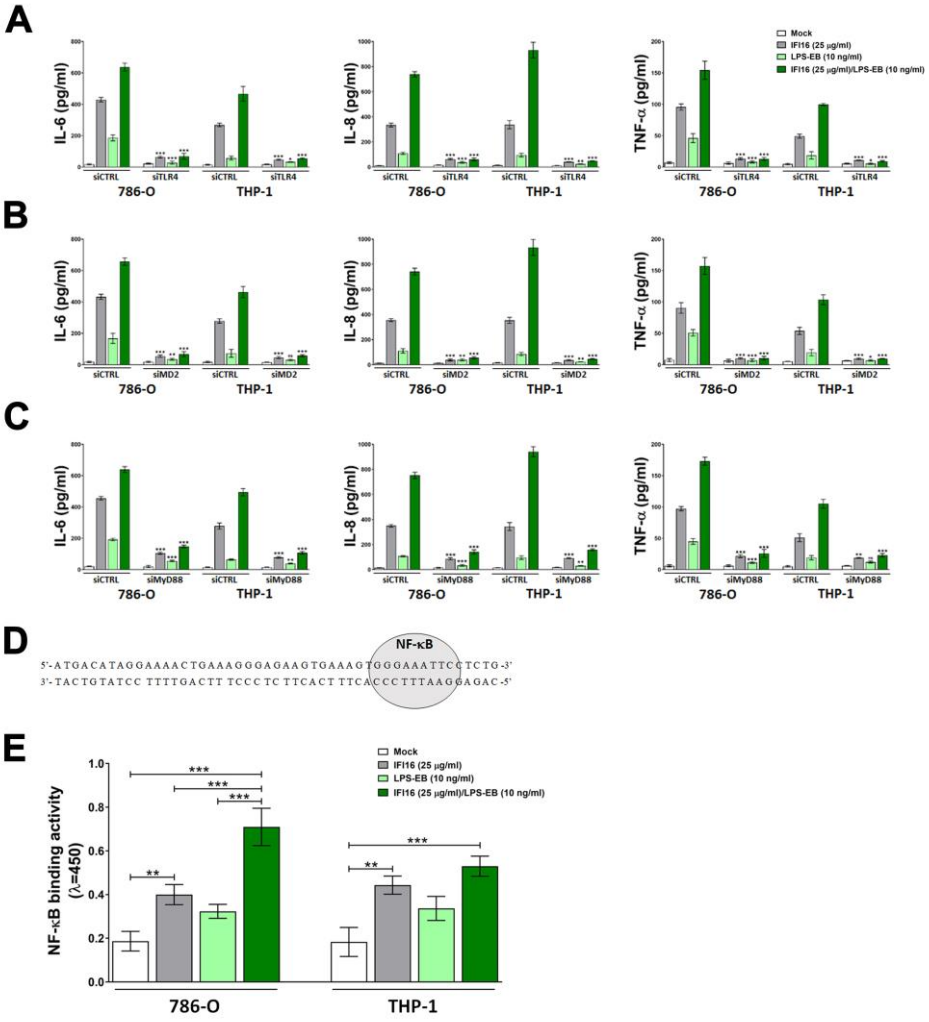

Fig 12. IFI16 exerts its proinflammatory activity in a TLR4/MyD88-dependent fashion. (A-C) Protein concentration of IL-6, IL-8 and TNF-α measured by ELISA in supernatants derived from 786-O or THP-1 cells transfected for 48 h with scramble control (siCTRL), or siRNAs against TLR4 (siTLR4, **A**), MD2 (siMD2, **B**) or MyD88 (siMyD88, **C**). Cells were then stimulated for 24 h with IFI16 (25 µg/ml), LPS from *E. coli* O111:B4 (LPS-EB, 10 ng/ml) or IFI16/LPS-EB complex (preincubated O/N at 4°C), or left untreated (mock). Data are expressed as mean values ± SD of three independent experiments (**P* < 0.05, ***P* < 0.01, ****P* < 0.001, ns: not significant; unpaired Student's *t*-test for comparison of silenced cells *vs.* their relative control counterpart). **(D)** Schematic representation of the probe containing the NF-κB binding site (highlighted in grey). **(E)** 786-O cells or THP-1 cells were stimulated with IFI16 (25 µg/ml), LPS from *E. coli* O111:B4 (LPS-EB, 10 ng/ml) or IFI16/LPS-EB complex (preincubated O/N at 4°C), or left untreated (mock). After 2 h, the cells were lysed and the nuclear fraction was analyzed for NF-κB binding activity using the Universal EZ-TFA transcription factor assay colorimetric kit and the probe described in **D**. Data are expressed as mean values ± SD of three independent experiments (**P* < 0.05, ***P* < 0.01, ****P* < 0.001; two-way ANOVA followed by Dunnett's test).

Finally, to circumvent potential issues of structural or functional differences between mammalian or bacterial expressed IFI16, we used wild-type and IFI16-knockout ($IFI16^{-/-}$) human osteosarcoma U2OS cells as a source of endogenous IFI16 released under stress stimuli. As shown in Fig 13A, and consistent with our previous report (Costa et al., 2011), UVB treatment (800 Jm^{-2} for 16h) led to massive release of IFI16 in the culture supernatants of U2OS cells that, as expected, did not occur in their $IFI16^{-/-}$ counterparts, thus serving as IFI16-depleted supernatant. The resulting conditioned media were preincubated with or without LPS-EB or LPS-RS and then added to THP-1 cells. After 24 h, the supernatants of the THP-1 cultures were harvested and assessed for cytokine expression by ELISA. Consistent with the results obtained with recombinant IFI16, exposure of THP-1 cells to conditioned medium from UVB-treated U2OS cells significantly stimulated the release of IL-6, IL-8 and TNF-α by THP-1 cells when compared to mock-treated cells—*i.e.,* 20.9-fold higher for IL-6; 83-fold for IL-8; and 33.4-fold for TNF-α (Fig 13B). When THP-1 cells were pre-treated with anti-TLR4 antibodies, the stimulatory activity of the conditioned medium form UVB-treated U2OS cells dropped significantly. Notably, cytokine release was significantly lower in THP-1 cells treated with conditioned medium from UVB-treated U2OS-$IFI16^{-/-}$ cells when compared to their UVB-treated normal counterparts—*i.e*., 2.8-fold lower for IL-6; 2.7-fold for IL-8; and 2.6-fold for TNF-α—, indicating that the effects observed were specifically due to the secretion of IFI16 protein. Consistent with the data obtained with the recombinant protein, cytokine release was enhanced when the conditioned media were preincubated with LPS-EB and, to a higher extent, with the conditioned medium of UVB-treated U2OS cells when compared to that of UVB-treated U2OS-$IFI16^{-/-}$ cells. As expected, this enhancement was not observed when LPS-RS was used.

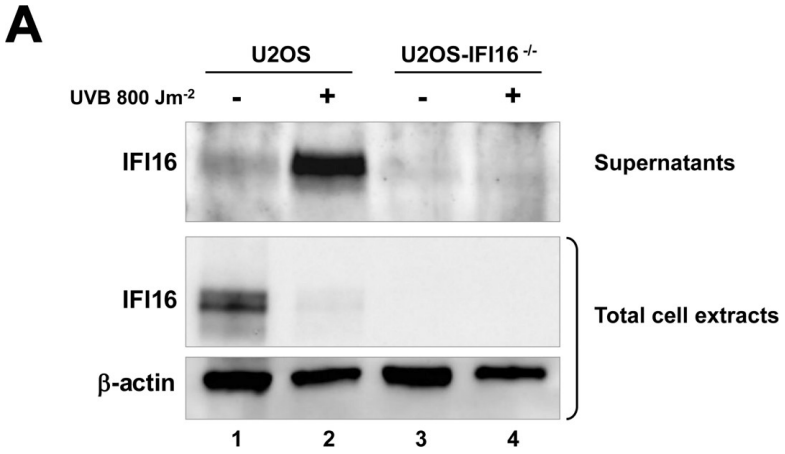
A
U2OS
U2OS-IFI16 -/-
UVB 800 Jm-2
-
+
-
+
IFI16
Supernatants
IFI16
β-actin
Total cell extracts
1
2
3
4

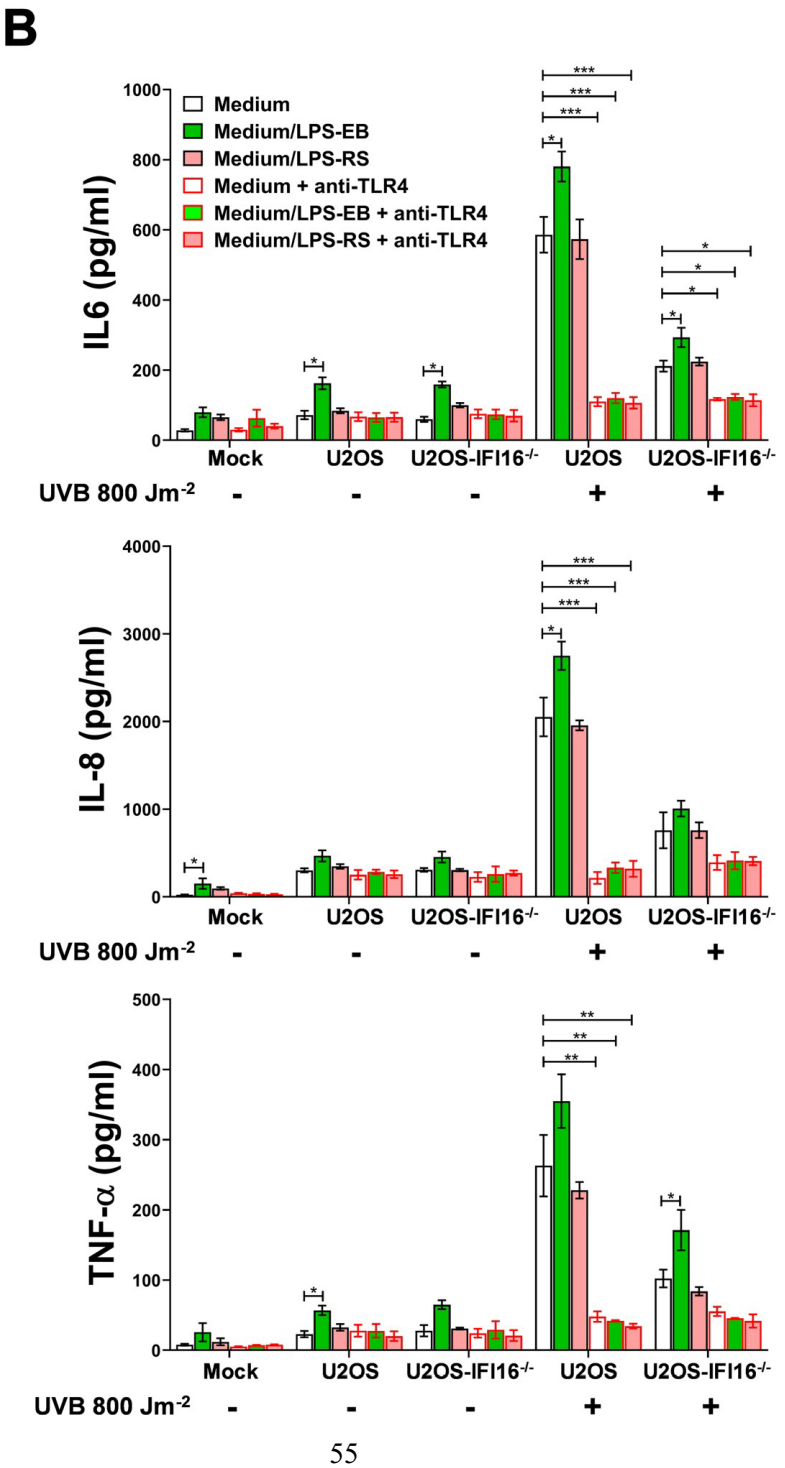
B
Medium
Medium/LPS-EB
Medium/LPS-RS
Medium + anti-TLR4
Medium/LPS-EB + anti-TLR4
Medium/LPS-RS + anti-TLR4
IL6 (pg/ml)
IL-8 (pg/ml)
TNF-α (pg/ml)
Mock
U2OS
U2OS-IFI16-/-
U2OS
U2OS-IFI16-/-
UVB 800 Jm-2

Fig 13. Endogenous IFI16 is released by UVB-exposed U2OS cells and triggers proinflammatory cytokines production in a TLR4-dependent fashion. (A) Western blot analysis of IFI16 in culture supernatants and total cell extracts of UVB-exposed (0 or 800 Jm^{-2}) U2OS or U2OS-IFI16$^{-/-}$ cells at 16 h after treatment. β-actin cellular expression was used for protein loading control. Data are representative of three independent experiments with similar results. **(B)** Protein concentration of IL-6, IL-8 and TNF-α evaluated by ELISA in supernatants derived from THP-1 cells stimulated for 24 h in the presence or absence of anti-TLR4 neutralizing antibodies (10 μg/ml) using conditioned medium from UVB-exposed (0 or 800 Jm^{-2}) U2OS and U2OS-IFI16$^{-/-}$ cells, or complete medium (mock), preincubated (O/N at 4°C), or not, with LPS from *E. coli* O111:B4 (LPS-EB, 10 ng/ml), or LPS from *R. sphaeroides* (LPS-RS, 10 ng/ml). Values were normalized to the initial protein concentration of the analyzed cytokines in the supernatants used for the treatment. Data are expressed as mean values ±SD of three independent experiments. The *P* values refer to comparison in each group with cells treated only with the medium without any addiction (white bar and black border; $*P < 0.05$, $**P < 0.01$, $***P < 0.001$; two-way ANOVA followed by Dunnett's test).

4.5. IFI16 binds to TLR4 *in vivo* and *in vitro*

We next sought to determine whether IFI16 could also bind to the TLR4/MD2 complex *in vivo*. To this end, co-immunoprecipitation assays were performed where TLR4 and interacting partners were immunoprecipitated using an anti-TLR4 antibody pre-adsorbed on protein G beads. The resulting immune complexes were then analyzed by SDS-PAGE followed by immunoblotting for TLR4, MD2, and IFI16. As shown in Fig 14A, IFI16 co-immunoprecipitated with TLR4/MD2 receptor when total extracts from cells treated with either IFI16 alone or IFI16/LPS-EB complex were used (lane 2 and 4, respectively). The specificity of this interaction was attested by the absence of co-immunoprecipitated IFI16 in extracts from cells untreated or treated with LPS-EB alone (lane 1 and 3, respectively). To ensure that residual DNA potentially present in the protein extracts would not affect Co-IPs, whole-cell extracts were treated with DNase and then subjected to Co-IP. As shown in Fig 14A (lane 5 and 6, respectively), the interaction between IFI16 or IFI16/LPS and TLR4 was maintained also in protein extracts

obtained from DNase-treated cells, indicating that the interaction between these molecules is not mediated by DNA binding.

The specificity of the interaction between IFI16 and TLR4 was then evaluated by surface plasmon resonance (SPR). Briefly, recombinant TLR4 was directly immobilized on a CM5 sensor chip by amine coupling and then probed with increasing concentration of recombinant IFI16—from 31.25 nM to 1 μM. As shown in Fig 14B, the resulting SPR sensorgrams revealed significant binding between TLR4 and IFI16 with an equilibrium dissociation constant (K_D) of 0.13 μM and a kinetic profile typical of dynamically interacting partners, with the dissociation rate being compatible with a rapid stimulation turnover of the ligand (*i.e.*, IFI16) on the TLR4 receptor. Thus, taken together these results indicate that the proinflammatory activity of IFI16, either alone or pre-complexed with LPS, is mediated by the TLR4/MD2/MyD88/NF-κB signaling pathways and requires a direct interaction between IFI16 and TLR4.

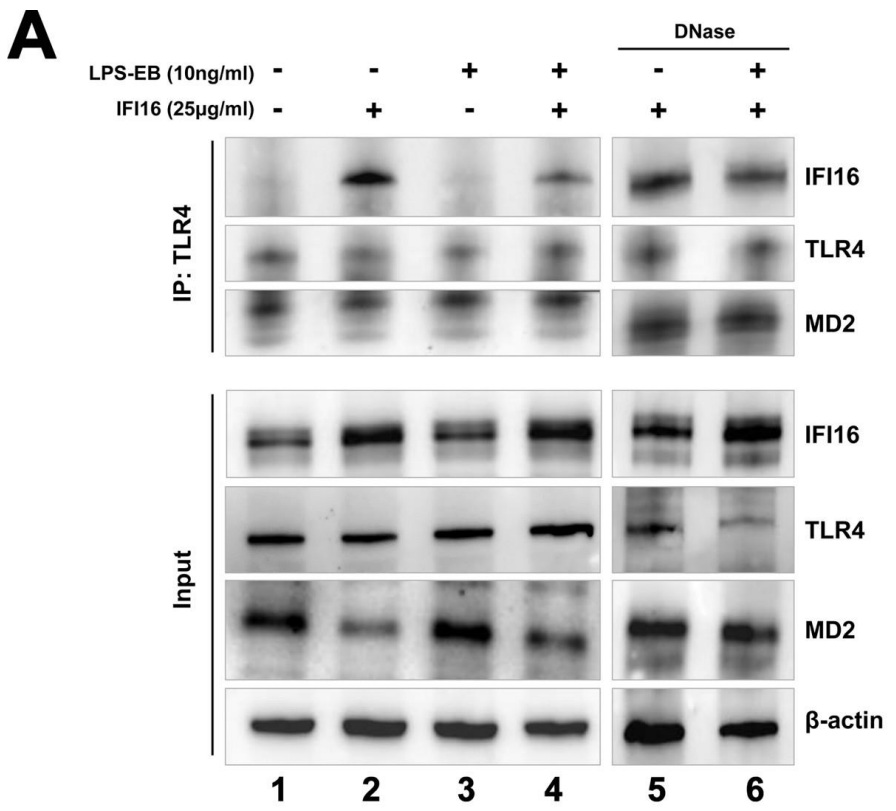

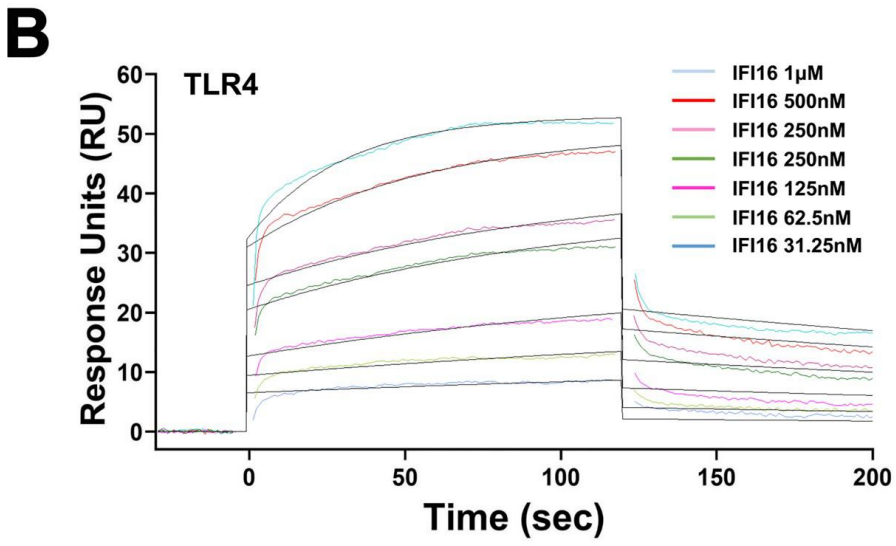

K_a (1/Ms)	K_d (1/s)	K_D (M)	Rmax (RU)	Chi^2 (RU)
$4.50*10^4$	$5.76*10^{-3}$	$1.28*10^{-7}$	25.35	1.83

Fig 14. IFI16 binds to TLR4 *in vitro* and *in vivo*. (A) 786-O cells were stimulated for 1 h in the presence or absence of the indicated concentrations of IFI16, LPS from *E. coli* O111:B4 (LPS-EB), or IFI16/LPS-EB complex. Total cell extracts, untreated or DNase I-treated, were subjected to immunoprecipitation using a TLR4 monoclonal antibody. Immunoprecipitates and whole-cell lysates were analyzed by immunoblotting with anti-IFI16, anti-TLR4 or anti-MD2 antibodies. β-actin protein expression was used for protein loading control. Data are representative of three independent experiments with similar results. **(B)** Surface plasmon resonance (SPR) analyses of IFI16 binding to immobilized TLR4. After immobilization of TLR4 on the CM5 sensor chip surface, increasing concentration of IFI16 (31.25-1000 nM) diluted

in running buffer were injected over immobilized TLR4. IFI16 binds to TLR4 with an equilibrium dissociation constant (K_D) of 0.13 μM. Data are representative of three independent experiments.

4.6. The IFI16/LPS complex proinflammatory activity is not affected by the presence of free LPS.

To gain more insights into the biological relevance of the IFI16/LPS complex *vs.* LPS, we sought to determine the proinflammatory activity of IFI16 or IFI16/LPS complex in the presence or absence of equal amounts of LPS simultaneously added to the cells. For this purpose, 786-O and THP-1 cells were stimulated with an array of different combinations as indicated in Fig 15. When IFI16 and LPS-EB were simultaneously added to the cells, without any pre-incubation step, induction of IL-6, IL-8 and TNF-α at both the mRNA and protein levels (Fig 15A and B, respectively) was comparable to that observed using LPS-EB alone, indicating that the affinity of IFI16 for the TLR4/MD2 receptor is lower than that of LPS. In contrast, when LPS-EB was simultaneously added to the cells together with the pre-formed IFI16/LPS-EB complex, induction of IL-6, IL-8 and TNF-α at both the mRNA and protein levels was comparable or even higher than that observed in cells stimulated with the IFI16/LPS-EB complex alone, suggesting that the affinity of the IFI16/LPS-EB complex for the TLR4 receptor is stronger than that of LPS-EB alone. Similar results were obtained when LPS-RS, a TLR4 antagonist, was used with the same combination treatment. Again, IFI16/LPS-RS complex activity, as measured by the induction of IL-6, IL-8 and TNF-α, was not affected by simultaneous addition of equal amounts of LPS-RS. Taken together, these findings clearly show that once IFI16 is complexed with LPS its proinflammatory activity is not affected by the simultaneous addition of LPS, regardless of its bacterial origin.

To better clarify the dynamics of interaction between IFI16/LPS-EB complex and TLR4/MD2 receptor, we performed further SPR analyses by means of a CM5 sensor chip coated with

recombinant TLR4/MD2. As shown in Table 3, the SPR-based studies demonstrated that the three receptor partners (*i.e.*, IFI16, LPS-EB and the IFI16/LPS-EB complex) had association rate (K_a) values in the same range, with IFI16/LPS-EB showing a 3- and 2-fold faster association compared to IFI16 or LPS-EB alone, respectively. Interestingly, in agreement with our previous findings, IFI16 interacted with the TLR4/MD2 complex in a concentration-dependent manner with a K_D of 0.68 μM, as calculated by the evaluation of the sensorgrams in Fig 15C. Moreover, LPS-EB alone revealed a much higher affinity, with a K_D of 0.15 nM. In contrast, IFI16/LPS-EB complex bound to TLR4/MD-2 with 6-fold lower affinity (K_D = 4.01 μM) when compared to IFI16 alone. The lower K_D displayed by LPS-EB was mainly due to the contribution of a lower dissociation rate constant ($K_d = 1.00*10^{-6}\ s^{-1}$), indicating that the kinetics of LPS-EB dissociation from the receptor is very slow. Interestingly, the sensorgrams demonstrated a much higher dissociation rate for both free IFI16 ($K_d = 6.14*10^{-3}\ s^{-1}$) and the IFI16/LPS-EB complex ($K_d = 1.43*10^{-2}\ s^{-1}$) in comparison with LPS-EB alone, indicating that bindings involving IFI16 are much less stable once formed. In agreement with the cytokine release, the aforementioned results indicate that, when added separately, LPS-EB binds to TLR4/MD2 more rapidly than IFI16 alone. In this setting, LPS-EB *per se* is able to trigger a weak inflammatory response highly likely due to its slow dissociation from the receptor, which in turn delays the optimal turnover of the receptor. In contrast, IFI16/LPS-EB complex binds to TLR4 more rapidly than LPS-EB simultaneously added to the cells, and it is released much more rapidly.

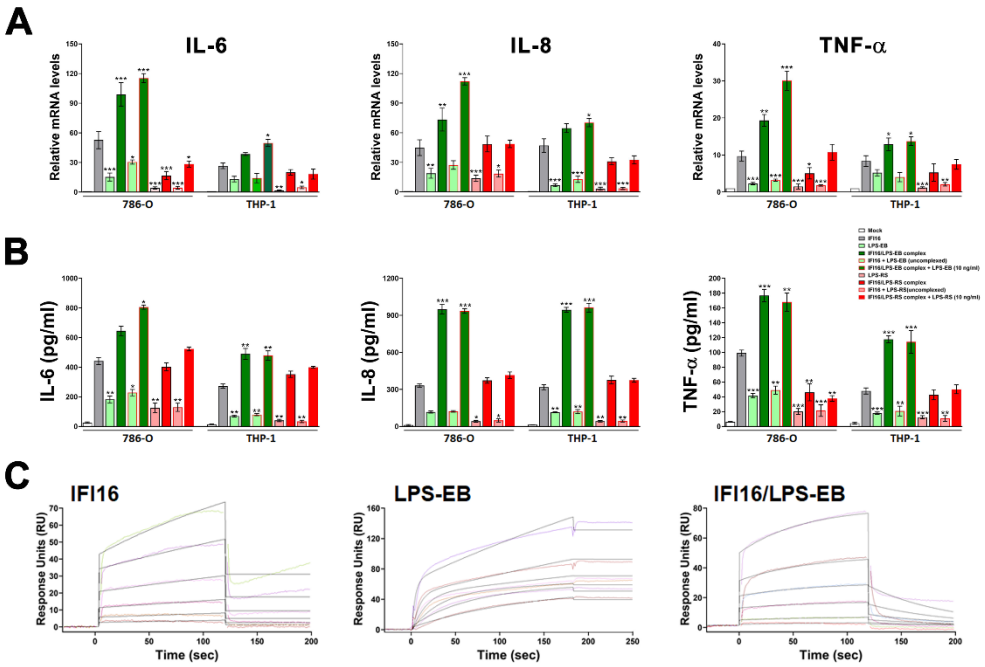

Fig 15. The IFI16/LPS complex proinflammatory activity is not affected by the presence of free LPS. (A) qRT-PCR analysis of IL-6, IL-8, TNF-α and mRNA expression levels in 786-O or THP-1 cells stimulated for 24 h with IFI16 (25 µg/ml), LPS from *E. coli* O111:B4 (LPS-EB, 10 ng/ml), IFI16/LPS-EB complex, IFI16 + LPS-EB (not complexed), IFI16/LPS-EB complex + LPS-EB (10 ng/ml), LPS from *Rhodobacter sphaeroides* (LPS-RS, 10 ng/ml), IFI16/LPS-RS complex, IFI16 + LPS-RS (not complexed), IFI16/LPS-RS complex + LPS-RS (10 ng/ml), or left untreated (mock). Values were normalized to GAPDH mRNA and plotted as fold induction over mock-treated cells. The *P* values refer to comparisons with IFI16-treated cells (**P* < 0.05, ***P* < 0.01, ****P* < 0.001; one-way ANOVA followed by Dunnett's test). **(B)** Protein concentration of IL-6, IL-8 and TNF-α was measured by ELISA in supernatants derived from 786-O or THP-1 cells stimulated for 24 h as described in **a**. Data are expressed as mean values ±SD of three independent experiments. The *P* values refer to comparisons with IFI16-treated cells (**P* < 0.05, ***P* < 0.01, ****P* < 0.001; one-way ANOVA followed by Dunnett's test). **(C)** Surface plasmon resonance (SPR) analyses of IFI16, LPS-EB and IFI16/LPS-EB complex binding to immobilized TLR4/MD2 receptor. After immobilization of recombinant TLR4/MD2 on the CM5 sensor chip surface, increasing concentration of the different analytes—31.25-1000 nM for IFI16, 3.125-100 µM for LPS-EB, 31.25-1000 nM for IFI16/LPS-EB complex—diluted in running buffer were injected over immobilized TLR4/MD2. IFI16, LPS-EB, and IFI16/LPS-EB bind to TLR4/MD2 with an equilibrium dissociation constant (K_D) of 0.68 µM, 0.15 nM, and 4.01 µM, respectively. Data are representative of three independent experiments.

Table 3. Binding kinetics of IFI16, LPS-EB and IFI16/LPS-EB to TLR4/MD2 receptor

	K_a (1/Ms)	K_d (1/s)	K_D (M)	Rmax (RU)	Chi^2 (RU)
IFI16	$9.07*10^3$	$6.14*10^{-3}$	$6.77*10^{-7}$	26.09	1.83
LPS-EB	$6.84*10^3$	$1.00*10^{-6}$	$1.47*10^{-10}$	745.00	14.30
IFI16/LPS-EB	$3.57*10^3$	$1.43*10^{-2}$	$4.01*10^{-6}$	90.30	6.89

K_a, association rate constant; M, molarity; s, seconds; K_d, dissociation rate constant; K_D, equilibrium dissociation constant; Rmax, maximum response; RU, response units; Chi^2, average squared residual.

4.7. The human IFI16 protein equally activates murine TLR4

Despite the huge number of murine HIN200 genes and pseudogenes, no data are currently available to demonstrate a clear counterpart for IFI16 in mice (Brunette et al., 2012; Deschamps et al., 2003). In order to establish a reliable *in vivo* model to test the IFI16 pro-inflammatory activity, and since human TLR4 and murine TLR4 display about 65% of homology (Hajjar et al., 2002), we aimed to determine whether human IFI16 could interact with murine TLR4. To this end, RAW 264.7 murine macrophages were treated with IFI16 and co-immunoprecipitation assays were performed immunoprecipitating TLR4 and interacting partners, as previously done. The resulting immune complexes were then analyzed by SDS-PAGE followed by immunoblotting for TLR4 and IFI16. As shown in Fig 16A, IFI16 co-immunoprecipitated with TLR4 receptor when total extracts from IFI16-treated cells were used. The specificity of this interaction was confirmed by the absence of co-immunoprecipitated IFI16 in extracts from untreated cells. As expected, there were no IFI16 bands in the input control of untreated cells, while IFI16 was clearly detectable in the input control of IFI16-treated cells. To further strengthen these results, RAW 264.7 cells were stimulated with full-length IFI16 and then total RNA was extracted to assess mRNA levels of IL-6 and IL-1β as read-out proinflammatory cytokines (Fig 16B). Interestingly, the results obtained were fully consistent with those found in

human cells. Indeed, IL-6 and IL-1β mRNA levels were strongly upregulated in cells treated with IFI16 when compared to mock-treated cells —*i.e.,* 359.7-fold higher for IL-6; 547.7-fold for IL-1β. Finally, to directly prove that the extracellular IFI16 released by human cells could lead to inflammatory activation in murine cells, we used the conditioned media from untreated or UVB-treated U2OS and U2OS-IFI16$^{-/-}$ cells as a source of endogenous IFI16 (Fig 13A). Consistent with the results obtained with recombinant IFI16, exposure of RAW 264.7 cells to conditioned medium from UVB-treated U2OS cells containing extracellular IFI16 caused a significant upregulation in the IL-6 and IL-1β mRNA levels when compared to untreated cells —*i.e.,* 124-fold higher for IL-6; 169.9-fold for IL-1β (Fig 16C).

Collectively, these results strongly suggest that IFI16 binds and activates also the murine TLR4/MD2 receptor, offering the opportunity of investigating the pro-inflammatory activity of IFI16 in mouse models.

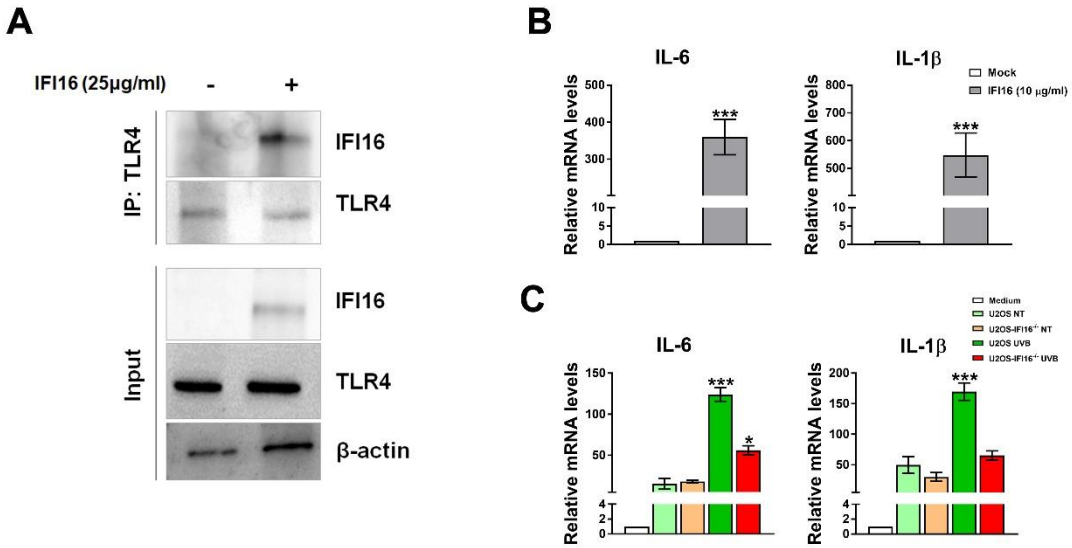

Fig 16. The human IFI16 protein equally activates murine TLR4. (A) RAW 264.7 cells were stimulated for 1 h in the presence or absence of the indicated concentration of IFI16. Total cell extracts were subjected to immunoprecipitation using a TLR4 monoclonal antibody. Immunoprecipitates and whole-cell lysates were analyzed by immunoblotting with anti-IFI16 or anti-TLR4 antibodies. β-actin protein expression was used for protein loading control. Data are representative of three independent experiments with similar results. **(B)** qRT-PCR analysis of IL-6 (left panel) and IL-

1β (right panel) mRNA expression levels in RAW264.7 mouse macrophages stimulated for 4 and 24 h with IFI16 (10 μg/ml) or left untreated (mock). Values are normalized to β-actin mRNA and plotted as fold of induction over mock-treated cells. qRT-PCR data are presented as mean values of biological triplicates. Error bars indicate SD (**P < 0.01, ***P < 0.001; unpaired t-test with Welch's correction). **(C)** qRT-PCR analysis of IL-6 and IL-β mRNA expression levels in RAW264.7 mouse macrophages stimulated for 24 h with conditioned medium from UVB-exposed (0 or 800 Jm^{-2}) U2OS and U2OS-IFI16$^{-/-}$ cells or with complete medium (mock). Values are normalized to β-actin mRNA and plotted as fold of induction over mock-treated cells. qRT-PCR data are shown as mean values of biological triplicates. Error bars indicate SD (*P < 0.05, **P < 0.01, ***P < 0.001; one-way ANOVA followed by Dunnett's test).

4.8. The PYRIN domain of IFI16 mediates TLR4 activation

Since previous work from our group demonstrated that the IFI16 N-terminal domain mediates its binding to the cell membrane of HUVEC (Gugliesi et al., 2013), we sought to determine whether IFI16 N-terminal domain inhibition could result in reduced levels of pro-inflammatory activity. To this end, RAW 264.7 cells were stimulated with different concentrations of full-length IFI16, alone or pre-incubated with increasing concentrations of rabbit polyclonal anti-IFI16 N-term antibodies, and then total RNA was extracted to assess mRNA levels of IL-6 and IL-1β. Consistent with our previous results, IL-6 and IL-1β mRNA levels were strongly upregulated in RAW 264.7 cells treated with all the concentrations of IFI16 tested. Interestingly, anti-IFI16 N-term antibodies significantly inhibited IFI16-mediated IL-6 and IL-1β upregulation in a concentration-dependent manner (Fig 17A). Accordingly, anti-IFI16 C-term antibodies did not have any effect on IFI16 proinflammatory activity (data not shown).

Next, to understand whether the inhibitory capability of anti-IFI16 N-term antibodies was associated with a reduced interaction between IFI16 and TLR4/MD2 receptor, SPR analyses were performed. As shown in Fig 17B, IFI16 bound to TLR4/MD2 receptor giving a response units (RUs) value of about 40. Interestingly, anti-IFI16 N-term antibodies significantly inhibited IFI16 binding to its receptor (about 75% of reduction when the highest concentration was used). In

contrast, anti-IFI16 C-term antibodies, even at the highest concentration, did not inhibit IFI16 binding to the receptor. Altogether, these data demonstrate that the IFI16 pro-inflammatory activity lies within its N-terminal portion.

These results prompted us to better characterize the pro-inflammatory activity of the N-terminal PYRIN domain of IFI16 (Chu et al., 2015; Jin et al., 2013). To this end, 786-O cells were stimulated with 25 μg/ml of full-length IFI16 or with equimolar concentrations of PYRIN, HINA and HINB domains (277 nM). As a control, IFI16ΔHINB and IFI16ΔPYRIN variants were used. Total RNA extracts prepared at 24h post-treatment were used to assess mRNA expression levels of IL-6, IL-8, and TNF-α genes. Consistent with the data previously obtained, IL-6, IL-8, and TNF-α mRNA were strongly upregulated when the full-length IFI16 or the IFI16ΔHINB variant were used (Fig 17C). By contrast, the IFI16 pro-inflammatory activity was strongly reduced when IFI16ΔPYRIN variant was added. Interestingly, out of the three IFI16 domains, only PYRIN domain still retained the ability to induce IL-6, IL-8, and TNF-α mRNA upregulation, although at a lower extent when compared to the full-length protein —*i.e.,* 23- fold higher for IL-6; 22-fold for IL-8, and 6-fold for TNF-α, respectively, compared to mock-treated cells (Fig 17C). Moreover, the same trend of pro-inflammatory activation was also confirmed when murine cells (*i.e.,* RAW 264.7) were used, suggesting that the mechanisms of activation are conserved across species (Fig 17D).

Taken together, these data strongly suggest that the IFI16 PYRIN domain is necessary and sufficient to induce a pro-inflammatory phenotype in target cells.

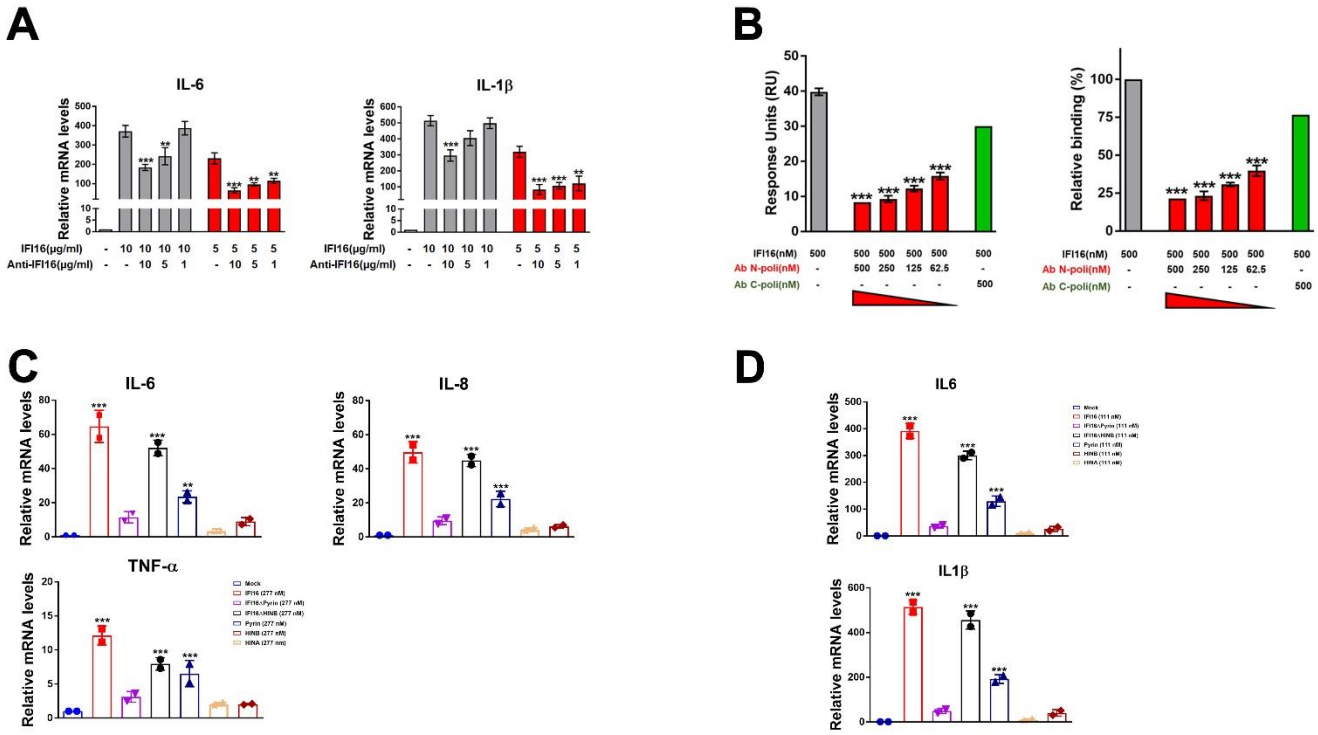

Fig 17. The PYRIN domain of IFI16 mediates TLR4 activation. (A) qRT-PCR analysis of IL-6 (left panel) and IL-1β (right panel) mRNA expression levels in RAW264.7 mouse macrophages stimulated for 24 h with IFI16 (10 μg/ml or 5 μg/ml) alone, or preincubated with the indicated concentrations of anti-IFI16 N-term antibodies, or left untreated (mock). Values are normalized to β-actin mRNA and plotted as fold of induction over mock-treated cells. qRT-PCR data are presented as mean values of biological triplicates. Error bars indicate SD (**P < 0.01, ***P < 0.001; one-way ANOVA followed by Dunnett's test). **(B)** Surface plasmon resonance (SPR) analyses of IFI16 binding to immobilized TLR4/MD2 receptor, in presence of anti-IFI16 N-term or C-term antibodies. After immobilization of recombinant TLR4/MD2 on the CM5 sensor chip surface, 500 nM of IFI16 alone or preincubated with different concentrations of anti-IFI16 N-term antibodies—500-62.5 nM— or C-term antibodies—500 nM— diluted in running buffer were injected over immobilized TLR4/MD2. The response units (left panel) and the relative binding inhibition compared to IFI16 alone (right panel) are shown. Data are representative of three independent experiments. **(C)** qRT-PCR analysis of IL-6, IL-8, and TNF-α mRNA expression levels in 786-O cells stimulated for 24 h with IFI16 (25 μg/ml, 277 nM), IFI16ΔHINB (277 nM), IFI16ΔPYRIN (277 nM), PYRIN (277 nM), HINA (277 nM), HINB (277 nM), or left untreated (mock). Values are normalized to GAPDH mRNA and plotted as fold induction over mock-treated cells. qRT-PCR data are presented as mean values of biological triplicates. Error bars indicate SD (***$P < 0.01$, ***$P < 0.001$ relative to mock-treated cells; one-way ANOVA followed by Dunnett's test). **(D)** qRT-PCR analysis of IL-6 and IL-1β mRNA expression levels in RAW264.7 mouse macrophages stimulated for 24 h with IFI16 (10 μg/ml, 111 nM), IFI16ΔHINB (111 nM),

IFI16ΔPYRIN (111 nM), PYRIN (111 nM), HINA (111 nM), HINB (111 nM), or left untreated (mock). Values are normalized to β-actin mRNA and plotted as fold of induction over mock-treated cells. qRT-PCR data are presented as mean values of biological triplicates. Error bars indicate SD (***P < 0.001 relative to mock-treated cells; one-way ANOVA followed by Dunnett's test).

5. Discussion

We previously reported that extracellular IFI16 promotes IL-6 and IL-8 production in endothelial cells, and that such proinflammatory activity is amplified in the presence of subtoxic concentrations of LPS-EB, a full activator of the TLR4 signaling pathway (Bawadekar et al., 2015b). Here, we expand on those observations by showing that, in renal and monocytic cell lines, IFI16 either alone or in complex with LPS binds to TLR4, thereby triggering a proinflammatory response through the TLR4/MD2/MyD88 signaling pathway. Specifically, by means of *in vitro* pull-down assays and saturation binding experiments, we provide the first evidence that the HINB domain of IFI16 mediates complex formation with LPS-EB or LPS-F583, two *E. coli*-derived variants of LPS capable of acting as strong TLR4 agonists (Bryant et al., 2010; Gao et al., 2006). This interaction follows a prototypical associative binding, with increasing rate of binding up to the plateau phase following addition of increasing amounts of the analytes. Furthermore, this binding is not dependent on the polysaccharide outer chain length as both LPS-EB and LPS-F583 display similar binding affinity for IFI16—the LPS-F583 variant is in fact characterized by the presence of a shorter polysaccharide chain compared to that of LPS-EB (Plevin et al., 2016). In addition, we show that both LPS-PG, a weak TLR4 agonist (Darveau et al., 2004), and LPS-RS, a TLR4 antagonist (Anwar et al., 2015)—these molecules display fewer acyl chains in their lipid A moieties compared to LPS-EB—, bind to IFI16 with similar affinities, albeit slightly lower than those of LPS-EB and LPS-F583. Finally, using the *E. coli* F583-derived DPLA and MPLA *lipid A variants* (Plevin et al., 2016; Stoddard et al., 2010), we demonstrate that lipid A is the LPS moiety interacting with IFI16-HINB, affording the highest affinity for LPS. Accordingly, the detoxified variant of LPS-EB, containing a lipid A moiety partially delipidated by alkaline hydrolysis, binds weakly to IFI16. The observation that the HINB domain of IFI16 has a much higher affinity for lipid A than that of the HINA domain, despite both molecules being highly similar in terms of primary sequence and overall structure topology, is only partially unexpected. Indeed, these two IFI16 domains have already been shown to have distinct modes of binding to

another paradigmatic PAMP—*i.e.*, viral DNA—most likely due to their different folding structures (Ni et al., 2016; Unterholzner et al., 2010).

In recent years, mounting evidence has shown how TLRs, besides sensing exogenous microbial components, are also capable of recognizing endogenous material released during cellular injury, thereby promoting a non-microbial-induced inflammatory state known as sterile inflammation, which if not resolved can lead to severe acute and chronic inflammatory conditions (Piccinini and Midwood, 2010; Rifkin et al., 2005; Schaefer, 2014). Here, we propose that IFI16 might represent a novel trigger of sterile inflammation acting through the TLR4 signaling pathway. In particular, we show that exposure to recombinant IFI16 can induce IL-6, IL-8 and TNF-α transcriptional activation and release of these cytokines into the culture supernatants. This induction is strictly dependent on the presence of the TLR4/MD2 receptor complex and the MyD88 adaptor. By contrast, the membrane-associated CD14 receptor seems to be only marginally involved in this signaling pathway given that undifferentiated THP-1 cells, displaying low levels of CD14 expression, and 786-O cells, expressing high levels of CD14, show similar cytokine induction patterns upon IFI16 exposure. The fact that IFI16 broadly activates inflammation through TLR4 signaling pathways strengthens the notion that extracellular IFI16 acts as a DAMP capable of promoting inflammation. Fittingly, aberrant IFI16 expression—*i.e.*, overexpression of IFI16 in otherwise negative cells or IFI16 delocalization to the cytoplasm—has been reported in a number of inflammatory conditions, such as SLE (skin, Costa et al., 2011), psoriasis (skin, Cao et al., 2016; Chiliveru et al., 2014; Tervaniemi et al., 2016), SSc (skin, Mondini et al., 2006), IBD (colonic epithelium, Caneparo et al., 2016; Vanhove et al., 2015) and SS (salivary epithelial and inflammatory infiltrating cells, Alunno et al., 2015, 2016; Antiochos et al., 2018). Additionally, aberrant IFI16 expression has been reported in virus-infected cells (Cigno et al., 2015; Dell'Oste et al., 2014; Singh et al., 2013) or cells treated with IFN-γ (Caposio et al., 2007). Importantly, in some of these and other pathological conditions, we and others have shown that IFI16 exists in a free, extracellular form in the blood or extracellular milieu (Alunno et al., 2015, 2016;

Antiochos et al., 2018; Gugliesi et al., 2013). Particularly, we found that high levels of circulating IFI16 (≥ 27 ng/ml) were associated to overall worse clinical parameters in three cohorts of RA, SS and PsA patients. Notably, among RA patients, circulating IFI16 was more frequently found in subjects with rheumatoid factor (RF)/anti-CCP-positive serum and significantly associated with pulmonary involvement (Alunno et al., 2016). Furthermore, in SS patients, circulating IFI16 is associated with increased prevalence of both RF and glandular infiltration degree (Alunno et al., 2015), while in PsA patients is associated with elevated C-reactive protein (CRP) levels (De Andrea et al., 2020). The release of extracellular IFI16 has also been shown by our group in a model of keratinocytes exposed to UVB radiation (Costa et al., 2011). Although the biological rationale of these findings is far from being completely understood, these observations clearly indicate that the IFI16 protein, whose expression in the natural setting is restricted to the nuclei of a limited number of cell types, such as keratinocytes, fibroblasts, endothelial and hematopoietic cells (Gariglio et al., 2002), can be released by a broad spectrum of injured cells, including damaged epithelial cells or the inflammatory cells recruited at the site of injury, which are known to massively express IFI16. In this setting, as mentioned above, extracellular IFI16 can act as a DAMP in promoting sterile inflammation (Gong et al., 2020). Accordingly, the exposure of THP-1 cells to conditioned medium from UVB-treated cells containing the IFI16 protein was able to significantly enhanced IL-6, IL-8 and TNF-α release when compared to the conditioned medium from UVB-treated IFI16 knockout cells. Addition of LPS-EB but not that of the weak TLR4-agonist LPS variant further enhanced cytokine induction, while pre-treatment of THP-1 cells with anti-TLR4 antibodies almost abolished the cytokine release. Thus, it is tempting to speculate that, similarly to pathogen-induced inflammation, binding of extracellularly-released IFI16 to TLR4 can activate both non-immune and innate immune cells, thus leading to the production of various cytokines and chemokines responsible for the recruitment of additional inflammatory cells (Chen and Nuñez, 2010). Interestingly, IFI16 pro-inflammatory activity lies within its PYRIN domain, which is necessary and sufficient to induce overexpression of pro-inflammatory cytokines. Since there are more than 20 PYRIN-containing proteins in the human

genome (Kwon et al., 2012), most of which shares several residues in their PYRIN domains (Jin et al., 2013), this result could pave the way toward the identification of a new class of DAMPs, which once extracellularly released by damaged cells can trigger sterile inflammation through the engagement of the TLR4/MD2 receptor.

In agreement with the emerging concept that DAMPs often potentiate their activity by binding to PAMPs, we demonstrate that the IFI16 proinflammatory activity is significantly enhanced when the protein is pre-incubated with subtoxic concentration of LPS and then added to the cells as pre-formed complex. Consistently, this effect is not observed when a truncated variant of IFI16 lacking the LPS-binding domain is used. Despite the fact that IFI16 binds with similar affinity to different variants of LPS, we could only achieve a significant increase in proinflammatory cytokine release with the strong TLR4 agonists LPS-EB and LPS-F583. Of note, these LPS molecules when added alone to the cells, even at high doses, were only able to induce marginally the transcriptional activation of such cytokines. Interestingly, the LPS-F583-derived lipid A DPLA and MPLA, carrying respectively a di- and a monophosphorylated glucosamine dimer, both lacking the sugar inner core, display a remarkably different ability to enhance IFI16 activity. Although both molecules show the highest affinity for IFI16 *in vitro*, only DPLA partially retains the ability to potentiate IFI16 downstream signaling. Fittingly, IFI16 binding to *Rhodobacter sphaeroides*-derived LPS, which is known to antagonize the response to strong TLR4 activators in human and mouse monocytes (Anwar et al., 2015), did not affect IFI16 proinflammatory activity. Interestingly, competition binding experiments in 786-O and THP-1 cells suggest that the affinity for TLR4 of either LPS-EB or LPS-RS is higher than that of IFI16. Indeed, when the cells are exposed to IFI16 and LPS-EB that were not pre-complexed, the release of proinflammatory cytokines in the culture supernatants is far lower than that of cells exposed to pre-complexed IFI16/LPS-EB or IFI16 alone. Accordingly, the binding kinetics revealed by SPR analysis clearly indicated that LPS-EB has a much higher affinity for TLR4 and a very slow kinetics of dissociation when compared to the IFI16 protein alone. Conversely, the

IFI16/LPS-EB complex retains a higher affinity for TLR4 and is not displaced upon co-treatment with LPS-EB, as attested by the release of cytokines at levels similar to those observed in the supernatants of cells exposed to the complex alone. Likewise, IFI16/LPS-RS complex activity is not affected by the simultaneous addition of an equal amount of LPS-RS. In good agreement with the immunoprecipitation and competition assays, binding kinetics analysis by SPR reveals that LPS-EB, regardless of its overall higher affinity for TLR4/MD2, cannot compete with the IFI16/LPS-EB complex for binding to the receptor. Indeed, the IFI16/LPS-EB complex appears to be continuously engaged for TLR4 activation, as indicated by its faster association and dissociation rates. Thus, these data strongly suggest that *in vivo* i) the proinflammatory activity of IFI16 is enhanced upon its interaction with small amounts of circulating LPS, and ii) the IFI16/LPS-EB complex has a rapid stimulation turnover on the receptor, successfully competing with LPS-EB alone and leading to a massive inflammatory response (Fig 18).

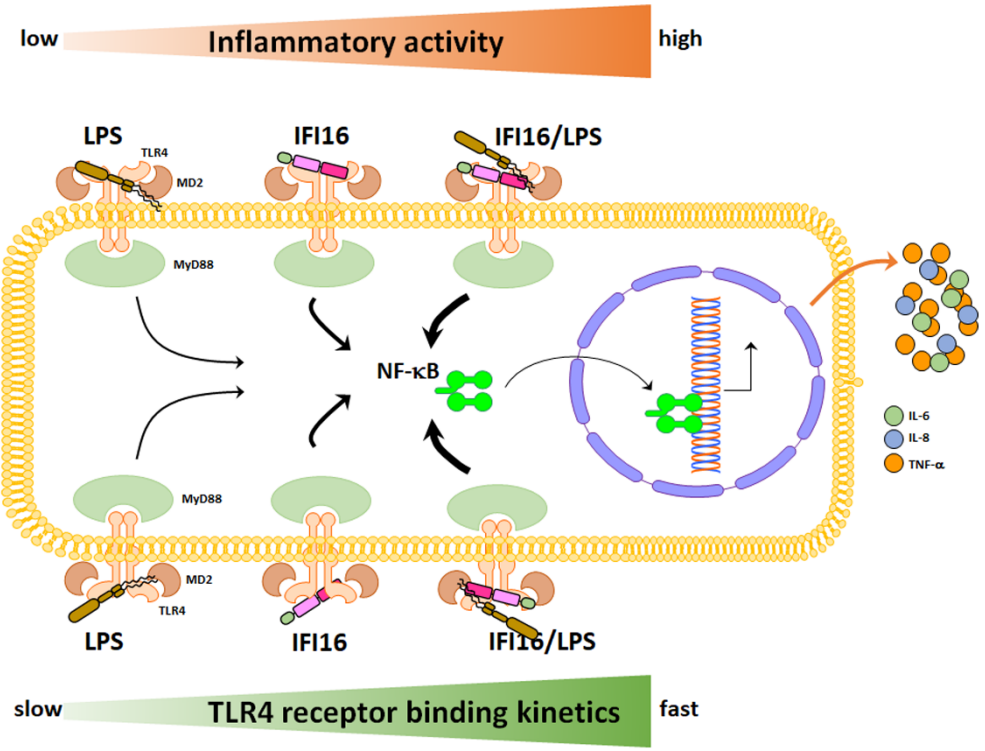

Fig 18. Proposed model depicting the inflammatory activities and binding kinetics to TLR4 of LPS and IFI16, alone or in combination. The relative inflammatory activities, from low to high, are reported in the upper part of the

scheme (orange arrow). The relative binding kinetics to TLR4 are reported in the lower part of the scheme (green arrow). The thickness of the black arrows is directly proportional to the ability of the pathway to induce NF-κB activation.

6. Conclusions and future perspectives

Overall, our findings unveil a central role of extracellular IFI16 in triggering inflammation through its ability to bind the TLR4/MD2 complex, thereby triggering TLR4/MyD88/NF-κB signaling. Given that IFI16 is able to form stable complexes with various LPS variants through interaction of its HINB domain with the lipid A moiety of LPS, we propose a new pathogenic mechanism regulated by extremely fine-tuned interactions between extracellular IFI16 and subtoxic doses of LPS, which are known to be present in various pathological settings other than gram-negative infections (Manco et al., 2010; Seki and Schnabl, 2012; Stoll et al., 2006).

Our observation that the IFI16 PYRIN domain is responsible for binding to the TLR4/MD2 receptor deserves a more comprehensive analysis of how these molecular entities are involved in this interaction. In addition, the molecular dynamic of the IFI16-LPS complex and the ensuing increased in TLR4 activation will be also further investigated. In the long term, we will identify novel therapeutic agents (*e.g.,* small molecules, small peptides, antibodies) that inhibit the IFI16-mediated inflammation and in turn dampen the chronic stimulation of the immune system during autoimmune/autoinflammatory diseases.

7. Bibliography

Aglipay, J.A., Lee, S.W., Okada, S., Fujiuchi, N., Ohtsuka, T., Kwak, J.C., Wang, Y., Johnstone, R.W., Deng, C., Qin, J., et al. (2003). A member of the Pyrin family, IFI16, is a novel BRCA1-associated protein involved in the p53-mediated apoptosis pathway. Oncogene *22*, 8931–8938.

Akashi, S., Shimazu, R., Ogata, H., Nagai, Y., Takeda, K., Kimoto, M., and Miyake, K. (2000). Cutting edge: cell surface expression and lipopolysaccharide signaling via the toll-like receptor 4-MD-2 complex on mouse peritoneal macrophages. J Immunol *164*, 3471–3475.

Albertini, S., Cigno, I.L., Calati, F., Andrea, M.D., Borgogna, C., Dell'Oste, V., Landolfo, S., and Gariglio, M. (2018). HPV18 Persistence Impairs Basal and DNA Ligand–Mediated IFN-β and IFN-λ1 Production through Transcriptional Repression of Multiple Downstream Effectors of Pattern Recognition Receptor Signaling. The Journal of Immunology *200*, 2076–2089.

Albrecht, M., Choubey, D., and Lengauer, T. (2005). The HIN domain of IFI-200 proteins consists of two OB folds. Biochemical and Biophysical Research Communications *327*, 679–687.

Alexander, C., and Rietschel, E.Th. (2001). Bacterial lipopolysaccharides and innate immunity. Journal of Endotoxin Research *7*, 167–202.

Almine, J.F., O'Hare, C.A.J., Dunphy, G., Haga, I.R., Naik, R.J., Atrih, A., Connolly, D.J., Taylor, J., Kelsall, I.R., Bowie, A.G., et al. (2017). IFI16 and cGAS cooperate in the activation of STING during DNA sensing in human keratinocytes. Nat Commun *8*, 14392.

Alunno, A., Caneparo, V., Carubbi, F., Bistoni, O., Caterbi, S., Bartoloni, E., Giacomelli, R., Gariglio, M., Landolfo, S., and Gerli, R. (2015). Interferon gamma-inducible protein 16 in primary Sjögren's syndrome: a novel player in disease pathogenesis? Arthritis Res Ther *17*, 208.

Alunno, A., Caneparo, V., Bistoni, O., Caterbi, S., Terenzi, R., Gariglio, M., Bartoloni, E., Manzo, A., Landolfo, S., and Gerli, R. (2016). Circulating Interferon-Inducible Protein IFI16 Correlates With Clinical and Serological Features in Rheumatoid Arthritis: IFI16 and Clinical/Serological Features in RA. Arthritis Care & Research *68*, 440–445.

Andersson, A., Covacu, R., Sunnemark, D., Danilov, A.I., Dal Bianco, A., Khademi, M., Wallström, E., Lobell, A., Brundin, L., Lassmann, H., et al. (2008). Pivotal advance: HMGB1 expression in active lesions of human and experimental multiple sclerosis. J Leukoc Biol *84*, 1248–1255.

Ansari, M.A., Singh, V.V., Dutta, S., Veettil, M.V., Dutta, D., Chikoti, L., Lu, J., Everly, D., and Chandran, B. (2013). Constitutive Interferon-Inducible Protein 16-Inflammasome Activation during Epstein-Barr Virus Latency I, II, and III in B and Epithelial Cells. Journal of Virology *87*, 8606–8623.

Antiochos, B., Matyszewski, M., Sohn, J., Casciola-Rosen, L., and Rosen, A. (2018). IFI16 filament formation in salivary epithelial cells shapes the anti-IFI16 immune response in Sjögren's syndrome. JCI Insight *3*, e120179.

Anwar, M.A., Panneerselvam, S., Shah, M., and Choi, S. (2015). Insights into the species-specific TLR4 signaling mechanism in response to *Rhodobacter sphaeroides* lipid A detection. Scientific Reports *5*, 7657.

Asefa, B. (2004). The interferon-inducible p200 family of proteins: a perspective on their roles in cell cycle regulation and differentiation. Blood Cells, Molecules, and Diseases *32*, 155–167.

Azzimonti, B., Pagano, M., Mondini, M., De Andrea, M., Valente, G., Monga, G., Tommasino, M., Aluffi, P., Landolfo, S., and Gariglio, M. (2004). Altered patterns of the interferon-inducible gene IFI16 expression

in head and neck squamous cell carcinoma: immunohistochemical study including correlation with retinoblastoma protein, human papillomavirus infection and proliferation index. Histopathology *45*, 560–572.

Baer, A.N., Petri, M., Sohn, J., Rosen, A., and Casciola-Rosen, L. (2016). Association of Antibodies to Interferon-Inducible Protein-16 With Markers of More Severe Disease in Primary Sjögren's Syndrome. Arthritis Care & Research *68*, 254–260.

Baillet, A., Trocmé, C., Berthier, S., Arlotto, M., Grange, L., Chenau, J., Quétant, S., Sève, M., Berger, F., Juvin, R., et al. (2010). Synovial fluid proteomic fingerprint: S100A8, S100A9 and S100A12 proteins discriminate rheumatoid arthritis from other inflammatory joint diseases. Rheumatology (Oxford) *49*, 671–682.

Barrat, F.J., Crow, M.K., and Ivashkiv, L.B. (2019). Interferon target-gene expression and epigenomic signatures in health and disease. Nat Immunol *20*, 1574–1583.

Bawadekar, M., De Andrea, M., Gariglio, M., and Landolfo, S. (2015a). Mislocalization of the interferon inducible protein IFI16 by environmental insults: implications in autoimmunity. Cytokine Growth Factor Rev. *26*, 213–219.

Bawadekar, M., De Andrea, M., Lo Cigno, I., Baldanzi, G., Caneparo, V., Graziani, A., Landolfo, S., and Gariglio, M. (2015b). The Extracellular IFI16 Protein Propagates Inflammation in Endothelial Cells Via p38 MAPK and NF-κB p65 Activation. J. Interferon Cytokine Res. *35*, 441–453.

Bhattacharyya, S., Wang, W., Morales-Nebreda, L., Feng, G., Wu, M., Zhou, X., Lafyatis, R., Lee, J., Hinchcliff, M., Feghali-Bostwick, C., et al. (2016). Tenascin-C drives persistence of organ fibrosis. Nature Communications *7*, 11703.

Bhattacharyya, S., Wang, W., Qin, W., Cheng, K., Coulup, S., Chavez, S., Jiang, S., Raparia, K., De Almeida, L.M.V., Stehlik, C., et al. (2018). TLR4-dependent fibroblast activation drives persistent organ fibrosis in skin and lung. JCI Insight *3*.

Borden, E.C., Sen, G.C., Uze, G., Silverman, R.H., Ransohoff, R.M., Foster, G.R., and Stark, G.R. (2007). Interferons at age 50: past, current and future impact on biomedicine. Nat Rev Drug Discov *6*, 975–990.

Bours, M.J.L., Swennen, E.L.R., Di Virgilio, F., Cronstein, B.N., and Dagnelie, P.C. (2006). Adenosine 5'-triphosphate and adenosine as endogenous signaling molecules in immunity and inflammation. Pharmacol Ther *112*, 358–404.

Brennan, T.V., Lin, L., Huang, X., Cardona, D.M., Li, Z., Dredge, K., Chao, N.J., and Yang, Y. (2012). Heparan sulfate, an endogenous TLR4 agonist, promotes acute GVHD after allogeneic stem cell transplantation. Blood *120*, 2899–2908.

Broz, P., and Dixit, V.M. (2016). Inflammasomes: mechanism of assembly, regulation and signalling. Nature Reviews Immunology *16*, 407–420.

Brunette, R.L., Young, J.M., Whitley, D.G., Brodsky, I.E., Malik, H.S., and Stetson, D.B. (2012). Extensive evolutionary and functional diversity among mammalian AIM2-like receptors. Journal of Experimental Medicine *209*, 1969–1983.

Bryant, C.E., Spring, D.R., Gangloff, M., and Gay, N.J. (2010). The molecular basis of the host response to lipopolysaccharide. Nat. Rev. Microbiol. *8*, 8–14.

Caneparo, V., Cena, T., De Andrea, M., Dell'oste, V., Stratta, P., Quaglia, M., Tincani, A., Andreoli, L., Ceffa, S., Taraborelli, M., et al. (2013). Anti-IFI16 antibodies and their relation to disease characteristics in systemic lupus erythematosus. Lupus *22*, 607–613.

Caneparo, V., Pastorelli, L., Pisani, L.F., Bruni, B., Prodam, F., Boldorini, R., Roggenbuck, D., Vecchi, M., Landolfo, S., Gariglio, M., et al. (2016). Distinct Anti-IFI16 and Anti-GP2 Antibodies in Inflammatory Bowel Disease and Their Variation with Infliximab Therapy: Inflammatory Bowel Diseases *22*, 2977–2987.

Caneparo, V., Landolfo, S., Gariglio, M., and De Andrea, M. (2018). The Absent in Melanoma 2-Like Receptor IFN-Inducible Protein 16 as an Inflammasome Regulator in Systemic Lupus Erythematosus: The Dark Side of Sensing Microbes. Front. Immunol. *9*.

Cao, T., Shao, S., Li, B., Jin, L., Lei, J., Qiao, H., and Wang, G. (2016). Up-regulation of Interferon-inducible protein 16 contributes to psoriasis by modulating chemokine production in keratinocytes. Sci Rep *6*, 25381.

Caposio, P., Gugliesi, F., Zannetti, C., Sponza, S., Mondini, M., Medico, E., Hiscott, J., Young, H.A., Gribaudo, G., Gariglio, M., et al. (2007). A Novel Role of the Interferon-inducible Protein IFI16 as Inducer of Proinflammatory Molecules in Endothelial Cells. J. Biol. Chem. *282*, 33515–33529.

Casella, C.R., and Mitchell, T.C. (2013). Inefficient TLR4/MD-2 heterotetramerization by monophosphoryl lipid A. PLoS ONE *8*, e62622.

Chan, Y.K., and Gack, M.U. (2016). Viral evasion of intracellular DNA and RNA sensing. Nat Rev Microbiol *14*, 360–373.

Chen, G.Y., and Nuñez, G. (2010). Sterile inflammation: sensing and reacting to damage. Nature Reviews Immunology *10*, 826–837.

Chiliveru, S., Rahbek, S.H., Jensen, S.K., Jørgensen, S.E., Nissen, S.K., Christiansen, S.H., Mogensen, T.H., Jakobsen, M.R., Iversen, L., Johansen, C., et al. (2014). Inflammatory Cytokines Break Down Intrinsic Immunological Tolerance of Human Primary Keratinocytes to Cytosolic DNA. J.I. *192*, 2395–2404.

Chu, L.H., Gangopadhyay, A., Dorfleutner, A., and Stehlik, C. (2015). An updated view on the structure and function of PYRIN domains. Apoptosis *20*, 157–173.

Cigno, I.L., Andrea, M.D., Borgogna, C., Albertini, S., Landini, M.M., Peretti, A., Johnson, K.E., Chandran, B., Landolfo, S., and Gariglio, M. (2015). The Nuclear DNA Sensor IFI16 Acts as a Restriction Factor for Human Papillomavirus Replication through Epigenetic Modifications of the Viral Promoters. Journal of Virology *89*, 7506–7520.

Costa, S., Borgogna, C., Mondini, M., De Andrea, M., Meroni, P.L., Berti, E., Gariglio, M., and Landolfo, S. (2011). Redistribution of the nuclear protein IFI16 into the cytoplasm of ultraviolet B-exposed keratinocytes as a mechanism of autoantigen processing. Br. J. Dermatol. *164*, 282–290.

Cridland, J.A., Curley, E.Z., Wykes, M.N., Schroder, K., Sweet, M.J., Roberts, T.L., Ragan, M.A., Kassahn, K.S., and Stacey, K.J. (2012). The mammalian PYHIN gene family: Phylogeny, evolution and expression. BMC Evol Biol *12*, 140.

Darveau, R.P., Pham, T.-T.T., Lemley, K., Reife, R.A., Bainbridge, B.W., Coats, S.R., Howald, W.N., Way, S.S., and Hajjar, A.M. (2004). Porphyromonas gingivalis lipopolysaccharide contains multiple lipid A species that functionally interact with both toll-like receptors 2 and 4. Infect Immun *72*, 5041–5051.

Dawson, M.J., Elwood, N.J., Johnstone, R.W., and Trapani, J.A. (1998). The IFN-inducible nucleoprotein IFI 16 is expressed in cells of the monocyte lineage, but is rapidly and markedly down-regulated in other myeloid precursor populations. J Leukoc Biol *64*, 546–554.

De Andrea, M., De Santis, M., Caneparo, V., Generali, E., Sirotti, S., Isailovic, N., Guidelli, G.M., Ceribelli, A., Fabbroni, M., Simpatico, A., et al. (2020). Serum IFI16 and anti-IFI16 antibodies in psoriatic arthritis. Clin Exp Immunol *199*, 88–96.

Dell'Oste, V., Gatti, D., Gugliesi, F., De Andrea, M., Bawadekar, M., Lo Cigno, I., Biolatti, M., Vallino, M., Marschall, M., Gariglio, M., et al. (2014). Innate Nuclear Sensor IFI16 Translocates into the Cytoplasm during the Early Stage of In Vitro Human Cytomegalovirus Infection and Is Entrapped in the Egressing Virions during the Late Stage. Journal of Virology *88*, 6970–6982.

Deng, M., Tang, Y., Li, W., Wang, X., Zhang, R., Zhang, X., Zhao, X., Liu, J., Tang, C., Liu, Z., et al. (2018). The Endotoxin Delivery Protein HMGB1 Mediates Caspase-11-Dependent Lethality in Sepsis. Immunity *49*, 740-753.e7.

Deschamps, S., Meyer, J., Chatterjee, G., Wang, H., Lengyel, P., and Roe, B.A. (2003). The mouse Ifi200 gene cluster: genomic sequence, analysis, and comparison with the human HIN-200 gene cluster☆. Genomics *82*, 34–46.

Dunzendorfer, S., Lee, H.-K., Soldau, K., and Tobias, P.S. (2004). TLR4 is the signaling but not the lipopolysaccharide uptake receptor. J Immunol *173*, 1166–1170.

Frey, E.A., Miller, D.S., Jahr, T.G., Sundan, A., Bažil, V., Espevik, T., Finlay, B.B., and Wright, S.D. (1992). Soluble cd14 participates in the response of cells to lipopolysaccharide. Journal of Experimental Medicine *176*, 1665–1671.

Frey, H., Schroeder, N., Manon-Jensen, T., Iozzo, R.V., and Schaefer, L. (2013). Biological interplay between proteoglycans and their innate immune receptors in inflammation. FEBS J *280*, 2165–2179.

Fujiuchi, N., Aglipay, J.A., Ohtsuka, T., Maehara, N., Sahin, F., Su, G.H., Lee, S.W., and Ouchi, T. (2004). Requirement of IFI16 for the maximal activation of p53 induced by ionizing radiation. J Biol Chem *279*, 20339–20344.

Gao, B., Wang, Y., and Tsan, M.-F. (2006). The heat sensitivity of cytokine-inducing effect of lipopolysaccharide. Journal of Leukocyte Biology *80*, 359–366.

Garcia, M.M., Goicoechea, C., Molina-Álvarez, M., and Pascual, D. (2020). Toll-like receptor 4: A promising crossroads in the diagnosis and treatment of several pathologies. European Journal of Pharmacology *874*, 172975.

Gariano, G.R., Dell'Oste, V., Bronzini, M., Gatti, D., Luganini, A., De Andrea, M., Gribaudo, G., Gariglio, M., and Landolfo, S. (2012). The Intracellular DNA Sensor IFI16 Gene Acts as Restriction Factor for Human Cytomegalovirus Replication. PLoS Pathog *8*, e1002498.

Gariglio, M., Azzimonti, B., Pagano, M., Palestro, G., De Andrea, M., Valente, G., Voglino, G., Navino, L., and Landolfo, S. (2002). Immunohistochemical expression analysis of the human interferon-inducible gene IFI16, a member of the HIN200 family, not restricted to hematopoietic cells. J Interferon Cytokine Res *22*, 815–821.

Gioannini, T.L., Teghanemt, A., Zhang, D., Coussens, N.P., Dockstader, W., Ramaswamy, S., and Weiss, J.P. (2004). Isolation of an endotoxin-MD-2 complex that produces Toll-like receptor 4-dependent cell activation at picomolar concentrations. Proc Natl Acad Sci U S A *101*, 4186–4191.

Goldstein, R.S., Bruchfeld, A., Yang, L., Qureshi, A.R., Gallowitsch-Puerta, M., Patel, N.B., Huston, B.J., Chavan, S., Rosas-Ballina, M., Gregersen, P.K., et al. (2007). Cholinergic Anti-Inflammatory Pathway Activity and High Mobility Group Box-1 (HMGB1) Serum Levels in Patients with Rheumatoid Arthritis. Mol Med *13*, 210–215.

Gondokaryono, S.P., Ushio, H., Niyonsaba, F., Hara, M., Takenaka, H., Jayawardana, S.T.M., Ikeda, S., Okumura, K., and Ogawa, H. (2007). The extra domain A of fibronectin stimulates murine mast cells via toll-like receptor 4. J Leukoc Biol *82*, 657–665.

Gong, T., Liu, L., Jiang, W., and Zhou, R. (2020). DAMP-sensing receptors in sterile inflammation and inflammatory diseases. Nat. Rev. Immunol. *20*, 95–112.

Gray, E.E., Winship, D., Snyder, J.M., Child, S.J., Geballe, A.P., and Stetson, D.B. (2016). The AIM2-like Receptors Are Dispensable for the Interferon Response to Intracellular DNA. Immunity *45*, 255–266.

Gugliesi, F., Mondini, M., Ravera, R., Robotti, A., de Andrea, M., Gribaudo, G., Gariglio, M., and Landolfo, S. (2005). Up-regulation of the interferon-inducible IFI16 gene by oxidative stress triggers p53 transcriptional activity in endothelial cells. J Leukoc Biol *77*, 820–829.

Gugliesi, F., Bawadekar, M., De Andrea, M., Dell'Oste, V., Caneparo, V., Tincani, A., Gariglio, M., and Landolfo, S. (2013). Nuclear DNA sensor IFI16 as circulating protein in autoimmune diseases is a signal of damage that impairs endothelial cells through high-affinity membrane binding. PLoS ONE *8*, e63045.

Hagar, J.A., Powell, D.A., Aachoui, Y., Ernst, R.K., and Miao, E.A. (2013). Cytoplasmic LPS Activates Caspase-11: Implications in TLR4-Independent Endotoxic Shock. Science *341*, 1250–1253.

Hajjar, A.M., Ernst, R.K., Tsai, J.H., Wilson, C.B., and Miller, S.I. (2002). Human Toll-like receptor 4 recognizes host-specific LPS modifications. Nat Immunol *3*, 354–359.

He, M., Bianchi, M.E., Coleman, T.R., Tracey, K.J., and Al-Abed, Y. (2018). Exploring the biological functional mechanism of the HMGB1/TLR4/MD-2 complex by surface plasmon resonance. Molecular Medicine *24*, 21.

d'Hennezel, E., Abubucker, S., Murphy, L.O., and Cullen, T.W. (2017). Total Lipopolysaccharide from the Human Gut Microbiome Silences Toll-Like Receptor Signaling. MSystems *2*.

Horng, T., Barton, G.M., and Medzhitov, R. (2001). TIRAP: An adapter molecule in the Toll signaling pathway. Nature Immunology *2*, 835–841.

Hulme, E.C., and Trevethick, M.A. (2010). Ligand binding assays at equilibrium: validation and interpretation. British Journal of Pharmacology *161*, 1219–1237.

Iqbal, J., Ansari, M.A., Kumar, B., Dutta, D., Roy, A., Chikoti, L., Pisano, G., Dutta, S., Vahedi, S., Veettil, M.V., et al. (2016). Histone H2B-IFI16 Recognition of Nuclear Herpesviral Genome Induces Cytoplasmic Interferon-β Responses. PLoS Pathog *12*, e1005967.

Ivashkiv, L.B. (2018). IFNγ: signalling, epigenetics and roles in immunity, metabolism, disease and cancer immunotherapy. Nat Rev Immunol *18*, 545–558.

Ivashkiv, L.B., and Donlin, L.T. (2014). Regulation of type I interferon responses. Nat Rev Immunol *14*, 36–49.

Jiang, J., Zhao, M., Chang, C., Wu, H., and Lu, Q. (2020). Type I Interferons in the Pathogenesis and Treatment of Autoimmune Diseases. Clinic Rev Allerg Immunol *59*, 248–272.

Jin, T., Perry, A., Smith, P., Jiang, J., and Xiao, T.S. (2013). Structure of the absent in melanoma 2 (AIM2) pyrin domain provides insights into the mechanisms of AIM2 autoinhibition and inflammasome assembly. J. Biol. Chem. *288*, 13225–13235.

Johnson, K.E., Bottero, V., Flaherty, S., Dutta, S., Singh, V.V., and Chandran, B. (2014). IFI16 Restricts HSV-1 Replication by Accumulating on the HSV-1 Genome, Repressing HSV-1 Gene Expression, and Directly or Indirectly Modulating Histone Modifications. PLoS Pathog *10*, e1004503.

Johnstone, R.W., Kershaw, M.H., and Trapani, J.A. (1998). Isotypic variants of the interferon-inducible transcriptional repressor IFI 16 arise through differential mRNA splicing. Biochemistry *37*, 11924–11931.

Jorgensen, I., Rayamajhi, M., and Miao, E.A. (2017). Programmed cell death as a defence against infection. Nature Reviews Immunology *17*, 151–164.

Kagan, J.C. (2017). Lipopolysaccharide Detection across the Kingdoms of Life. Trends Immunol. *38*, 696–704.

Kagan, J.C., Magupalli, V.G., and Wu, H. (2014). SMOCs: supramolecular organizing centres that control innate immunity. Nature Reviews Immunology *14*, 821–826.

Kawahara, K., Tsukano, H., Watanabe, H., Lindner, B., and Matsuura, M. (2002). Modification of the Structure and Activity of Lipid A in Yersinia pestis Lipopolysaccharide by Growth Temperature. Infect Immun *70*, 4092–4098.

Kawai, T., and Akira, S. (2009). The roles of TLRs, RLRs and NLRs in pathogen recognition. Int Immunol *21*, 317–337.

Kayagaki, N., Warming, S., Lamkanfi, M., Vande Walle, L., Louie, S., Dong, J., Newton, K., Qu, Y., Liu, J., Heldens, S., et al. (2011). Non-canonical inflammasome activation targets caspase-11. Nature *479*, 117–121.

Kayagaki, N., Wong, M.T., Stowe, I.B., Ramani, S.R., Gonzalez, L.C., Akashi-Takamura, S., Miyake, K., Zhang, J., Lee, W.P., Muszyński, A., et al. (2013). Noncanonical Inflammasome Activation by Intracellular LPS Independent of TLR4. Science *341*, 1246–1249.

Kayagaki, N., Stowe, I.B., Lee, B.L., O'Rourke, K., Anderson, K., Warming, S., Cuellar, T., Haley, B., Roose-Girma, M., Phung, Q.T., et al. (2015). Caspase-11 cleaves gasdermin D for non-canonical inflammasome signalling. Nature *526*, 666–671.

Kerur, N., Veettil, M.V., Sharma-Walia, N., Bottero, V., Sadagopan, S., Otageri, P., and Chandran, B. (2011). IFI16 Acts as a Nuclear Pathogen Sensor to Induce the Inflammasome in Response to Kaposi Sarcoma-Associated Herpesvirus Infection. Cell Host & Microbe *9*, 363–375.

Kieser, K.J., and Kagan, J.C. (2017). Multi-receptor detection of individual bacterial products by the innate immune system. Nat Rev Immunol *17*, 376–390.

Kim, E.-J., Park, J.-I., and Nelkin, B.D. (2005). IFI16 is an essential mediator of growth inhibition, but not differentiation, induced by the leukemia inhibitory factor/JAK/STAT pathway in medullary thyroid carcinoma cells. J Biol Chem *280*, 4913–4920.

Kono, H., Chen, C.-J., Ontiveros, F., and Rock, K.L. (2010). Uric acid promotes an acute inflammatory response to sterile cell death in mice. J Clin Invest *120*, 1939–1949.

Kwon, D., Yoon, J.H., Shin, S.-Y., Jang, T.-H., Kim, H.-G., So, I., Jeon, J.-H., and Park, H.H. (2012). A comprehensive manually curated protein–protein interaction database for the Death Domain superfamily. Nucleic Acids Res *40*, D331–D336.

Land, W. (2003). Allograft injury mediated by reactive oxygen species: from conserved proteins of Drosophila to acute and chronic rejection of human transplants. Part III: interaction of (oxidative) stress-induced heat shock proteins with toll-like receptor-bearing cells of innate immunity and its consequences for the development of acute and chronic allograft rejection. Transplantation Reviews *17*, 67–86.

Landolfo, S., Gariglio, M., Gribaudo, G., and Lembo, D. (1998). The Ifi 200 genes: An emerging family of IFN-inducible genes. Biochimie *80*, 721–728.

Lee, J.D., Kravchenko, V., Kirkland, T.N., Han, J., Mackman, N., Moriarty, A., Leturcq, D., Tobias, P.S., and Ulevitch, R.J. (1993). Glycosyl-phosphatidylinositol-anchored or integral membrane forms of CD14 mediate identical cellular responses to endotoxin. Proc Natl Acad Sci U S A *90*, 9930–9934.

Li, T., Diner, B.A., Chen, J., and Cristea, I.M. (2012). Acetylation modulates cellular distribution and DNA sensing ability of interferon-inducible protein IFI16. PNAS *109*, 10558–10563.

Li, T., Chen, J., and Cristea, I.M. (2013). Human Cytomegalovirus Tegument Protein pUL83 Inhibits IFI16-Mediated DNA Sensing for Immune Evasion. Cell Host & Microbe *14*, 591–599.

Liao, J.C.C., Lam, R., Brazda, V., Duan, S., Ravichandran, M., Ma, J., Xiao, T., Tempel, W., Zuo, X., Wang, Y.-X., et al. (2011). Interferon-Inducible Protein 16: Insight into the Interaction with Tumor Suppressor p53. Structure *19*, 418–429.

Ludlow, L.E.A., Johnstone, R.W., and Clarke, C.J.P. (2005). The HIN-200 family: More than interferon-inducible genes? Experimental Cell Research *308*, 1–17.

MacMicking, J.D. (2012). Interferon-inducible effector mechanisms in cell-autonomous immunity. Nat Rev Immunol *12*, 367–382.

Malara, A., Gruppi, C., Abbonante, V., Cattaneo, D., De Marco, L., Massa, M., Iurlo, A., Gianelli, U., Balduini, C.L., Tira, M.E., et al. (2019). EDA fibronectin-TLR4 axis sustains megakaryocyte expansion and inflammation in bone marrow fibrosis. J Exp Med *216*, 587–604.

Managò, A., Audrito, V., Mazzola, F., Sorci, L., Gaudino, F., Gizzi, K., Vitale, N., Incarnato, D., Minazzato, G., Ianniello, A., et al. (2019). Extracellular nicotinate phosphoribosyltransferase binds Toll like receptor 4 and mediates inflammation. Nature Communications *10*, 4116.

Manco, M., Putignani, L., and Bottazzo, G.F. (2010). Gut Microbiota, Lipopolysaccharides, and Innate Immunity in the Pathogenesis of Obesity and Cardiovascular Risk. Endocr Rev *31*, 817–844.

Matzinger, P. (1994). Tolerance, danger, and the extended family. Annu Rev Immunol *12*, 991–1045.

Midwood, K., Sacre, S., Piccinini, A.M., Inglis, J., Trebaul, A., Chan, E., Drexler, S., Sofat, N., Kashiwagi, M., Orend, G., et al. (2009). Tenascin-C is an endogenous activator of Toll-like receptor 4 that is essential for maintaining inflammation in arthritic joint disease. Nat Med *15*, 774–780.

Miller, S.I., Ernst, R.K., and Bader, M.W. (2005). LPS, TLR4 and infectious disease diversity. Nature Reviews Microbiology *3*, 36–46.

Mondini, M., Vidali, M., De Andrea, M., Azzimonti, B., Airò, P., D'Ambrosio, R., Riboldi, P., Meroni, P.L., Albano, E., Shoenfeld, Y., et al. (2006). A novel autoantigen to differentiate limited cutaneous systemic sclerosis from diffuse cutaneous systemic sclerosis: the interferon-inducible gene IFI16. Arthritis Rheum. *54*, 3939–3944.

Mondini, M., Vidali, M., Airò, P., De Andrea, M., Riboldi, P., Meroni, P.L., Gariglio, M., and Landolfo, S. (2007). Role of the interferon-inducible gene IFI16 in the etiopathogenesis of systemic autoimmune disorders. Ann N Y Acad Sci *1110*, 47–56.

Monroe, K.M., Yang, Z., Johnson, J.R., Geng, X., Doitsh, G., Krogan, N.J., and Greene, W.C. (2014). IFI16 DNA Sensor Is Required for Death of Lymphoid CD4 T Cells Abortively Infected with HIV. Science *343*, 428–432.

Nagai, Y., Akashi, S., Nagafuku, M., Ogata, M., Iwakura, Y., Akira, S., Kitamura, T., Kosugi, A., Kimoto, M., and Miyake, K. (2002). Essential role of MD-2 in LPS responsiveness and TLR4 distribution. Nat Immunol *3*, 667–672.

Ni, X., Ru, H., Ma, F., Zhao, L., Shaw, N., Feng, Y., Ding, W., Gong, W., Wang, Q., Ouyang, S., et al. (2016). New insights into the structural basis of DNA recognition by HINa and HINb domains of IFI16. J Mol Cell Biol *8*, 51–61.

Orvain, C., Lin, Y.-L., Jean-Louis, F., Hocini, H., Hersant, B., Bennasser, Y., Ortonne, N., Hotz, C., Wolkenstein, P., Boniotto, M., et al. (2020). Hair follicle stem cell replication stress drives IFI16/STING-dependent inflammation in hidradenitis suppurativa. J. Clin. Invest. *130*, 3777–3790.

Orzalli, M.H., DeLuca, N.A., and Knipe, D.M. (2012). Nuclear IFI16 induction of IRF-3 signaling during herpesviral infection and degradation of IFI16 by the viral ICP0 protein. Proceedings of the National Academy of Sciences *109*, E3008–E3017.

Orzalli, M.H., Conwell, S.E., Berrios, C., DeCaprio, J.A., and Knipe, D.M. (2013). Nuclear interferon-inducible protein 16 promotes silencing of herpesviral and transfected DNA. Proceedings of the National Academy of Sciences *110*, E4492–E4501.

Paciello, I., Silipo, A., Lembo-Fazio, L., Curcurù, L., Zumsteg, A., Noël, G., Ciancarella, V., Sturiale, L., Molinaro, A., and Bernardini, M.L. (2013). Intracellular Shigella remodels its LPS to dampen the innate immune recognition and evade inflammasome activation. PNAS *110*, E4345–E4354.

Pandolfi, F., Altamura, S., Frosali, S., and Conti, P. (2016). Key Role of DAMP in Inflammation, Cancer, and Tissue Repair. Clinical Therapeutics *38*, 1017–1028.

Park, B.S., Song, D.H., Kim, H.M., Choi, B.-S., Lee, H., and Lee, J.-O. (2009). The structural basis of lipopolysaccharide recognition by the TLR4–MD-2 complex. Nature *458*, 1191–1195.

Petes, C., Mintsopoulos, V., Finnen, R.L., Banfield, B.W., and Gee, K. (2018). The effects of CD14 and IL-27 on induction of endotoxin tolerance in human monocytes and macrophages. J. Biol. Chem. *293*, 17631–17645.

Piccinini, A.M., and Midwood, K.S. (2010). DAMPening Inflammation by Modulating TLR Signalling (Hindawi).

Plevin, R.E., Knoll, M., McKay, M., Arbabi, S., and Cuschieri, J. (2016). The Role of Lipopolysaccharide Structure in Monocyte Activation and Cytokine Secretion. Shock *45*, 22–27.

Quintana, F.J., and Cohen, I.R. (2005). Heat shock proteins as endogenous adjuvants in sterile and septic inflammation. J Immunol *175*, 2777–2782.

Raffaella, R., Gioia, D., De Andrea, M., Cappello, P., Giovarelli, M., Marconi, P., Manservigi, R., Gariglio, M., and Landolfo, S. (2004). The interferon-inducible IFI16 gene inhibits tube morphogenesis and proliferation of primary, but not HPV16 E6/E7-immortalized human endothelial cells. Experimental Cell Research *293*, 331–345.

Rifkin, I.R., Leadbetter, E.A., Busconi, L., Viglianti, G., and Marshak-Rothstein, A. (2005). Toll-like receptors, endogenous ligands, and systemic autoimmune disease. Immunol. Rev. *204*, 27–42.

Roh, J.S., and Sohn, D.H. (2018). Damage-Associated Molecular Patterns in Inflammatory Diseases. Immune Netw *18*.

Romerio, A., and Peri, F. (2020). Increasing the Chemical Variety of Small-Molecule-Based TLR4 Modulators: An Overview. Front Immunol *11*, 1210.

Roy, A., Ghosh, A., Kumar, B., and Chandran, B. (2019). IFI16, a nuclear innate immune DNA sensor, mediates epigenetic silencing of herpesvirus genomes by its association with H3K9 methyltransferases SUV39H1 and GLP. ELife *8*, e49500.

Rühl, S., and Broz, P. (2015). Caspase-11 activates a canonical NLRP3 inflammasome by promoting K(+) efflux. Eur J Immunol *45*, 2927–2936.

Ryu, J.-K., Kim, S.J., Rah, S.-H., Kang, J.I., Jung, H.E., Lee, D., Lee, H.K., Lee, J.-O., Park, B.S., Yoon, T.-Y., et al. (2017). Reconstruction of LPS Transfer Cascade Reveals Structural Determinants within LBP, CD14, and TLR4-MD2 for Efficient LPS Recognition and Transfer. Immunity *46*, 38–50.

Santos, J.C., Boucher, D., Schneider, L.K., Demarco, B., Dilucca, M., Shkarina, K., Heilig, R., Chen, K.W., Lim, R.Y.H., and Broz, P. (2020). Human GBP1 binds LPS to initiate assembly of a caspase-4 activating platform on cytosolic bacteria. Nature Communications *11*, 3276.

Scaffidi, P., Misteli, T., and Bianchi, M.E. (2002). Release of chromatin protein HMGB1 by necrotic cells triggers inflammation. Nature *418*, 191–195.

Schaefer, L. (2014). Complexity of danger: the diverse nature of damage-associated molecular patterns. J. Biol. Chem. *289*, 35237–35245.

Schaefer, L., Babelova, A., Kiss, E., Hausser, H.-J., Baliova, M., Krzyzankova, M., Marsche, G., Young, M.F., Mihalik, D., Götte, M., et al. (2005). The matrix component biglycan is proinflammatory and signals through Toll-like receptors 4 and 2 in macrophages. J Clin Invest *115*, 2223–2233.

Schattgen, S.A., and Fitzgerald, K.A. (2011). The PYHIN protein family as mediators of host defenses: PYHIN/p200 family in innate immunity. Immunological Reviews *243*, 109–118.

Schenk, S., Muser, J., Vollmer, G., and Chiquet-Ehrismann, R. (1995). Tenascin-C in serum: a questionable tumor marker. Int J Cancer *61*, 443–449.

Schumann, R.R., Leong, S.R., Flaggs, G.W., Gray, P.W., Wright, S.D., Mathison, J.C., Tobias, P.S., and Ulevitch, R.J. (1990). Structure and function of lipopolysaccharide binding protein. Science *249*, 1429–1431.

Seelig, H.P., Ehrfeld, H., and Renz, M. (1994). Interferon-γ–inducible protein p16. a new target of antinuclear antibodies in patients with systemic lupus erythematosus. Arthritis & Rheumatism *37*, 1672–1683.

Seki, E., and Schnabl, B. (2012). Role of innate immunity and the microbiota in liver fibrosis: crosstalk between the liver and gut. The Journal of Physiology *590*, 447–458.

Shi, J., Zhao, Y., Wang, Y., Gao, W., Ding, J., Li, P., Hu, L., and Shao, F. (2014). Inflammatory caspases are innate immune receptors for intracellular LPS. Nature *514*, 187–192.

Shi, J., Zhao, Y., Wang, K., Shi, X., Wang, Y., Huang, H., Zhuang, Y., Cai, T., Wang, F., and Shao, F. (2015). Cleavage of GSDMD by inflammatory caspases determines pyroptotic cell death. Nature *526*, 660–665.

Shimazu, R., Akashi, S., Ogata, H., Nagai, Y., Fukudome, K., Miyake, K., and Kimoto, M. (1999). MD-2, a molecule that confers lipopolysaccharide responsiveness on Toll-like receptor 4. J Exp Med *189*, 1777–1782.

Singh, V.V., Kerur, N., Bottero, V., Dutta, S., Chakraborty, S., Ansari, M.A., Paudel, N., Chikoti, L., and Chandran, B. (2013). Kaposi's Sarcoma-Associated Herpesvirus Latency in Endothelial and B Cells Activates Gamma Interferon-Inducible Protein 16-Mediated Inflammasomes. Journal of Virology *87*, 4417–4431.

Song, Y., Wu, X., Xu, Y., Zhu, J., Li, J., Zou, Z., Chen, L., Zhang, B., Hua, C., Rui, H., et al. (2020). HPV E7 inhibits cell pyroptosis by promoting TRIM21-mediated degradation and ubiquitination of the IFI16 inflammasome. Int. J. Biol. Sci. *16*, 2924–2937.

Sponza, S., De Andrea, M., Mondini, M., Gugliesi, F., Gariglio, M., and Landolfo, S. (2009). Role of the interferon-inducible IFI16 gene in the induction of ICAM-1 by TNF-α. Cellular Immunology *257*, 55–60.

Stoddard, M.B., Pinto, V., Keiser, P.B., and Zollinger, W. (2010). Evaluation of a Whole-Blood Cytokine Release Assay for Use in Measuring Endotoxin Activity of Group B Neisseria meningitidis Vaccines Made from Lipid A Acylation Mutants. Clin. Vaccine Immunol. *17*, 98–107.

Stoll, L.L., Denning, G.M., and Weintraub, N.L. (2006). Endotoxin, TLR4 signaling and vascular inflammation: potential therapeutic targets in cardiovascular disease. Curr Pharm Des *12*, 4229–4245.

Takeda, K., and Akira, S. (2004). TLR signaling pathways. Seminars in Immunology *16*, 3–9.

Tan, Y., and Kagan, J.C. (2014). A Cross-Disciplinary Perspective on the Innate Immune Responses to Bacterial Lipopolysaccharide. Molecular Cell *54*, 212–223.

Tan, Y., Zanoni, I., Cullen, T.W., Goodman, A.L., and Kagan, J.C. (2015). Mechanisms of Toll-like Receptor 4 Endocytosis Reveal a Common Immune-Evasion Strategy Used by Pathogenic and Commensal Bacteria. Immunity *43*, 909–922.

Tang, D., Kang, R., Coyne, C.B., Zeh, H.J., and Lotze, M.T. (2012). PAMPs and DAMPs: signal 0s that spur autophagy and immunity. Immunol Rev *249*, 158–175.

Tervaniemi, M.H., Katayama, S., Skoog, T., Siitonen, H.A., Vuola, J., Nuutila, K., Sormunen, R., Johnsson, A., Linnarsson, S., Suomela, S., et al. (2016). NOD-like receptor signaling and inflammasome-related pathways are highlighted in psoriatic epidermis. Sci Rep *6*, 22745.

Tian, J., Avalos, A.M., Mao, S.-Y., Chen, B., Senthil, K., Wu, H., Parroche, P., Drabic, S., Golenbock, D., Sirois, C., et al. (2007). Toll-like receptor 9-dependent activation by DNA-containing immune complexes is mediated by HMGB1 and RAGE. Nat Immunol *8*, 487–496.

Tobias, P.S., Soldau, K., and Ulevitch, R.J. (1986). Isolation of a lipopolysaccharide-binding acute phase reactant from rabbit serum. J Exp Med *164*, 777–793.

Trapani, J.A., Dawson, M., Apostolidis, V.A., and Browne, K.A. (1994). Genomic organization of IFI16, an interferon-inducible gene whose expression is associated with human myeloid cell differentiation: correlation of predicted protein domains with exon organization. Immunogenetics *40*, 415–424.

Uchida, K., Akita, Y., Matsuo, K., Fujiwara, S., Nakagawa, A., Kazaoka, Y., Hachiya, H., Naganawa, Y., Oh-iwa, I., Ohura, K., et al. (2005). Identification of specific autoantigens in Sjogren's syndrome by SEREX. Immunology *116*, 53–63.

Unterholzner, L., Keating, S.E., Baran, M., Horan, K.A., Jensen, S.B., Sharma, S., Sirois, C.M., Jin, T., Latz, E., Xiao, T.S., et al. (2010). IFI16 is an innate immune sensor for intracellular DNA. Nat Immunol *11*, 997–1004.

Vanhove, W., Peeters, P.M., Staelens, D., Schraenen, A., Van der Goten, J., Cleynen, I., De Schepper, S., Van Lommel, L., Reynaert, N.L., Schuit, F., et al. (2015). Strong Upregulation of AIM2 and IFI16 Inflammasomes in the Mucosa of Patients with Active Inflammatory Bowel Disease: Inflammatory Bowel Diseases *21*, 2673–2682.

Veeranki, S., and Choubey, D. (2012). Interferon-inducible p200-family protein IFI16, an innate immune sensor for cytosolic and nuclear double-stranded DNA: Regulation of subcellular localization. Molecular Immunology *49*, 567–571.

Velkov, T., Roberts, K.D., Nation, R.L., Thompson, P.E., and Li, J. (2013). Pharmacology of polymyxins: new insights into an "old" class of antibiotics. Future Microbiol *8*, 711–724.

Vénéreau, E., Ceriotti, C., and Bianchi, M.E. (2015). DAMPs from Cell Death to New Life. Front Immunol *6*.

Vinogradov, E., Perry, M.B., and Conlan, J.W. (2002). Structural analysis of Francisella tularensis lipopolysaccharide. European Journal of Biochemistry *269*, 6112–6118.

Wack, A., Terczyńska-Dyla, E., and Hartmann, R. (2015). Guarding the frontiers: the biology of type III interferons. Nat Immunol *16*, 802–809.

Wähämaa, H., Schierbeck, H., Hreggvidsdottir, H.S., Palmblad, K., Aveberger, A.-C., Andersson, U., and Harris, H.E. (2011). High mobility group box protein 1 in complex with lipopolysaccharide or IL-1 promotes an increased inflammatory phenotype in synovial fibroblasts. Arthritis Research & Therapy *13*, R136.

Wang, H., Bloom, O., Zhang, M., Vishnubhakat, J.M., Ombrellino, M., Che, J., Frazier, A., Yang, H., Ivanova, S., Borovikova, L., et al. (1999). HMG-1 as a late mediator of endotoxin lethality in mice. Science *285*, 248–251.

Wei, W., Clarke, C.J.P., Somers, G.R., Cresswell, K.S., Loveland, K.A., Trapani, J.A., and Johnstone, R.W. (2003). Expression of IFI 16 in epithelial cells and lymphoid tissues. Histochem Cell Biol *119*, 45–54.

Wright, S.D., Ramos, R.A., Tobias, P.S., Ulevitch, R.J., and Mathison, J.C. (1990). CD14, a receptor for complexes of lipopolysaccharide (LPS) and LPS binding protein. Science *249*, 1431–1433.

Xia, C., Braunstein, Z., Toomey, A.C., Zhong, J., and Rao, X. (2018). S100 Proteins As an Important Regulator of Macrophage Inflammation. Front Immunol *8*.

Xin, H., Curry, J., Johnstone, R.W., Nickoloff, B.J., and Choubey, D. (2003). Role of IFI 16, a member of the interferon-inducible p200-protein family, in prostate epithelial cellular senescence. Oncogene *22*, 4831–4840.

Yamamoto, M., Sato, S., Hemmi, H., Hoshino, K., Kaisho, T., Sanjo, H., Takeuchi, O., Sugiyama, M., Okabe, M., Takeda, K., et al. (2003). Role of adaptor TRIF in the MyD88-independent toll-like receptor signaling pathway. Science *301*, 640–643.

Yan, H., Dalal, K., Hon, B.K., Youkharibache, P., Lau, D., and Pio, F. (2008). RPA nucleic acid-binding properties of IFI16-HIN200. Biochimica et Biophysica Acta (BBA) - Proteins and Proteomics *1784*, 1087–1097.

Yang, H., Hreggvidsdottir, H.S., Palmblad, K., Wang, H., Ochani, M., Li, J., Lu, B., Chavan, S., Rosas-Ballina, M., Al-Abed, Y., et al. (2010). A critical cysteine is required for HMGB1 binding to Toll-like receptor 4 and activation of macrophage cytokine release. PNAS *107*, 11942–11947.

Yang, H., Wang, H., Ju, Z., Ragab, A.A., Lundbäck, P., Long, W., Valdes-Ferrer, S.I., He, M., Pribis, J.P., Li, J., et al. (2015a). MD-2 is required for disulfide HMGB1–dependent TLR4 signaling. J Exp Med *212*, 5–14.

Yang, H., Wang, H., Chavan, S.S., and Andersson, U. (2015b). High Mobility Group Box Protein 1 (HMGB1): The Prototypical Endogenous Danger Molecule. Mol Med *21*, S6–S12.

Youn, J.H., Oh, Y.J., Kim, E.S., Choi, J.E., and Shin, J.-S. (2008). High mobility group box 1 protein binding to lipopolysaccharide facilitates transfer of lipopolysaccharide to CD14 and enhances lipopolysaccharide-mediated TNF-alpha production in human monocytes. J Immunol *180*, 5067–5074.

Youn, J.H., Kwak, M.S., Wu, J., Kim, E.S., Ji, Y., Min, H.J., Yoo, J.-H., Choi, J.E., Cho, H.-S., and Shin, J.-S. (2011). Identification of lipopolysaccharide-binding peptide regions within HMGB1 and their effects on subclinical endotoxemia in a mouse model. Eur J Immunol *41*, 2753–2762.

Zanoni, I., Ostuni, R., Marek, L.R., Barresi, S., Barbalat, R., Barton, G.M., Granucci, F., and Kagan, J.C. (2011). CD14 Controls the LPS-Induced Endocytosis of Toll-like Receptor 4. Cell *147*, 868–880.

Zanoni, I., Tan, Y., Di Gioia, M., Springstead, J.R., and Kagan, J.C. (2017). By Capturing Inflammatory Lipids Released from Dying Cells, the Receptor CD14 Induces Inflammasome-Dependent Phagocyte Hyperactivation. Immunity *47*, 697-709.e3.

Zuliani-Alvarez, L., Marzeda, A.M., Deligne, C., Schwenzer, A., McCann, F.E., Marsden, B.D., Piccinini, A.M., and Midwood, K.S. (2017). Mapping tenascin-C interaction with toll-like receptor 4 reveals a new subset of endogenous inflammatory triggers. Nat Commun *8*, 1595.

8. Publication

Iannucci A, Caneparo V, Raviola S, Debernardi I, Colangelo D, et al. (2020) Toll-like receptor 4-mediated inflammation triggered by extracellular IFI16 is enhanced by lipopolysaccharide binding. PLOS Pathogens 16(9): e1008811. https://doi.org/10.1371/journal.ppat.1008811

PLOS PATHOGENS

RESEARCH ARTICLE

Toll-like receptor 4-mediated inflammation triggered by extracellular IFI16 is enhanced by lipopolysaccharide binding

Andrea Iannucci[1,2], Valeria Caneparo[1,2], Stefano Raviola[1,2], Isacco Debernardi[2], Donato Colangelo[3], Riccardo Miggiano[4], Gloria Griffante[2,5], Santo Landolfo[5], Marisa Gariglio[1,2]*, Marco De Andrea[1,5]*

1 CAAD—Center for Translational Research on Autoimmune and Allergic Disease, University of Eastern Piedmont, Novara, Italy, **2** Department of Translational Medicine, University of Eastern Piedmont, Novara, Italy, **3** Department of Health Sciences, University of Eastern Piedmont, Novara, Italy, **4** Department of Pharmaceutical Sciences, University of Eastern Piedmont, Novara, Italy, **5** Department of Public Health and Pediatric Sciences, University of Turin, Medical School, Turin, Italy

* marisa.gariglio@uniupo.it (MG); marco.deandrea@unito.it (MDA)

Citation: Iannucci A, Caneparo V, Raviola S, Debernardi I, Colangelo D, Miggiano R, et al. (2020) Toll-like receptor 4-mediated inflammation triggered by extracellular IFI16 is enhanced by lipopolysaccharide binding. PLoS Pathog 16(9): e1008811. https://doi.org/10.1371/journal.ppat.1008811

Editor: Victor Robert DeFilippis, Oregon Health and Sciences University, UNITED STATES

Received: February 8, 2020

Accepted: July 14, 2020

Published: September 9, 2020

Peer Review History: PLOS recognizes the benefits of transparency in the peer review process; therefore, we enable the publication of all of the content of peer review and author responses alongside final, published articles. The editorial history of this article is available here: https://doi.org/10.1371/journal.ppat.1008811

Data Availability Statement: All relevant data are within the manuscript and its Supporting Information files.

Abstract

Damage-associated molecular patterns (DAMPs) are endogenous molecules activating the immune system upon release from injured cells. Here we show that the IFI16 protein, once freely released in the extracellular milieu of chronically inflamed tissues, can function as a DAMP either alone or upon binding to lipopolysaccharide (LPS). Specifically, using pull-down and saturation binding experiments, we show that IFI16 binds with high affinity to the lipid A moiety of LPS. Remarkably, IFI16 DAMP activity is potentiated upon binding to subtoxic concentrations of strong TLR4-activating LPS variants, as judged by TLR4-MD2/TIRAP/MyD88-dependent IL-6, IL-8 and TNF-α transcriptional activation and release in stimulated monocytes and renal cells. Consistently, using co-immunoprecipitation (co-IP) and surface plasmon resonance (SPR) approaches, we show that IFI16 is a specific TLR4-ligand and that IFI16/LPS complexes display a faster stimulation turnover on TLR4 than LPS alone. Altogether, our findings point to a novel pathomechanism of inflammation involving the formation of multiple complexes between extracellular IFI16 and subtoxic doses of LPS variants, which then signal through TLR4.

Author summary

IFI16 is a nuclear protein involved in a variety of physiological processes, including cell cycle regulation, tumor suppression, and virus sensing. Emerging evidence indicates that IFI16 is released in the extracellular milieu under injury or stress conditions. Here we show that extracellular IFI16 acts as a damage-associated molecular pattern (DAMP), triggering inflammation through Toll-like receptor 4 (TLR4) activation. Furthermore, we demonstrate that IFI16 activity is potentiated upon binding to subtoxic concentrations of strong TLR4-activating lipopolysaccharide (LPS) variants, which are known to be present

Funding: The investigators were supported by grant 2015W729WH from the Italian Ministry for University and Research (PRIN2015 to MDA), grant CSTO168881 from the Compagnia di San Paolo (CSP2016 to MDA), and grant from the European Commission under the Horizon2020 program (H2020-MSCA-ITN-2015 to SL). This study was partially funded by the AGING Project – Department of Excellence– DIMET, University of Eastern Piedmont. The funders had no role in study design, data collection and analysis, decision to publish, or preparation of the manuscript.

Competing interests: The authors have declared that no competing interests exist.

in various pathological settings other than gram-negative infections. Our study provides new insights into the role of extracellular IFI16 during low-grade endotoxemia.

Introduction

In the absence of stress stimuli, expression of the nuclear IFI16 protein is restricted to hematopoietic cells, vascular endothelial cells and keratinocytes [1]. Since its discovery in the early 90s, IFI16 has been involved in a growing number of physiological processes, such as cell cycle regulation, tumor suppression, apoptosis, DNA damage signaling, virus sensing and virus restriction [2–5]. More recently, we and others have found that IFI16 can also be aberrantly expressed in chronically inflamed tissues such as the intestinal epithelium of patients with inflammatory bowel disease (IBD) [6,7] and the epidermis and inflammatory dermal infiltrates of systemic lupus erythematosus (SLE) patients [8,9]. In addition, abnormal IFI16 expression has been also detected in the skin of individuals affected by systemic sclerosis (SSc) [10] or psoriasis (Pso) [11–13], as well as in salivary epithelial cells and infiltrating lymphocytes of subjects with Sjögren's syndrome (SS) [14,15]. Noteworthy, serum circulating IFI16 protein and its specific autoantibodies have also been reported in various autoimmune diseases, including SSc, rheumatoid arthritis (RA), SLE, SS, psoriatic arthritis (PsA) and IBD [6,8,16–20]. Our group and others have also reported IFI16 de-localization to the cytoplasm upon viral infection or UVB exposure [8,21–23]. Importantly, under these conditions, IFI16 is eventually released in the extracellular matrix where it acts as a damage-associated molecular pattern (DAMP), inducing a proinflammatory phenotype [8,24]. However, the molecular mechanisms underlying the extracellular DAMP activity of IFI16 have yet to be determined.

Lipopolysaccharide (LPS) is the main cause of gram-negative bacterial sepsis and among the best-characterized pathogen-associated molecular patterns (PAMPs). It is made up of a lipid component (lipid A), playing an essential role in promoting inflammation, and two sugar moieties subdivided in a core polysaccharide and an O-polysaccharide of variable length [25]. Serum LPS is recognized by the LPS binding protein (LBP), which then forms transient ternary complexes with soluble or membrane-anchored CD14 (sCD14 or mCD14, respectively). Subsequently, CD14 dissociates from LBP to extract monomeric LPS [26, 27] and through mCD14, LPS is finally presented to the TLR4/MD2 complex, thereby leading to the activation of multiple signaling components, including NF-κB and IRF3, which in turn transcriptionally activate proinflammatory cytokines [28].

Since we previously demonstrated that recombinant IFI16 can synergize with subtoxic concentrations of LPS to induce proinflammatory cytokine production in endothelial cells [24], here we have explored the possibility that aberrant expression of IFI16 and its ensuing release into the extracellular matrix may favor its interaction with exogenous molecules, such as LPS, thereby triggering an inflammatory state also in other target cells.

In this study, we show for the first time that IFI16 binds with high affinity to the lipid A moiety of LPS through its HINB domain. Moreover, we provide further evidence that IFI16 functions as a DAMP by triggering proinflammatory cytokine production in renal and monocytic cell lines through the Toll-like receptor 4 (TLR4) signaling pathway, either alone or, more potently, when complexed with strong TLR4-activating LPS variants.

Results

IFI16 binds to LPS of different bacterial origin and inflammatory activity

To investigate the occurrence of a direct association between IFI16 and LPS, we performed an *in vitro* pull-down assay using biotin-labeled LPS from *E. coli* O111:B4 (biotin-LPS-EB) and

human recombinant IFI16 protein. As shown in Fig 1A, we could readily detect a highly reproducible ~100-kDa band corresponding to biotin-LPS-bound IFI16. To rule out that this binding was due to bacterial contaminants, we next performed a pull-down assay using a recombinant glutathione-S transferase (GST) protein prepared with the same procedure as that employed to obtain recombinant IFI16. As shown in Fig 1B, we failed to isolate any GST-containing band following incubation of GST with biotin-LPS-EB and streptavidin beads, demonstrating the specificity of the IFI16/LPS interaction. Furthermore, saturation binding experiments using IFI16-coated microtiter plates challenged with increasing amounts of biotin-LPS-EB revealed biotin-labeled LPS bound to solid-phase IFI16 in a concentration-dependent manner, reaching saturation at 100,000 ng/ml of biotin-LPS-EB (Fig 1C). When recombinant GST or BSA were coated onto the microtiter plates, no binding occurred in the presence of biotin-LPS-EB (Fig 1C). To assess binding specificity, we asked whether polymyxin B (PMB), an LPS-sequestering agent able to bind to negatively charged phosphate groups of lipid A [29], would disrupt IFI16/LPS interaction. As shown in Fig 1C, when PMB was pre-incubated with biotin-LPS-EB and then added to the IFI16-coated wells, it completely prevented IFI16 from binding to LPS. Next, IFI16/LPS-EB interaction was confirmed by surface plasmon resonance (SPR) analysis flowing increasing amounts of LPS-EB over a CM5 IFI16-coated chip. As shown in Fig 1D, LPS interacted with IFI16 in a concentration-dependent manner, with a kinetic association constant (K_a) of $1.13^{*}10^{4}$ 1/Ms and a kinetic dissociation constant (K_d) of $1.94^{*}10^{-3}$ 1/s, respectively.

Altogether, these results indicate that IFI16 binds to LPS-EB with high affinity and that such interaction is inhibited by PMB, presumably by masking the negatively charged groups of the LPS lipid A moiety.

We next sought to determine whether IFI16 could bind to LPS in its natural setting, such as the outer membrane of fixed gram-negative bacteria. To this end, a panel of gram-negative bacteria, including a laboratory strain of *E. coli* and a clinical isolate of *Klebsiella pneumoniae*, were assessed as solid phase antigens by whole cell ELISA. Gram-positive clinical isolates of *Staphylococcus aureus*, *Staphylococcus epidermidis* and *Streptococcus pyogenes* were used as negative controls. As shown in Fig 1E, IFI16 strongly associated with the surface of both gram-negative bacteria species. By contrast, no IFI16 binding could be detected when gram-positive bacteria were used as solid phase antigens (Fig 1E). Thus, IFI16-LPS binding can also occur in the natural setting where LPS is anchored to the bacterial outer membrane by its lipid A moiety.

We next asked whether IFI16 would bind with the same affinity to LPS variants derived from different gram-negative strains with highly variable structure and broad-spectrum activity. For this purpose, microtiter plates were coated with the following LPS variants: 1) the two full TLR4 agonists *E. coli* O111:B4 (LPS-EB) and *E. coli* F583 (LPS-F583), with the latter harboring a similar lipid A moiety but a shorter polysaccharide chain length compared to that of the O111:B4 strain; 2) the weak TLR4 agonist *P. gingivalis* (LPS-PG), carrying a mixture of di-, mono- and de-phosphorylated penta- or tetra-acylated lipid A moieties; or 3) the TLR4 antagonist *R. sphaeroides* (LPS-RS), harboring a di-phosphorylated lipid A loaded with 3 long and 2 short acyl chains (Fig 1F). As shown in Fig 1G, IFI16 was able to bind to all the aforementioned solid-phase LPS variants in a concentration-dependent manner, although with slightly different kinetics. Specifically, we obtained similar K_Ds for the two *E. coli* LPS variants—*i.e.*, 4.2 nM and 4.3 nM for LPS-EB and LPS-F583, respectively—, while we observed slightly higher K_Ds for LPS-PG and LPS-RS—*i.e.*, 12.0 nM and 19.3 nM, respectively (Table 1). Consistently, treatment of immobilized LPS molecules with PMB prior to the addition of IFI16 completely abolished IFI16 binding. Thus, IFI16 binds to not only the canonical TLR4-activating LPS but also variants characterized by weaker triggering activity.

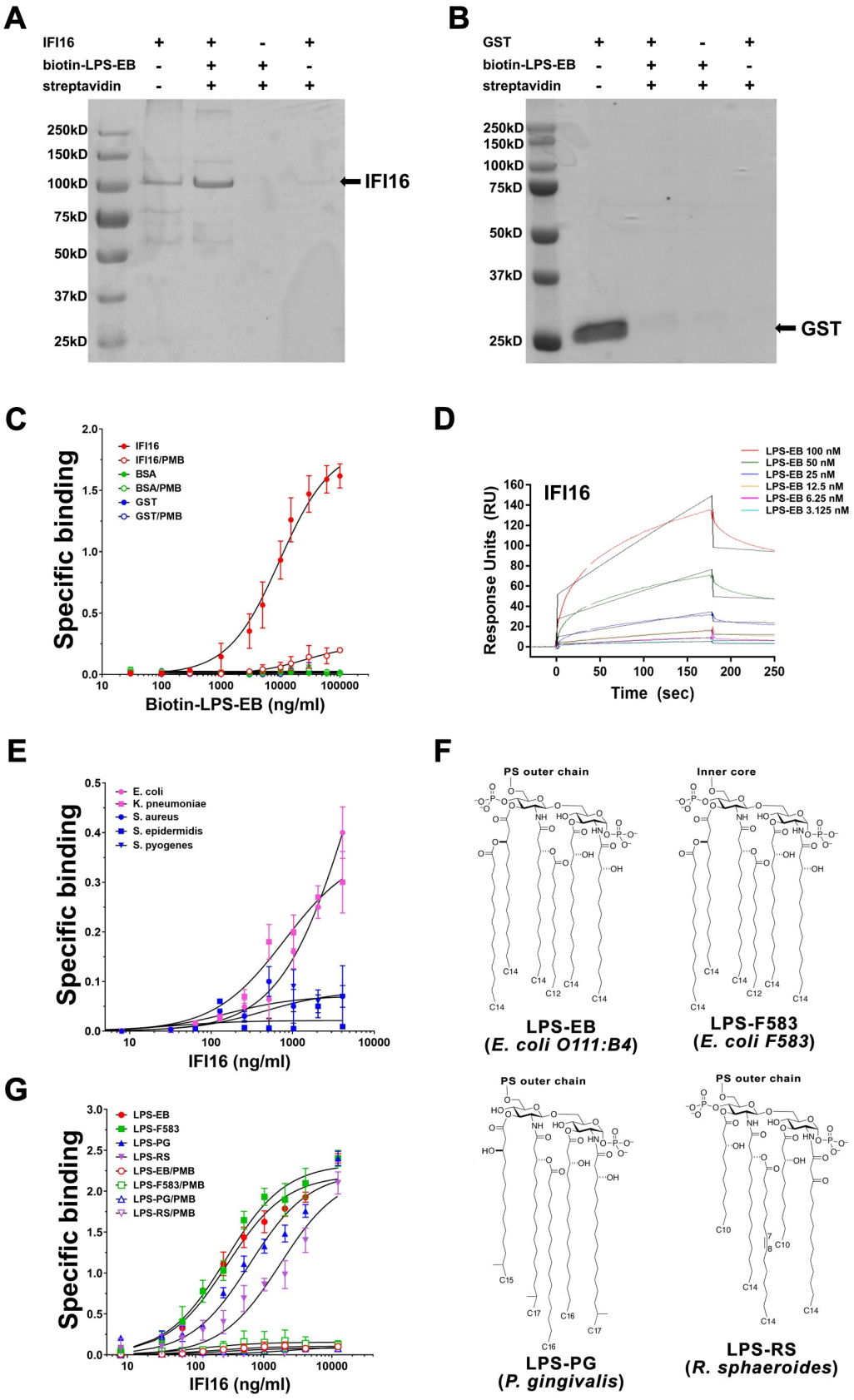
A
IFI16 + + - +
biotin-LPS-EB - + + -
streptavidin - + + +
250kD
150kD
100kD
75kD
50kD
37kD
25kD
IFI16
B
GST + + - +
biotin-LPS-EB - + + -
streptavidin - + + +
250kD
150kD
100kD
75kD
50kD
37kD
25kD
GST
C
Specific binding
IFI16
IFI16/PMB
BSA
BSA/PMB
GST
GST/PMB
Biotin-LPS-EB (ng/ml)
D
IFI16
LPS-EB 100 nM
LPS-EB 50 nM
LPS-EB 25 nM
LPS-EB 12.5 nM
LPS-EB 6.25 nM
LPS-EB 3.125 nM
Response Units (RU)
Time (sec)
E
Specific binding
E. coli
K. pneumoniae
S. aureus
S. epidermidis
S. pyogenes
IFI16 (ng/ml)
F
PS outer chain
Inner core
LPS-EB
(E. coli O111:B4)
LPS-F583
(E. coli F583)
G
Specific binding
LPS-EB
LPS-F583
LPS-PG
LPS-RS
LPS-EB/PMB
LPS-F583/PMB
LPS-PG/PMB
LPS-RS/PMB
IFI16 (ng/ml)
PS outer chain
LPS-PG
(P. gingivalis)
PS outer chain
LPS-RS
(R. sphaeroides)

Fig 1. IFI16 binds to LPS of different bacterial origin and inflammatory activity. Coomassie brilliant blue staining of pull-down assays performed with 3 μg of recombinant IFI16 **(A)** or GST **(B)** in the presence or absence of biotin-labeled lipopolysaccharide (LPS) from *E. coli* O111:B4 (biotin-LPS-EB). **(C)** Saturation binding experiments performed with 2 μg/ml of IFI16 (red circles) and increasing amount of biotin-LPS-EB. Binding was detected by ELISA using HRP-conjugated streptavidin. Optical density (OD) of samples was measured at 450 nm. An excess of recombinant GST (blue circles) or BSA (green circles) and pre-treatment of biotin-LPS-EB with polymyxin B (PMB, empty circles) were used as negative controls. Data are expressed as mean values ± SD of three independent experiments. **(D)** Surface plasmon resonance (SPR) analysis of LPS-EB binding to immobilized IFI16. After immobilization of IFI16 on the CM5 sensor chip surface, increasing concentration of LPS-EB (3.125–100 nM) diluted in running buffer were injected over immobilized IFI16. Data are representative of three independent experiments. **(E)** *Ex-vivo* interaction analysis between increasing amount of recombinant IFI16 and formalin-fixed gram-negative (*E. coli* and *K. pneumonia*; pink circles and pink squares, respectively) or gram-positive (*S. aureus*, *S. epidermidis*, *S. pyogenes*; blue circles, squares and triangles, respectively) bacteria. Data are expressed as mean values ± SD of three independent experiments. **(F)** Lipid A structures of LPS derived from *E. coli* O111:B4 or F583 LPS (LPS-EB and LPS-F583, respectively; strong TLR4 agonists), *P. gingivalis* (LPS-PG; weak TLR4 agonist) and *R. sphaeroides* (LPS-RS, TLR4 antagonist). For LPS-PG, which harbors a mixture of di-, mono- and de-phosphorylated penta- or tetra-acylated lipid A moieties, a single isoform is represented for simplicity. PS-outer chain = polysaccharide outer chain. **(G)** Saturation binding experiments with increasing amount of recombinant IFI16 (8 to 12,288 ng/ml) and 10 μg/ml of LPS-EB (red line), LPS-F583 (green line), LPS-PG (blue line) or LPS-RS (purple line). Anti-IFI16 antibodies against the N-terminus of the protein and HRP-labelled anti-rabbit IgG were added as primary and secondary antibody, respectively, and binding was detected by ELISA at 450 nm. Data are expressed as mean values ± SD of three independent experiments.

https://doi.org/10.1371/journal.ppat.1008811.g001

IFI16 binds to the lipid A moiety of LPS through its HINB domain

To identify which LPS moiety is involved in IFI16 binding, we performed saturation binding experiments using two different variants of lipid A derived from the *E. coli* F583 strain, namely diphosphorylated and monophosphorylated lipid A (DPLA and MPLA, respectively), alongside a detoxified LPS molecule derived from the *E. coli* strain O111:B4 (detoxLPS) (Fig 2A). The first two molecules lack the heteropolysaccharide outer chain and differ in the number of phosphate groups, with MPLA being a weaker agonist than DPLA [30]. On the other hand, the detoxLPS lipid A moiety is partially delipidated by alkaline hydrolysis, resulting in only four primary acyl chains being directly esterified with the sugar moiety, in which the outer chain is however preserved. DetoxLPS endotoxin levels are about 10,000 times lower than that of parental LPS [31]. As shown in Fig 2B, IFI16 readily bound to both forms of lipid A in a concentration-dependent fashion. The K_D values showed higher affinity for the lipid A moieties (either form) in comparison with LPS-F583–0.9 nM and 1.2 nM, respectively, *vs*. 4.3 nM (Table 1). Interestingly, the K_D value for IFI16 binding to detoxLPS (55.6 nM) was the highest among all LPS forms, indicating that the canonical acyl chain is required for IFI16 binding to LPS. When lipid A was pre-treated with PMB, no signal was detected. Thus, LPS binds to IFI16 through its lipid A moiety. To corroborate these data, a competition ELISA was performed by immobilizing LPS from the *E. coli* strain O111:B4 (LPS-EB) onto the microtiter

Table 1. Full-length IFI16 and IFI16 domains binding affinities to LPS.

LPS variant	Equilibrium dissociation constant (K_D), nM			
	IFI16	PYRIN	HINA	HINB
LPS *E. coli* O111:B4 (LPS-EB)	4.2	116.5	85.3	3.3
LPS *E. coli* F583 (LPS-F583)	4.3	-	-	-
LPS *P. gingivalis* (LPS-PG)	12.0	46.9	84.0	1.6
LPS *R. sphaeroides* (LPS-RS)	19.3	-	-	-
DPLA *E. coli* F583 (DPLA)	0.9	47.5	67.7	2.8
MPLA *E. coli* F583 (MPLA)	1.2	47.2	94.1	2.7
Detoxified LPS *E. coli* O111:B4 (detoxLPS)	> 20	-	-	-

K_D, equilibrium dissociation constant

https://doi.org/10.1371/journal.ppat.1008811.t001

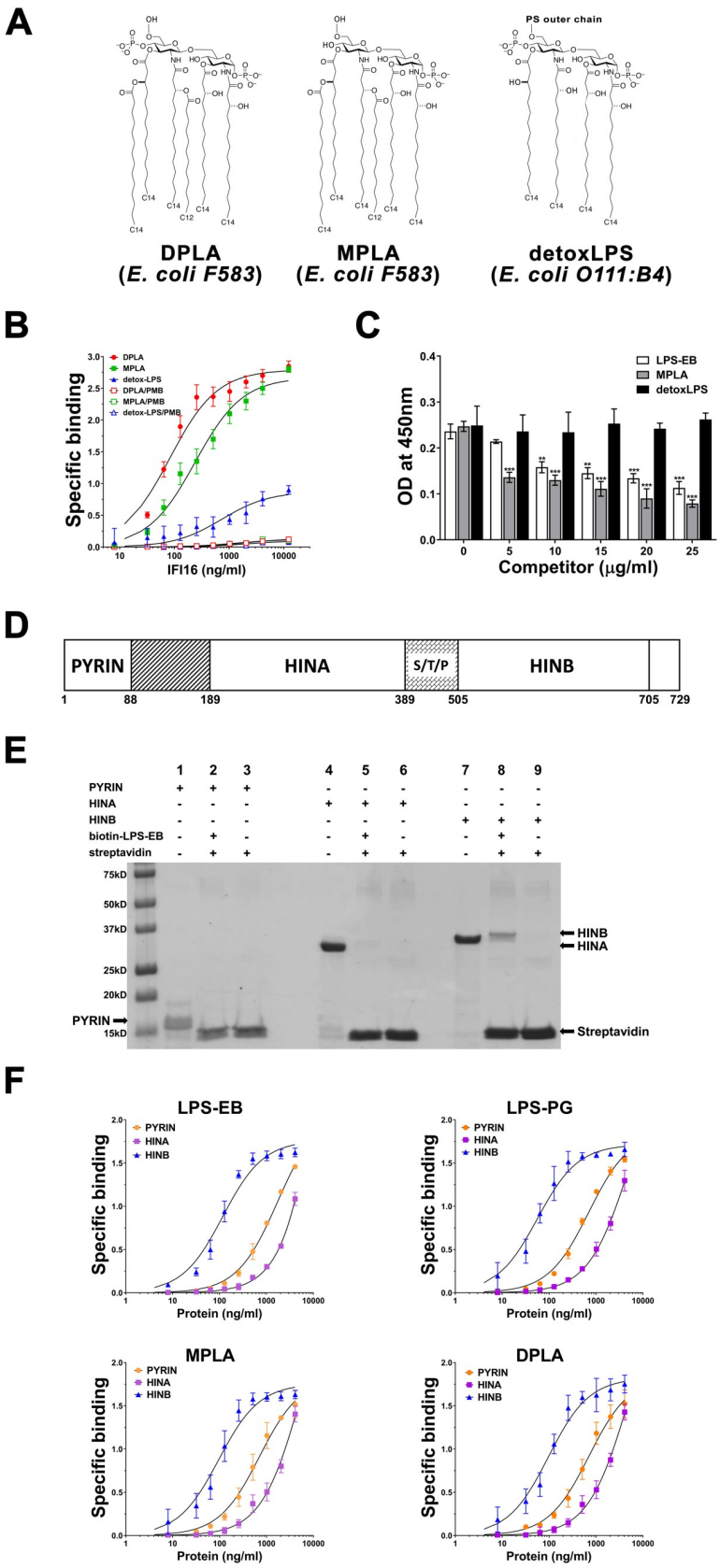
A
PS outer chain
DPLA
(E. coli F583)
MPLA
(E. coli F583)
detoxLPS
(E. coli O111:B4)
B
Specific binding
IFI16 (ng/ml)
DPLA
MPLA
detox-LPS
DPLA/PMB
MPLA/PMB
detox-LPS/PMB
C
OD at 450nm
Competitor (μg/ml)
LPS-EB
MPLA
detoxLPS
D
PYRIN
HINA
S/T/P
HINB
1
88
189
389
505
705
729
E
PYRIN
HINA
HINB
biotin-LPS-EB
streptavidin
75kD
50kD
37kD
25kD
20kD
15kD
HINB
HINA
Streptavidin
F
LPS-EB
LPS-PG
MPLA
DPLA
Specific binding
Protein (ng/ml)
PYRIN
HINA
HINB

Fig 2. FI16 binds to the lipid A moiety of LPS through its HINB domain. (A) Structures of di- or mono-phosphorylated lipid A from *E. coli* F583 (DPLA and MPLA, respectively) and detoxified LPS (detox-LPS) derived from *E. coli* O111:B4. PS-outer chain = polysaccharide outer chain. **(B)** Saturation binding experiments with increasing amount of recombinant IFI16 (from 8 to 12,288 ng/ml) and 10 μg/ml of MPLA (green line), DPLA (red line) or detox-LPS (purple line). Binding was detected by ELISA as described in the legend to Fig 1G. Data are expressed as mean values ± SD of three different experiments. **(C)** Competition ELISA assay for LPS-EB binding to IFI16 with increasing amount of LPS-EB, MPLA or detox-LPS as competitors. Briefly, microtiter plates were coated with 1 μg/ml LPS-EB, then 2 μg/ml of IFI16 were added to the wells in the presence of increasing concentration (5 to 25 μg/ml) of competitor. Binding was detected by ELISA as described in the legend to Fig 1F. Data are expressed as mean values ± SD of three independent experiments ($^{***}P<0.001$, $^{**}P<0.01$, Student's t test). **(D)** Domain organization of the IFI16 protein. The numbers represent the amino acid positions based on NCBI Reference Sequence NP_005522. From the N- to the C-terminal (left to right), IFI16 comprises a pyrin domain involved in protein-protein interaction, and two hematopoietic interferon-inducible nuclear protein with 200-amino-acid repeats (HINA and HINB) domains, which are a hallmark of the absent in melanoma 2-like receptors (ALRs). S/T/P = serine/threonine/proline-rich repeats, which are regulated by alternative mRNA splicing. **(E)** Coomassie brilliant blue staining of pull-down assays performed with 3 μg of recombinant PYRIN, HINA, and HINB domains, in presence or absence of biotin-labeled LPS from *E. coli* O111:B4 (biotin-LPS-EB). **(F)** Saturation binding experiments performed by using increasing amount (8 to 4,096 ng/ml) of recombinant PYRIN, HINA or HINB domains (orange, purple and blue lines, respectively) and 10 μg/ml of LPS-EB, LPS-PG, MPLA or DPLA. Anti-IFI16 antibodies against the N- or C-terminus of the protein and HRP-labeled anti-rabbit IgG were added as primary and secondary antibody, respectively, and binding detected in ELISA at 450 nm. Data are expressed as mean values ± SD of three independent experiments.

https://doi.org/10.1371/journal.ppat.1008811.g002

plates followed by the addition of a mixture of a constant amount of IFI16 and increasing concentrations of LPS-EB, MPLA or detoxLPS, in this case used as competitors. As expected, addition of LPS-EB reduced IFI16 binding to immobilized LPS in a concentration-dependent manner (Fig 2C, white bars). Interestingly, a concentration of 5 μg/ml of MPLA was sufficient enough to achieve a much stronger reduction in IFI16 binding to LPS compared to a similar dose of LPS-EB (Fig 2C, grey bars). Binding inhibition was further enhanced at higher concentrations of MPLA, but the difference between the two variants was less evident. By contrast, detoxLPS did not interfere with the binding of IFI16 to the canonical agonist LPS, even at the highest concentrations used (25 μg/ml: LPS-*EB vs*. detoxLPS, $P = 0.0059$; MPLA *vs*. detoxLPS, $P < 0.0004$; LPS-EB *vs*. MPLA, ns; unpaired t-test) (Fig 2C, black bars). Taken together, these findings indicate that lipid A is the LPS moiety involved in the binding to IFI16 and that the heteropolysaccharide outer chain, absent in MPLA, might constitute a steric hindrance for such interaction.

To identify the domain of IFI16 mediating binding to LPS, an *in vitro* pull-down assay was performed using three distinct recombinant domains of IFI16 spanning either the N-terminal portion containing the pyrin domain (PYRIN) or each of the 200 amino acid-long HIN domains (namely HINA or HINB) (Fig 2D). As shown in Fig 2E, a signal at ~35 kDa was only detected when the HINB fragment was incubated with biotin-LPS-EB bound to streptavidin beads (lane 9), while neither the PYRIN nor the HINA fragment was co-precipitated in the presence of biotinylated LPS (lanes 3 and 6). To corroborate these data, an *in vitro* pull-down assay was performed using a truncated variant of IFI16 lacking the HINB domain (IFI16Δ-HINB) (S1A Fig). As expected, no binding was observed when IFI16ΔHINB was incubated with biotin-LPS-EB and streptavidin beads (S1B Fig, lane 2), confirming that the HINB is required for LPS binding. To further support a role of the HINB domain in mediating the binding of IFI16 to LPS, we performed saturation binding experiments using increasing concentrations of the three IFI16 domains (*i.e*., PYRIN, HINA, and HINB) with fixed amounts of different interactors. As shown in Fig 2F (blue lines), the HINB domain was able to bind to both LPS variants, displaying either strong or weak TLR4 agonist activity, as well as to lipid A. The binding was not affected by the origin of bacterial LPS or by the number of phosphate groups, and displayed K_D values in a similar range to that obtained with the full-length recombinant IFI16 protein (Table 1). Conversely, the PYRIN (orange lines) and HINA (purple lines)

domains displayed very low affinity for the immobilized molecules when compared to HINB, with K_D values indicative of unspecific binding (Table 1). Thus, the HINB domain displays the highest affinity for LPS, indicating that HINB may play a major role in the interaction between IFI16 and LPS.

Only potent TLR4-activating endotoxins can potentiate the proinflammatory activity of IFI16

The results so far obtained prompted us to investigate whether IFI16 binding to the strong agonist variant LPS-EB would modulate IFI16-mediated transcriptional activation of proinflammatory cytokines *in vitro*. For these experiments, in addition to the standard human monocytic cell line THP-1, we chose as a model the renal tubular carcinoma cell line 786-O. We first assessed protein expression levels of the main components of the LPS recognition complex (*i.e.*, TLR4, MD2, MyD88 and CD14) by Western blotting and/or flow cytometry (S2 Fig). While TLR4 and MD2 were expressed at similar levels in both cell lines, CD14 expression was 4-fold lower in THP-1 *vs*. 786-O cells, as judged by FACS analysis (S2B Fig), in good agreement with a previous report [32]. The expression of the TLR4 canonical adaptor MyD88 was similar in both cell lines (S2A Fig).

Next, cells were stimulated with full-length IFI16 or the IFI16ΔHINB variant, alone or pre-incubated with LPS-EB, and then total RNA was extracted to assess mRNA levels of a panel of proinflammatory cytokines (Fig 3A). Consistent with IFI16 acting as a DAMP, IL-6, IL-8 and tumor necrosis factor-α (TNF-α) mRNA levels were strongly upregulated in cells treated with IFI16 alone when compared to mock- or LPS-treated cells in the presence of either low or high LPS concentration. Interestingly, we detected a further increase in mRNA expression levels of the aforementioned genes in cells treated with the IFI16/LPS-EB complex compared to IFI16 alone—*i.e.*, 1.8- and 1.6-fold induction for IL-6; 1.7- and 1.3-fold induction for IL-8; and 2.1- and 1.6-fold induction for TNF-α in 786-O and THP-1 cells, respectively. Likewise, IL-1β gene expression levels were also significantly induced by IFI16 alone or IFI16/LPS-EB complex treatment of THP-1 cells—*i.e.*, 72- and 83-fold induction, respectively—and, albeit to a lower extent, 786-O cells—*i.e.*, 13- and 27-fold induction, respectively. When IFI16ΔHINB alone or pre-incubated with LPS-EB was used to stimulate the cells, the degree of cytokine induction was similar to that observed with the full-length protein, while it was not enhanced following pre-incubation with LPS-EB.

Altogether, these findings further strengthen the notion that the HINB moiety is necessary for the formation of the functional IFI16/LPS complex.

Consistent with the mRNA data, the amounts of IL-6, IL-8 and TNF-α secreted into the culture supernatants were significantly higher in cells treated with the IFI16/LPS-EB complex than those of cells treated with IFI16 alone, while they did not vary upon pre-incubation with LPS-EB in the case of the IFI16ΔHINB variant (Fig 3B). In contrast, neither IFI16 nor IFI16ΔHINB *per se* or after forming a complex with LPS induced IL-1β release in both cell lines, indicating lack of inflammasome-mediated IL-1β processing at 24 h post-treatment.

Next, we asked whether the LPS derivatives DPLA and MPLA or the TLR4 antagonist LPS-RS would be equally able to modulate the biological activity of IFI16. The full agonist LPS-F583, from which DPLA and MPLA were derived, was included as positive control (full TLR4 activator). Cells were treated with the aforementioned compounds, alone or pre-complexed with IFI16 protein, and then total RNA and supernatants were collected to assess the mRNA expression and cytokine production profiles of IL-6, IL-8 and TNF-α. As expected, cells treated with the IFI16/LPS-F583 displayed a similar transcriptional activation pattern to that previously observed in IFI16/LPS-EB-treated cells (Fig 4A). On the other hand, when cells

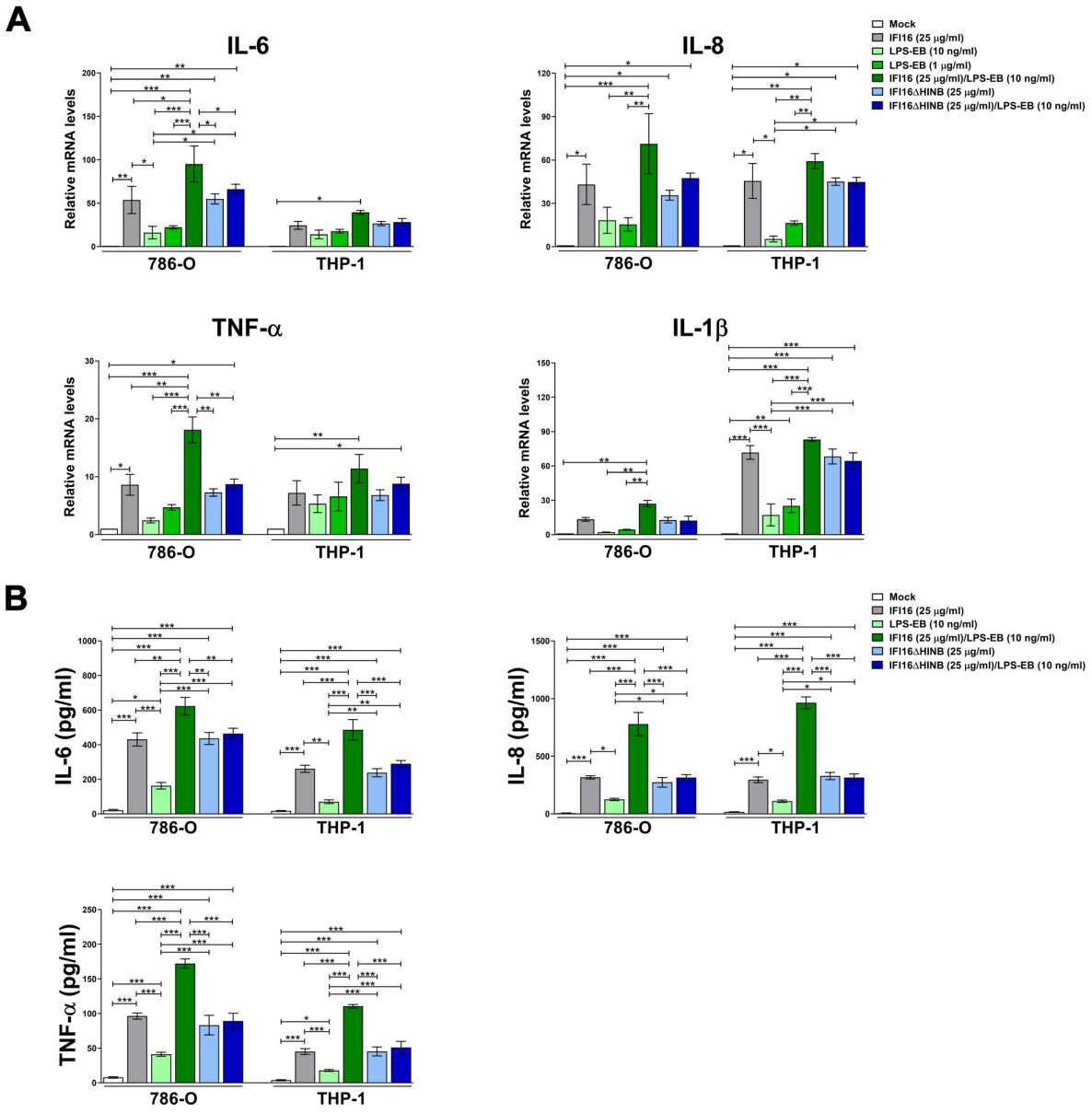

Fig 3. IFI16 proinflammatory activity is potentiated by the strong TLR4 activator LPS-EB. (A) qRT-PCR analysis of IL-6, IL-8, TNF-α and IL-1β mRNA expression levels in 786-O or THP-1 cells stimulated for 24 h with IFI16 (25 μg/ml), IFI16ΔHINB (25 μg/ml), LPS from *E. coli* O111:B4 (LPS-EB, 10 ng/ml or 1 μg/ml), IFI16/LPS-EB complex (preincubated O/N at 4˚C), IFI16ΔHINB/LPS-EB (preincubated O/N at 4˚C), or left untreated (mock). Values are normalized to GAPDH mRNA and plotted as fold induction over mock-treated cells. qRT-PCR data are presented as mean values of biological triplicates. Error bars indicate SD ($^{*}P < 0.05$, $^{**}P < 0.01$, $^{***}P < 0.001$; two-way ANOVA followed by Dunnett's test). **(B)** Protein concentration of IL-6, IL-8 and TNF-α evaluated by ELISA in supernatants derived from 786-O or THP-1 cells stimulated for 24 h as described in **A**. Data are expressed as mean values ± SD of three independent experiments ($^{*}P < 0.05$, $^{**}P < 0.01$, $^{***}P < 0.001$; two-way ANOVA followed by Dunnett's test).

https://doi.org/10.1371/journal.ppat.1008811.g003

were treated with IFI16 complexed with LPS-RS, MPLA or DPLA, we failed to observe any transcriptional enhancement in comparison with IFI16 alone. A similar pattern was found when the same cytokines were measured in the culture supernatants by ELISA (Fig 4B), although a significant increase in IFI16-induced secretion of IL-6 and IL-8 was only observed when cells were treated with the IFI16-DPLA complex—*i.e.*, 1.4-fold induction for IL-6 in THP-1 cells, 1.3- and 1.8-fold induction for IL-8 in 786-O and THP-1, respectively.

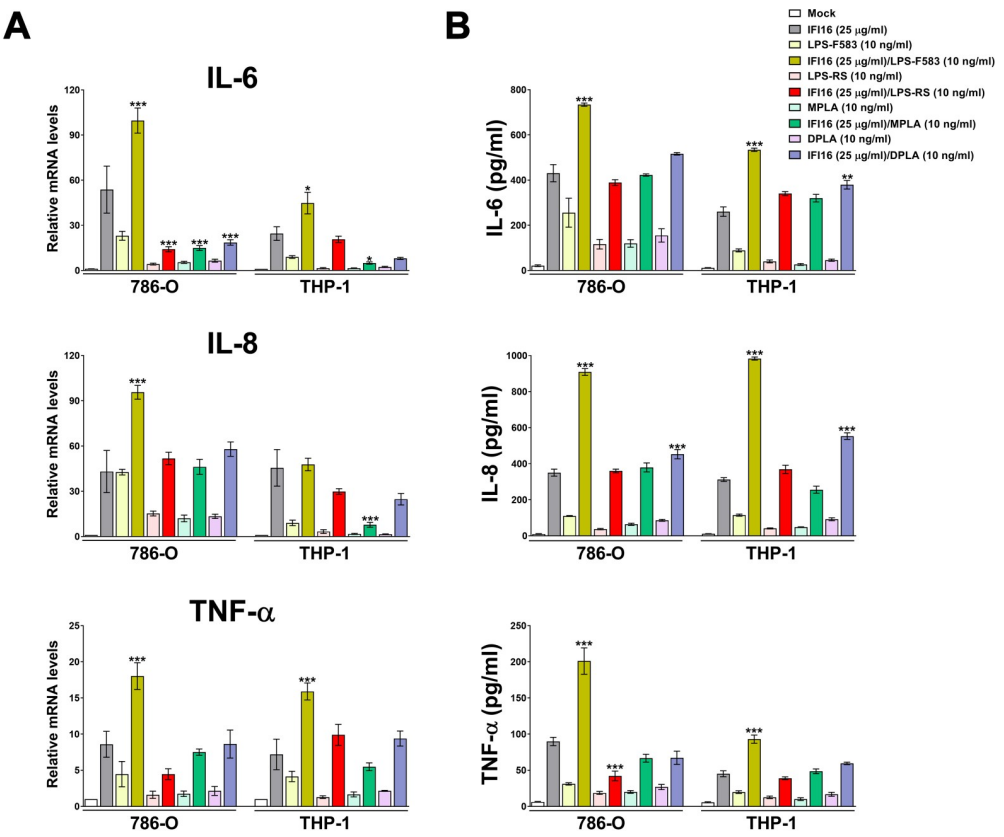

Fig 4. Weak TLR4-activating LPS variants and the TLR4 antagonist LPS-RS do not potentiate IFI16 proinflammatory activity. (A) qRT-PCR analysis of IL-6, IL-8 and TNF-α mRNA expression levels in 786-O or THP-1 cells stimulated for 24 h with or without IFI16 (25 μg/ml), LPS from *E. coli* F583 (LPS-F583, 10 ng/ml) or LPS from *R. sphaeroides* (LPS-RS, 10 ng/ml), MPLA (10 ng/ml), DPLA (10 ng/ml) or in the presence of one of the following complexes: IFI16/LPS-F583, IFI16/LPS-RS, IFI16/MPLA or IFI16/DPLA. Values are normalized to GAPDH mRNA and plotted as fold induction over mock-treated cells. qRT-PCR data are presented as mean values of biological triplicates. Error bars indicate SD, and the *P* values refer to comparisons between IFI16 *vs*. IFI16/LPS or IFI16/lipid A complex-treated cells ($^{*}P < 0.05$, $^{**}P < 0.01$, $^{***}P < 0.001$; two-way ANOVA followed by Dunnett's test). **(B)** Protein concentration of IL-6, IL-8 and TNF-α evaluated by ELISA in supernatants derived from 786-O or THP-1 cells stimulated for 24 h as described in the legend to panel **A**. Data are expressed as mean values ± SD of three independent experiments ($^{*}P < 0.05$, $^{**}P < 0.01$, $^{***}P < 0.001$; ns, not significant; two-way ANOVA followed by Dunnett's test). The *P* values are relative to comparisons between IFI16- and IFI16/LPS- or IFI16/lipid A-treated cells.

https://doi.org/10.1371/journal.ppat.1008811.g004

Collectively, these data indicate that the proinflammatory activity of full-length IFI16 is potentiated when this protein is complexed with potent TLR4-activating LPS variants *via* the HINB moiety, while it is not affected when it forms a complex with the TLR4 antagonist LPS-RS or the weak agonists MPLA and DPLA.

IFI16 exerts its proinflammatory activity in a TLR4/MyD88-dependent fashion

Since we had previously implicated TLR4 signaling in IFI16-mediated cytokine release in endothelial cells [24], we sought to determine whether ablation of the TLR4/MD2 complex would affect IFI16/LPS proinflammatory activity. To this end, we performed gene silencing of TLR4 and MD2 genes in both 786-O and THP-1 cells, achieving complete knockdown of both genes, as judged by immunoblotting and flow cytometric analysis (S3A–S3C Fig). As shown in S4 Fig, the transcriptional activation of IL-6, IL-8 and TNF-α genes (panels A and B) as well as

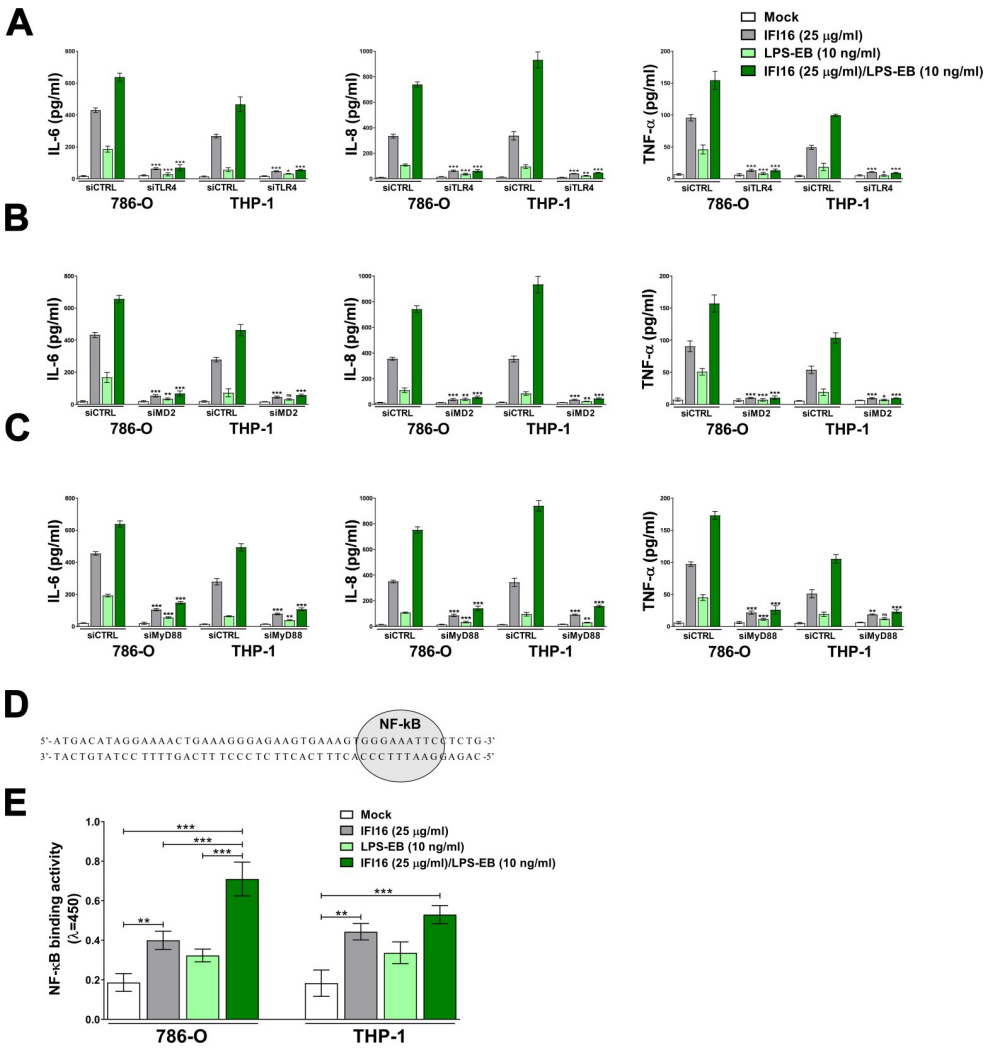

Fig 5. IFI16 exerts its proinflammatory activity in a TLR4/MyD88-dependent fashion. (A-C) Protein concentration of IL-6, IL-8 and TNF-α measured by ELISA in supernatants derived from 786-O or THP-1 cells transfected for 48 h with scramble control (siCTRL), or siRNAs against TLR4 (siTLR4, **A**), MD2 (siMD2, **B**) or MyD88 (siMyD88, **C**). Cells were then stimulated for 24 h with IFI16 (25 μg/ml), LPS from *E. coli* O111:B4 (LPS-EB, 10 ng/ml) or IFI16/LPS-EB complex (preincubated O/N at 4˚C), or left untreated (mock). Data are expressed as mean values ± SD of three independent experiments ($^{*}P < 0.05$, $^{**}P < 0.01$, $^{***}P < 0.001$, ns: not significant; unpaired Student's *t*-test for comparison of silenced cells *vs*. their relative control counterpart). **(D)** Schematic representation of the probe containing the NF-κB binding site (highlighted in grey). **(E)** 786-O cells or THP-1 cells were stimulated with IFI16 (25 μg/ml), LPS from *E. coli* O111:B4 (LPS-EB, 10 ng/ml) or IFI16/LPS-EB complex (preincubated O/N at 4˚C), or left untreated (mock). After 2 h, the cells were lysed and the nuclear fraction was analyzed for NF-κB binding activity using the Universal EZ-TFA transcription factor assay colorimetric kit and the probe described in **D**. Data are expressed as mean values ± SD of three independent experiments ($^{*}P < 0.05$, $^{**}P < 0.01$, $^{***}P < 0.001$; two-way ANOVA followed by Dunnett's test).

https://doi.org/10.1371/journal.ppat.1008811.g005

the release of the same cytokines (Fig 5A, B) in the culture supernatants upon exposure to both IFI16 or IFI16/LPS-EB was almost completely abolished in siTLR4- and siMD2-silenced cells when compared to siRNA control (siCTRL)-transfected cells. Similar results were obtained in both 786-O and THP-1 cells, indicating that IFI16 signaling through the TLR4-MD2 complex is not cell type-specific.

Upon LPS stimulation, TLR4 induces two independent signaling pathways regulated by either the TIRAP/MyD88 or TRAM/TRIF pair of adaptors, which promote the production of

proinflammatory cytokines and type I interferons (IFN-I), respectively [33,34]. As IFN-β could never be detected in IFI16- or IFI16/LPS-stimulated cells, we assumed that the TRAM-TRIF pathway would not play a role in our model. To address a potential role of the TIRAP-MyD88 complex, we performed siRNA-mediated knockdown of MyD88 in both 786-O and THP-1 cells (S3D Fig). In MyD88-silenced cells treated with IFI16 alone or IFI16/LPS-EB, transcription of IL-6, IL-8 and TNF-α genes (S4C Fig) and release of the corresponding cytokines (Fig 5C) were dramatically reduced in comparison with siCTRL-transfected cells, indicating that IFI16 or the IFI16/LPS complex signals through the TIRAP-MyD88 axis. Fittingly, ELISA-based transcription factor binding assay, performed using a probe containing the NF-κB binding site (Fig 5D), showed NF-κB binding activity to be significantly increased in cells challenged with IFI16 alone or pre-complexed with LPS-EB in comparison with untreated cells—*i.e.*, 2.2- and 3.9-fold induction in 786-O cells; 2.4- and 2.9-fold induction in THP-1 cells, respectively (Fig 5E). Overall, these results demonstrate that IFI16-mediated proinflammatory cytokine production requires the TLR4-MD2/TIRAP-MyD88 signaling pathway, which then promotes NF-κB nuclear binding activity to target DNA.

Finally, to circumvent potential issues of structural or functional differences between mammalian or bacterial expressed IFI16, we used wild-type and IFI16-knockout ($IFI16^{-/-}$) human osteosarcoma U2OS cells as a source of endogenous IFI16 released under stress stimuli. As shown in Fig 6A, and consistent with our previous report [8], UVB treatment (800 Jm^{-2} for 16h) led to massive release of IFI16 in the culture supernatants of U2OS cells that, as expected, did not occur in their $IFI16^{-/-}$ counterparts, thus serving as IFI16-depleted supernatant. The resulting conditioned media were preincubated with or without LPS-EB or LPS-RS and then added to THP-1 cells. After 24 h, the supernatants of the THP-1 cultures were harvested and assessed for cytokine expression by ELISA. Consistent with the results obtained with recombinant IFI16, exposure of THP-1 cells to conditioned medium from UVB-treated U2OS cells significantly stimulated the release of IL-6, IL-8 and TNF-α by THP-1 cells when compared to mock-treated cells—*i.e.*, 20.9-fold higher for IL-6; 83-fold for IL-8; and 33.4-fold for TNF-α (Fig 6B). When THP-1 cells were pre-treated with anti-TLR4 antibodies, the stimulatory activity of the conditioned medium form UVB-treated U2OS cells dropped significantly. Notably, cytokine release was significantly lower in THP-1 cells treated with conditioned medium from UVB-treated U2OS-$IFI16^{-/-}$ cells when compared to their UVB-treated normal counterparts—*i.e.*, 2.8-fold lower for IL-6; 2.7-fold for IL-8; and 2.6-fold for TNF-α—, indicating that the effects observed were specifically due to the secretion of IFI16 protein. Consistent with the data obtained with the recombinant protein, cytokine release was enhanced when the conditioned media were preincubated with LPS-EB and, to a higher extent, with the conditioned medium of UVB-treated U2OS cells when compared to that of UVB-treated U2OS-$IFI16^{-/-}$ cells. As expected, this enhancement was not observed when LPS-RS was used.

IFI16 binds to TLR4 *in vivo* and *in vitro*

We next sought to determine whether IFI16 could also bind to the TLR4/MD2 complex *in vivo*. To this end, co-immunoprecipitation assays were performed where TLR4 and interacting partners were immunoprecipitated using an anti-TLR4 antibody pre-adsorbed on protein G beads. The resulting immune complexes were then analyzed by SDS-PAGE followed by immunoblotting for TLR4, MD2, and IFI16. As shown in Fig 7A, IFI16 co-immunoprecipitated with TLR4/MD2 receptor when total extracts from cells treated with either IFI16 alone or IFI16/LPS-EB complex were used (lane 2 and 4, respectively). The specificity of this interaction was attested by the absence of co-immunoprecipitated IFI16 in extracts from cells untreated or treated with LPS-EB alone (lane 1 and 3, respectively). To ensure that residual DNA potentially

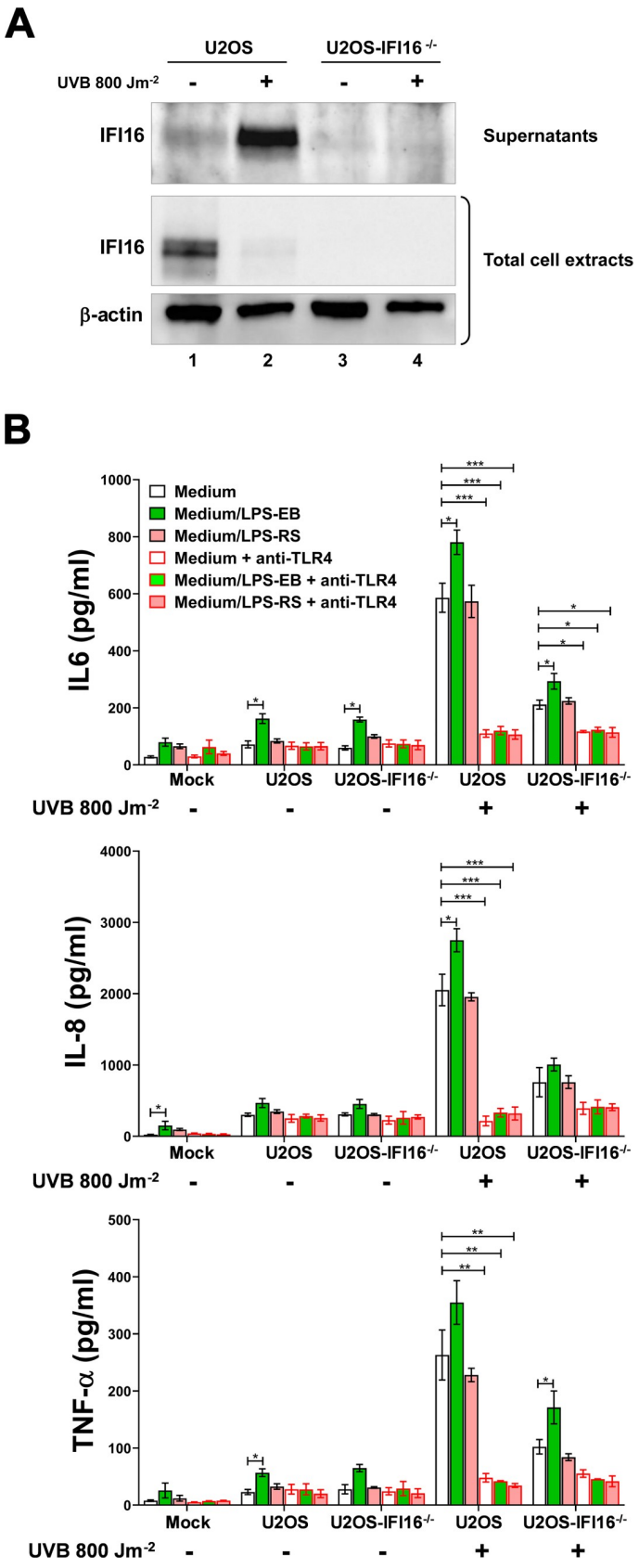
A
U2OS
U2OS-IFI16 -/-
UVB 800 Jm-2
-
+
-
+
IFI16
Supernatants
IFI16
Total cell extracts
β-actin
1
2
3
4
B
Medium
Medium/LPS-EB
Medium/LPS-RS
Medium + anti-TLR4
Medium/LPS-EB + anti-TLR4
Medium/LPS-RS + anti-TLR4
IL6 (pg/ml)
IL-8 (pg/ml)
TNF-α (pg/ml)
Mock
U2OS
U2OS-IFI16-/-
U2OS
U2OS-IFI16-/-
UVB 800 Jm-2

Fig 6. Endogenous IFI16 is released by UVB-exposed U2OS cells and triggers proinflammatory cytokines production in a TLR4-dependent fashion. (A) Western blot analysis of IFI16 in culture supernatants and total cell extracts of UVB-exposed (0 or 800 Jm^{-2}) U2OS or U2OS-IFI16$^{-/-}$ cells at 16 h after treatment. β-actin cellular expression was used for protein loading control. Data are representative of three independent experiments with similar results. **(B)** Protein concentration of IL-6, IL-8 and TNF-α evaluated by ELISA in supernatants derived from THP-1 cells stimulated for 24 h in the presence or absence of anti-TLR4 neutralizing antibodies (10 μg/ml) using conditioned medium from UVB-exposed (0 or 800 Jm^{-2}) U2OS and U2OS-IFI16$^{-/-}$ cells, or complete medium (mock), preincubated (O/N at 4˚C), or not, with LPS from *E. coli* O111:B4 (LPS-EB, 10 ng/ml), or LPS from *R. sphaeroides* (LPS-RS, 10 ng/ml). Values were normalized to the initial protein concentration of the analyzed cytokines in the supernatants used for the treatment. Data are expressed as mean values ± SD of three independent experiments. The *P* values refer to comparison in each group with cells treated only with the medium without any addiction (white bar and black border; $^{*}P < 0.05$, $^{**}P < 0.01$, $^{***}P < 0.001$; two-way ANOVA followed by Dunnett's test).

https://doi.org/10.1371/journal.ppat.1008811.g006

present in the protein extracts would not affect Co-IPs, whole-cell extracts were treated with DNase and then subjected to Co-IP. As shown in Fig 7A (lane 5 and 6, respectively), the interaction between IFI16 or IFI16/LPS and TLR4 was maintained also in protein extracts obtained from DNase-treated cells, indicating that the interaction between these molecules is not mediated by DNA binding.

The specificity of the interaction between IFI16 and TLR4 was then evaluated by surface plasmon resonance (SPR). Briefly, recombinant TLR4 was directly immobilized on a CM5 sensor chip by amine coupling and then probed with increasing concentration of recombinant IFI16—from 31.25 nM to 1 μM. As shown in Fig 7B, the resulting SPR sensorgrams revealed significant binding between TLR4 and IFI16 with an equilibrium dissociation constant (K_D) of 0.13 μM and a kinetic profile typical of dynamically interacting partners, with the dissociation rate being compatible with a rapid stimulation turnover of the ligand (*i.e.*, IFI16) on the TLR4 receptor. Thus, taken together these results indicate that the proinflammatory activity of IFI16, either alone or pre-complexed with LPS, is mediated by the TLR4/MD2/MyD88/NF-κB signaling pathways and requires a direct interaction between IFI16 and TLR4.

The IFI16/LPS complex proinflammatory activity is not affected by the presence of free LPS

To gain more insights into the biological relevance of the IFI16/LPS complex *vs*. LPS, we sought to determine the proinflammatory activity of IFI16 or IFI16/LPS complex in the presence or absence of equal amounts of LPS simultaneously added to the cells. For this purpose, 786-O and THP-1 cells were stimulated with an array of different combinations as indicated in Fig 8. When IFI16 and LPS-EB were simultaneously added to the cells, without any pre-incubation step, induction of IL-6, IL-8 and TNF-α at both the mRNA and protein levels (Fig 8A and 8B, respectively) was comparable to that observed using LPS-EB alone, indicating that the affinity of IFI16 for the TLR4/MD2 receptor is lower than that of LPS. In contrast, when LPS-EB was simultaneously added to the cells together with the pre-formed IFI16/LPS-EB complex, induction of IL-6, IL-8 and TNF-α at both the mRNA and protein levels was comparable or even higher than that observed in cells stimulated with the IFI16/LPS-EB complex alone, suggesting that the affinity of the IFI16/LPS-EB complex for the TLR4 receptor is stronger than that of LPS-EB alone. Similar results were obtained when LPS-RS, a TLR4 antagonist, was used with the same combination treatment. Again, IFI16/LPS-RS complex activity, as measured by the induction of IL-6, IL-8 and TNF-α, was not affected by simultaneous addition of equal amounts of LPS-RS. Taken together, these findings clearly show that once IFI16 is complexed with LPS its proinflammatory activity is not affected by the simultaneous addition of LPS, regardless of its bacterial origin.

To better clarify the dynamics of interaction between IFI16/LPS-EB complex and TLR4/MD2 receptor, we performed further SPR analyses by means of a CM5 sensor chip coated with

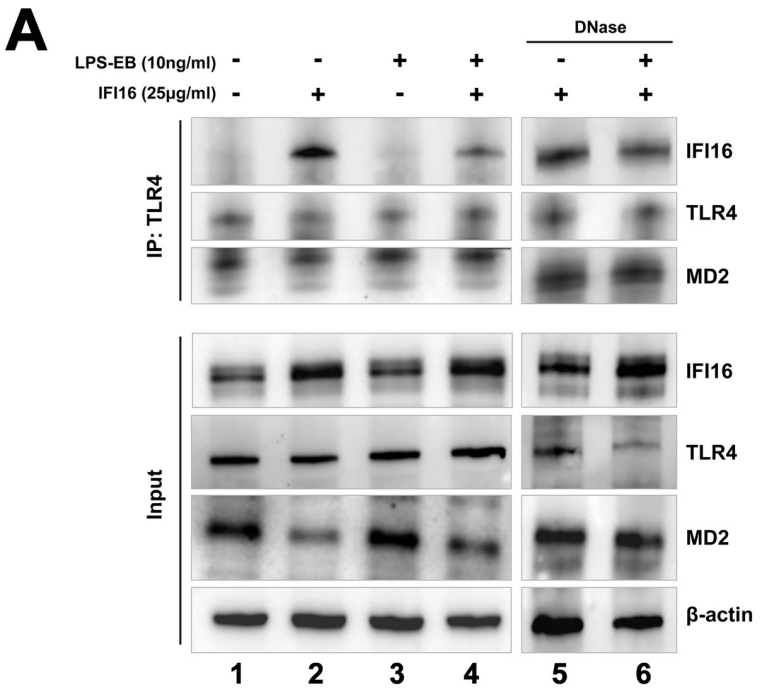

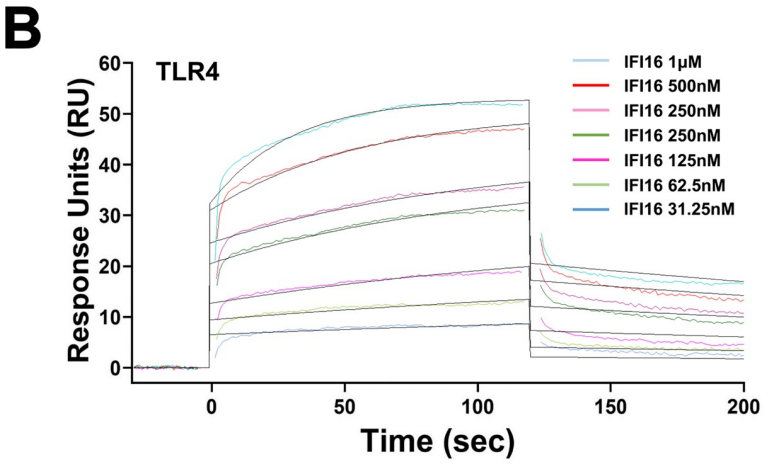

K_a (1/Ms)	K_d (1/s)	K_D (M)	Rmax (RU)	Chi^2 (RU)
$4.50*10^4$	$5.76*10^{-3}$	$1.28*10^{-7}$	25.35	1.83

Fig 7. IFI16 binds to TLR4 *in vitro* and *in vivo*. **(A)** 786-O cells were stimulated for 1 h in the presence or absence of the indicated concentrations of IFI16, LPS from *E. coli* O111:B4 (LPS-EB), or IFI16/LPS-EB complex. Total cell extracts, untreated or DNase I-treated, were subjected to immunoprecipitation using a TLR4 monoclonal antibody. Immunoprecipitates and whole-cell lysates were analyzed by immunoblotting with anti-IFI16, anti-TLR4 or anti-MD2 antibodies. β-actin protein expression was used for protein loading control. Data are representative of three independent experiments with similar results. **(B)** Surface plasmon resonance (SPR) analyses of IFI16 binding to immobilized TLR4. After immobilization of TLR4 on the CM5 sensor chip surface, increasing concentration of IFI16 (31.25–1,000 nM) diluted in running buffer were injected over immobilized TLR4. IFI16 binds to TLR4 with an equilibrium dissociation constant (K_D) of 0.13 μM. Data are representative of three independent experiments.

https://doi.org/10.1371/journal.ppat.1008811.g007

recombinant TLR4/MD2. As shown in Table 2, the SPR-based studies demonstrated that the three receptor partners (*i.e.*, IFI16, LPS-EB and the IFI16/LPS-EB complex) had association rate (K_a) values in the same range, with IFI16/LPS-EB showing a 3- and 2-fold faster association compared to IFI16 or LPS-EB alone, respectively. Interestingly, in agreement with our

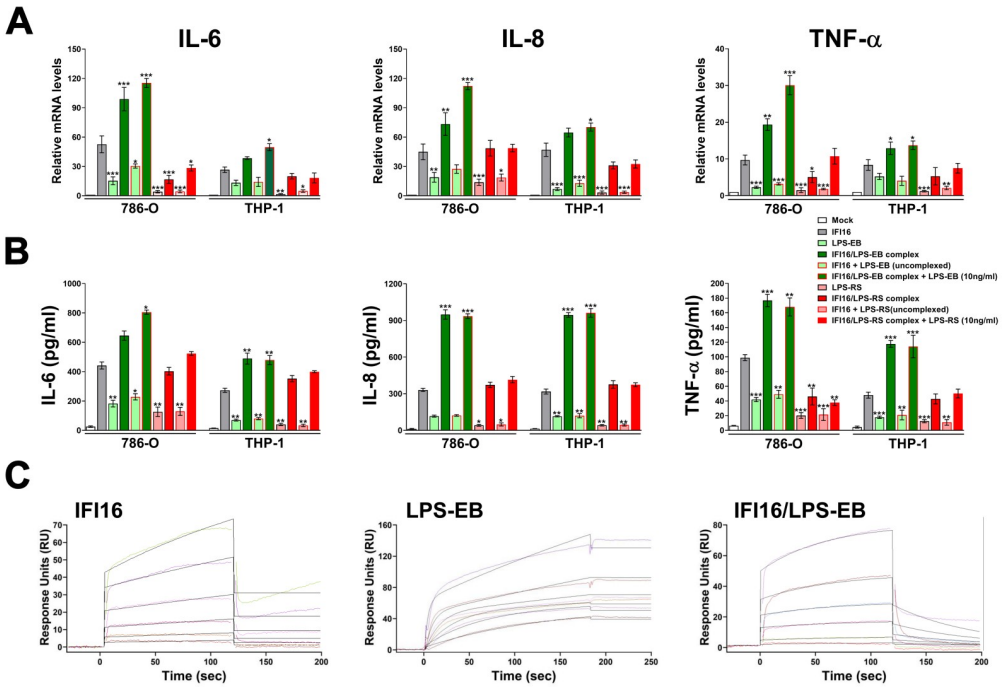

Fig 8. The IFI16/LPS complex proinflammatory activity is not affected by the presence of free LPS. (A) qRT-PCR analysis of IL-6, IL-8, TNF-α and mRNA expression levels in 786-O or THP-1 cells stimulated for 24 h with IFI16 (25 μg/ml), LPS from *E. coli* O111:B4 (LPS-EB, 10 ng/ml), IFI16/LPS-EB complex, IFI16 + LPS-EB (not complexed), IFI16/LPS-EB complex + LPS-EB (10 ng/ml), LPS from *Rhodobacter sphaeroides* (LPS-RS, 10 ng/ml), IFI16/LPS-RS complex, IFI16 + LPS-RS (not complexed), IFI16/LPS-RS complex + LPS-RS (10 ng/ml), or left untreated (mock). Values were normalized to GAPDH mRNA and plotted as fold induction over mock-treated cells. The *P* values refer to comparisons with IFI16-treated cells ($^{*}P < 0.05$, $^{**}P < 0.01$, $^{***}P < 0.001$; one-way ANOVA followed by Dunnett's test). **(B)** Protein concentration of IL-6, IL-8 and TNF-α was measured by ELISA in supernatants derived from 786-O or THP-1 cells stimulated for 24 h as described in **A**. Data are expressed as mean values ± SD of three independent experiments. The *P* values refer to comparisons with IFI16-treated cells ($^{*}P < 0.05$, $^{**}P < 0.01$, $^{***}P < 0.001$; one-way ANOVA followed by Dunnett's test). **(C)** Surface plasmon resonance (SPR) analyses of IFI16, LPS-EB and IFI16/LPS-EB complex binding to immobilized TLR4/MD2 receptor. After immobilization of recombinant TLR4/MD2 on the CM5 sensor chip surface, increasing concentration of the different analytes—31.25–1000 nM for IFI16, 3.125–100 μM for LPS-EB, 31.25–1000 nM for IFI16/LPS-EB complex—diluted in running buffer were injected over immobilized TLR4/MD2. IFI16, LPS-EB, and IFI16/LPS-EB bind to TLR4/MD2 with an equilibrium dissociation constant (K_D) of 0.68 μM, 0.15 nM, and 4.01 μM, respectively. Data are representative of three independent experiments.

https://doi.org/10.1371/journal.ppat.1008811.g008

previous findings, IFI16 interacted with the TLR4/MD2 complex in a concentration-dependent manner with a K_D of 0.68 μM, as calculated by the evaluation of the sensorgrams in Fig 8C. Moreover, LPS-EB alone revealed a much higher affinity, with a K_D of 0.15 nM. In contrast, IFI16/LPS-EB complex bound to TLR4/MD2 with 6-fold lower affinity (K_D = 4.01 μM)

Table 2. Binding kinetics of IFI16, LPS-EB and IFI16/LPS-EB to TLR4/MD2 receptor.

	K_a (1/Ms)	K_d (1/s)	K_D (M)	Rmax (RU)	Chi^2 (RU)
IFI16	$9.07^{*}10^{3}$	$6.14^{*}10^{-3}$	$6.77^{*}10^{-7}$	26.09	1.83
LPS-EB	$6.84^{*}10^{3}$	$1.00^{*}10^{-6}$	$1.47^{*}10^{-10}$	745.00	14.30
IFI16/LPS-EB	$3.57^{*}10^{3}$	$1.43^{*}10^{-2}$	$4.01^{*}10^{-6}$	90.30	6.89

K_a, association rate constant; M, molarity; s, seconds; K_d, dissociation rate constant; K_D, equilibrium dissociation constant; Rmax, maximum response; RU, response units; Chi^2, average squared residual.

https://doi.org/10.1371/journal.ppat.1008811.t002

when compared to IFI16 alone. The lower K_D displayed by LPS-EB was mainly due to the contribution of a lower dissociation rate constant ($K_d = 1.00^{*}10^{-6}$ s^{-1}), indicating that the kinetics of LPS-EB dissociation from the receptor is very slow. Interestingly, the sensorgrams demonstrated a much higher dissociation rate for both free IFI16 ($K_d = 6.14^{*}10^{-3}$ s^{-1}) and the IFI16/LPS-EB complex ($K_d = 1.43^{*}10^{-2}$ s^{-1}) in comparison with LPS-EB alone, indicating that bindings involving IFI16 are much less stable once formed. In agreement with the cytokine release, the aforementioned results indicate that, when added separately, LPS-EB binds to TLR4/MD2 more rapidly than IFI16 alone. In this setting, LPS-EB *per se* is able to trigger a weak inflammatory response highly likely due to its slow dissociation from the receptor, which in turn delays the optimal turnover of the receptor. In contrast, IFI16/LPS-EB complex binds to TLR4 more rapidly than LPS-EB simultaneously added to the cells, and it is released much more rapidly.

Discussion

We previously reported that extracellular IFI16 promotes IL-6 and IL-8 production in endothelial cells, and that such proinflammatory activity is amplified in the presence of subtoxic concentrations of LPS-EB, a full activator of the TLR4 signaling pathway [24]. Here, we expand on those observations by showing that, in renal and monocytic cell lines, IFI16 either alone or in complex with LPS binds to TLR4, thereby triggering a proinflammatory response through the TLR4/MD2/MyD88 signaling pathway. Specifically, by means of *in vitro* pull-down assays and saturation binding experiments, we provide the first evidence that the HINB domain of IFI16 mediates complex formation with LPS-EB or LPS-F583, two *E. coli*-derived variants of LPS capable of acting as strong TLR4 agonists [35,36]. This interaction follows a prototypical associative binding, with increasing rate of binding up to the plateau phase following addition of increasing amounts of the analytes. Furthermore, this binding is not dependent on the polysaccharide outer chain length as both LPS-EB and LPS-F583 display similar binding affinity for IFI16—the LPS-F583 variant is in fact characterized by the presence of a shorter polysaccharide chain compared to that of LPS-EB [37]. In addition, we show that both LPS-PG, a weak TLR4 agonist [38], and LPS-RS, a TLR4 antagonist [39]—these molecules display fewer acyl chains in their lipid A moieties compared to LPS-EB—, bind to IFI16 with similar affinities, albeit slightly lower than those of LPS-EB and LPS-F583. Finally, using the *E. coli* F583-derived DPLA and MPLA *lipid A variants* [37,40], we demonstrate that lipid A is the LPS moiety interacting with IFI16-HINB, affording the highest affinity for LPS. Accordingly, the detoxified variant of LPS-EB, containing a lipid A moiety partially delipidated by alkaline hydrolysis, binds weakly to IFI16. The observation that the HINB domain of IFI16 has a much higher affinity for lipid A than that of the HINA domain, despite both molecules being highly similar in terms of primary sequence and overall structure topology, is only partially unexpected. Indeed, these two IFI16 domains have already been shown to have distinct modes of binding to another paradigmatic PAMP—*i.e.*, viral DNA—most likely due to their different folding structures [41,42].

In recent years, mounting evidence has shown how TLRs, besides sensing exogenous microbial components, are also capable of recognizing endogenous material released during cellular injury, thereby promoting a non-microbial-induced inflammatory state known as sterile inflammation, which if not resolved can lead to severe acute and chronic inflammatory conditions [43–45]. Here, we propose that IFI16 might represent a novel trigger of sterile inflammation acting through the TLR4 signaling pathway. In particular, we show that exposure to recombinant IFI16 can induce IL-6, IL-8 and TNF-α transcriptional activation and release of these cytokines into the culture supernatants. This induction is strictly dependent on the presence of the TLR4/MD2 receptor complex and the MyD88 adaptor. By contrast, the

membrane-associated CD14 receptor seems to be only marginally involved in this signaling pathway given that undifferentiated THP-1 cells, displaying low levels of CD14 expression, and 786-O cells, expressing high levels of CD14, show similar cytokine induction patterns upon IFI16 exposure. The fact that IFI16 broadly activates inflammation through TLR4 signaling pathways strengthens the notion that extracellular IFI16 acts as a DAMP capable of promoting inflammation. Fittingly, aberrant IFI16 expression—*i.e*., overexpression of IFI16 in otherwise negative cells or IFI16 delocalization to the cytoplasm—has been reported in a number of inflammatory conditions, such as SLE (skin) [8], psoriasis (skin) [11–13], SSc (skin) [10], IBD (colonic epithelium) [6,7] and SS (salivary epithelial and inflammatory infiltrating cells) [14,15,17]. Additionally, aberrant IFI16 expression has been reported in virus-infected cells [21–23] or cells treated with IFN-γ [46]. Importantly, in some of these and other pathological conditions, we and others have shown that IFI16 exists in a free, extracellular form in the blood or extracellular milieu [14–16,47]. Particularly, we found that high levels of circulating IFI16 ($\geq$ 27 ng/ml) were associated to overall worse clinical parameters in three cohorts of RA, SS and PsA patients. Notably, among RA patients, circulating IFI16 was more frequently found in subjects with rheumatoid factor (RF)/anti-CCP-positive serum and significantly associated with pulmonary involvement [16]. Furthermore, in SS patients, circulating IFI16 is associated with increased prevalence of both RF and glandular infiltration degree [14], while in PsA patients is associated with elevated C-reactive protein (CRP) levels [19]. The release of extracellular IFI16 has also been shown by our group in a model of keratinocytes exposed to UVB radiation [8]. Although the biological rationale of these findings is far from being completely understood, these observations clearly indicate that the IFI16 protein, whose expression in the natural setting is restricted to the nuclei of a limited number of cell types, such as keratinocytes, fibroblasts, endothelial and hematopoietic cells [1], can be released by a broad spectrum of injured cells, including damaged epithelial cells or the inflammatory cells recruited at the site of injury, which are known to massively express IFI16. In this setting, as mentioned above, extracellular IFI16 can act as a DAMP in promoting sterile inflammation [48]. Accordingly, the exposure of THP-1 cells to conditioned medium from UVB-treated cells containing the IFI16 protein was able to significantly enhanced IL-6, IL-8 and TNF-α release when compared to the conditioned medium from UVB-treated IFI16 knockout cells. Addition of LPS-EB but not that of the weak TLR4-agonist LPS variant further enhanced cytokine induction, while pre-treatment of THP-1 cells with anti-TLR4 antibodies almost abolished the cytokine release. Thus, it is tempting to speculate that, similarly to pathogen-induced inflammation, binding of extracellularly-released IFI16 to TLR4 can activate both non-immune and innate immune cells, thus leading to the production of various cytokines and chemokines responsible for the recruitment of additional inflammatory cells [49].

In agreement with the emerging concept that DAMPs often potentiate their activity by binding to PAMPs, we demonstrate that the IFI16 proinflammatory activity is significantly enhanced when the protein is pre-incubated with subtoxic concentration of LPS and then added to the cells as pre-formed complex. Consistently, this effect is not observed when a truncated variant of IFI16 lacking the LPS-binding domain is used. Despite the fact that IFI16 binds with similar affinity to different variants of LPS, we could only achieve a significant increase in proinflammatory cytokine release with the strong TLR4 agonists LPS-EB and LPS-F583. Of note, these LPS molecules when added alone to the cells, even at high doses, were only able to induce marginally the transcriptional activation of such cytokines. Interestingly, the LPS-F583-derived lipid A DPLA and MPLA, carrying respectively a di- and a monophosphorylated glucosamine dimer, both lacking the sugar inner core, display a remarkably different ability to enhance IFI16 activity. Although both molecules show the highest affinity for IFI16 *in vitro*, only DPLA partially retains the ability to potentiate IFI16 downstream

signaling. Fittingly, IFI16 binding to *Rhodobacter sphaeroides*-derived LPS, which is known to antagonize the response to strong TLR4 activators in human and mouse monocytes [39], did not affect IFI16 proinflammatory activity. Interestingly, competition binding experiments in 786-O and THP-1 cells suggest that the affinity for TLR4 of either LPS-EB or LPS-RS is higher than that of IFI16. Indeed, when the cells are exposed to IFI16 and LPS-EB that were not pre-complexed, the release of proinflammatory cytokines in the culture supernatants is far lower than that of cells exposed to pre-complexed IFI16/LPS-EB or IFI16 alone. Accordingly, the binding kinetics revealed by SPR analysis clearly indicated that LPS-EB has a much higher affinity for TLR4 and a very slow kinetics of dissociation when compared to the IFI16 protein alone. Conversely, the IFI16/LPS-EB complex retains a higher affinity for TLR4 and is not displaced upon co-treatment with LPS-EB, as attested by the release of cytokines at levels similar to those observed in the supernatants of cells exposed to the complex alone. Likewise, IFI16/LPS-RS complex activity is not affected by the simultaneous addition of an equal amount of LPS-RS. In good agreement with the immunoprecipitation and competition assays, binding kinetics analysis by SPR reveals that LPS-EB, regardless of its overall higher affinity for TLR4/MD2, cannot compete with the IFI16/LPS-EB complex for binding to the receptor. Indeed, the IFI16/LPS-EB complex appears to be continuously engaged for TLR4 activation, as indicated by its faster association and dissociation rates. Thus, these data strongly suggest that *in vivo* i) the proinflammatory activity of IFI16 is enhanced upon its interaction with small amounts of circulating LPS, and ii) the IFI16/LPS-EB complex has a rapid stimulation turnover on the receptor, successfully competing with LPS-EB alone and leading to a massive inflammatory response (Fig 9).

Overall, our findings unveil a central role of extracellular IFI16 in triggering inflammation thanks to its ability to bind to the TLR4/MD2 complex, thereby triggering TLR4/MyD88/NF-κB signaling. Given that IFI16 is able to form stable complexes with various LPS variants through interaction of its HINB domain with the lipid A moiety of LPS, we propose a new pathogenic mechanism regulated by extremely fine-tuned interactions between extracellular IFI16 and subtoxic doses of LPS, which are known to be present in various pathological settings other than gram-negative infections [50–52].

Materials and methods

Reagents, antibodies, and recombinant proteins

LPS from *Escherichia coli* O111:B4 (LPS-EB), *Porphyromonas gingivalis* (LPS-PG) or *Rhodobacter sphaeroides* (LPS-RS), biotin-labeled LPS from *Escherichia coli* O111:B4 (biotin-labeled LPS-EB), detoxified LPS from *Escherichia coli* O111:B4 (detoxLPS) and polimixin B (PMB) were all purchased from InvivoGen. LPS from *Escherichia coli* F583 (LPS-F583), monophosphoryl lipid A from *Escherichia coli* F583 (MPLA), diphosphoryl lipid A from *Escherichia coli* F583 (DPLA) were purchased from Sigma-Aldrich. Bovine serum albumin Fraction V pH 7 (BSA) was purchased from Euroclone.

The following antibodies were used: rabbit polyclonal anti-IFI16 N-term and C-term (produced as described in [1], mAb anti-human TLR4 (sc-293072, Santa Cruz Biotechnologies), mAb anti-human TLR4 (sc-13593, Santa Cruz Biotechnologies), mAb anti-human TLR4 (mabg-htlr4, InvivoGen), rabbit polyclonal anti-MD2 (AHP1717T, Bio-Rad), rabbit monoclonal anti-MyD88 (4283, Cell Signaling Technology), mAb anti-NF-κB p65 (sc-8008 X, Santa Cruz Biotechnologies), PE mouse anti-human CD14 (555398, BD Pharmingen), mAb anti-β-actin (A1978, Sigma-Aldrich), rabbit IgG-HRP (A6154, Sigma-Aldrich,), mouse IgG-HRP (NA931V, GE Healthcare), streptavidin-HRP (E2886, Sigma-Aldrich,), mouse IgG-Alexa Flour 488 (A11001, Thermo Fisher Scientific), normal mouse IgG2a isotype control (sc-3878, Santa Cruz Biotechnologies).

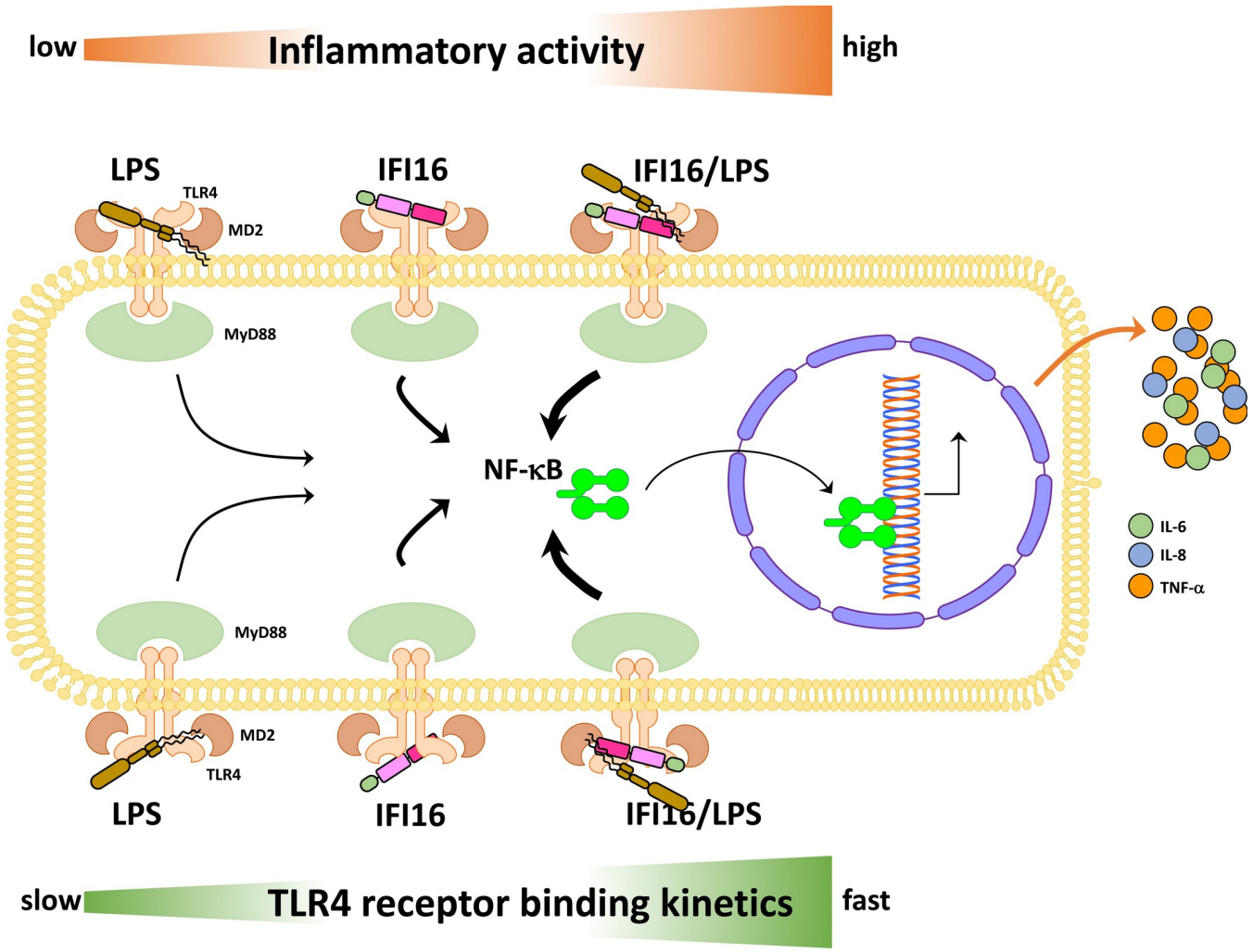

Fig 9. Proposed model depicting the inflammatory activities and binding kinetics to TLR4 of LPS and IFI16, alone or in combination. The relative inflammatory activities, from low to high, are reported in the upper part of the scheme (orange arrow). The relative binding kinetics to TLR4 are reported in the lower part of the scheme (green arrow). The thickness of the black arrows is directly proportional to the ability of the pathway to induce NF-κB activation.

https://doi.org/10.1371/journal.ppat.1008811.g009

Human recombinant IFI16 was produced as previously described [24]. The purified protein was then processed with Toxin Eraser Endotoxin Removal Kit (GenScript) to remove endotoxins, and the final endotoxin concentration was measured using Toxin Sensor Chromogenic LAL Endotoxin Assay Kit (GenScript). The endotoxin level was always below 0.05 EU/ml. Purified IFI16 was stored at—80˚C in endotoxin-free vials.

The coding regions of the three IFI16 domains (*i.e.*, PYRIN, HINA and HINB) and of the IFI16 variant lacking the HINB domain (IFI16ΔHINB) were amplified from full-length human IFI16 cDNA (isoform b) and cloned in pET30a expression vector (Novagen). The three domains and IFI16ΔHINB were then synthesized and processed following the same procedure as that for the full-length protein [24].

GST recombinant protein was expressed using pGEX-4T2 vector and purified according to standard procedures. The purity of the proteins was assessed by 12% SDS-polyacrylamide gel electrophoresis. Recombinant TLR4 protein and TLR4/MD2 complex (478-TR-050 and 3146-TM-050/CF, respectively) were purchased from R&D Systems.

Pull-down assay, ELISA and competitive ELISA

Biotin-labeled LPS-EB (10 μg) was incubated with 30 μl of streptavidin sepharose high performance beads (GE Healthcare) for 3 h at 4˚C. After a washing step, 3 μg of recombinant IFI16, PYRIN, HINA, HINB, IFI16ΔHINB, or GST were added and incubated O/N at 4˚C. After five washes with 1X PBS with 0.25% Triton X-100 (Sigma-Aldrich), samples were boiled in sample buffer containing SDS and β-mercaptoethanol and centrifuged. Supernatants were separated on a 7.5% or 12% SDS-polyacrylamide gel (Bio-Rad). Gels were stained with Coomassie brilliant blue (Serva Electrophoresis GmbH) for protein visualization.

For saturation binding experiments, microtiter plates (Nunc-Immuno MaxiSorp, Thermo Fischer Scientific) were coated with 2 μg/ml of recombinant IFI16 or 10 μg/ml of BSA or GST in 1X PBS O/N at 4˚C. After a washing step with 1X PBS and 0.25% Tween 20 (v/v, Sigma-Aldrich) and blocking step with 1X PBS with 3% BSA and 0.05% Tween 20 for 1 h, increasing concentrations of biotin-labeled LPS-EB, preincubated with 10 μg/ml of polymyxin B (PMB) when specified, were added to the wells and incubated for 1 h at room temperature (RT). Bound proteins were then detected using HRP-conjugated streptavidin. TMB solution (Thermo Fischer Scientific) was used for color development, and OD was measured at 450 nm. Alternatively, microtiter plates were coated with 10 μg/ml of LPS-EB, LPS-PG, LPS-RS, LPS-F583, MPLA, DPLA, or detoxLPS in 1X PBS for 24 h at RT. After washing and blocking for 2 h, increasing concentrations of IFI16, PYRIN, HINA, or HINB were added to the wells, preincubated with 10 μg/ml of PMB when specified, for 2 h. Anti-IFI16 antibodies against the N- or the C-terminus of the protein and HRP-labeled anti-rabbit IgG were then added as primary and secondary antibodies, respectively. The binding was detected as described above.

For whole-cell ELISA, different strains of bacteria (*i.e*., gram-positive: *Staphylococcus aureus*, *Staphylococcus epidermidis* and *Streptococcus pyogenes*; gram-negative: *Escherichia coli* and *Klebsiella pneumonia*) were grown in LB medium without antibiotics and, after washing with 1X PBS, fixed in 0.5% formalin O/N at 4˚C. Subsequently, the bacteria were diluted to an OD_{600} of 0.5 and were used to coat microtiter plates O/N at 37˚C. After blocking, increasing concentrations of IFI16 were added to the wells and incubated for 2 h at RT. Anti-IFI16 antibodies against the N-terminus of the protein and HRP-labelled anti-rabbit IgG were then added as primary and secondary antibody, respectively, and binding was detected as described above.

For competitive ELISA, microtiter plates were coated with 1 μg/ml LPS-EB in 1X PBS O/N at RT. Successively, a constant amount of 2 μg/ml IFI16 was added to the wells in the presence of increasing concentration of LPS-EB, MPLA or detoxLPS. After incubation for 4 h at RT under gentle agitation, plates were incubated with an anti-IFI16 N-terminal primary antibody and an HRP-conjugated anti-rabbit IgG secondary antibody. The binding was detected as described above. To determine K_D constants, saturation binding experiments were performed, and data were fitted to the Langmuir isotherm equation, which describes the equilibrium binding of the ligands [53]. Data are reported as sigmoid concentration-response curves plotted against log concentrations.

Cell cultures, treatments and transfection

Human kidney adenocarcinoma cells 786-O and human leukemia monocytes THP-1 were obtained from ATCC and grown in RPMI 1640 Medium (Sigma-Aldrich) containing 10% of fetal bovine serum (FBS, Immunological Sciences) and 1% of penicillin/streptomycin/glutamine solution (PSG, Gibco) at 37˚C and 5% CO_2. Wild-type and IFI16-knockout ($U2OS\text{-}IFI16^{-/-}$) human osteosarcoma cells U2OS were kindly gifted by Dr. Bala Chandraniversity of South Florida, FL, USA) [22] and grown in Dulbecco's modified Eagle's medium

(Sigma-Aldrich) containing 10% of FBS and 1% of PSG at 37˚C and 5% CO_2. UVB irradiations were performed as previously described [8]. The resulting cell culture supernatants were centrifuged to remove any cellular pellet and stored at -80˚C for the following experiments.

For treatments, cells were stimulated in complete medium with endotoxin-free IFI16 (25 μg/ml), endotoxin-free IFI16ΔHINB (25 μg/ml), MPLA, DPLA, LPS-F583, LPS-EB, LPS-RS, alone or pre-complexed by O/N incubation at 4˚C, unless specified otherwise. Additionally, cells were stimulated with supernatants of untreated or UVB-treated U2OS or U2OS-IFI16$^{-/-}$ cells alone or preincubated O/N at 4˚C with LPS-EB, or LPS-RS. LPS variants or lipid A moieties were used at a concentration of 10 ng/ml. All treatments were carried out at 37˚C and 5% CO_2.

For TLR4 neutralization, THP-1 cells were pretreated with 10 μg/ml of anti-TLR4 antibodies for 1 h before treatments.

For TLR4, MD2 or Myd88 gene silencing, cells were transfected with specific human TLR4, MD2, Myd88 or control siRNAs (Dharmacon, siGENOME smart pool) using DharmaFect1 transfection reagent (Dharmacon). The efficiency of knockdown was confirmed by FACS analysis and immunoblotting at 48 h after transfection.

FACS analysis

Single cell suspensions were incubated for 30 min on ice with anti-TLR4 (sc-13593), PE-conjugated anti-CD14 (555398) or with isotype control diluted in staining buffer (PBS 1% FBS 0.1% NaN_3). To detect TLR4 staining, cells were further washed and incubated for 30 min on ice with Alexa Fluor 488-conjugated secondary antibody. Cell counts and fluorescence intensity measurements were calculated by Attune NxT Flow Cytometer (Thermo Fisher Scientific). Background fluorescence was subtracted using unlabeled cells, and channel compensation was performed using Attune performance tracking beads (Thermo Fisher Scientific). A total of 10,000 events were recorded. Data were analyzed by FlowJo cell analysis software (BD Life Sciences).

Western blot and immunoprecipitation

Whole-cell extracts were prepared using RIPA lysis and extraction buffer (Pierce) with halt protease and phosphatase inhibitor (Thermo Fisher Scientific) on ice, and total protein concentration was quantified by Bradford Reagent (Sigma-Aldrich) measuring absorbance at 595 nm. Twenty μg of cell extracts, or 30 μl of U2OS culture supernatants were separated by electrophoresis on 7.5% or 12% SDS-polyacrylamide gels (Bio-Rad), transferred to nitrocellulose membranes, blocked with 10% non-fat milk in tris-buffered saline-tween (TBST), and probed with specific primary antibodies O/N at 4˚C. After being washed with TBST, membranes were incubated with specific HRP-conjugated secondary antibodies, and binding was detected by ECL (Thermo Fisher Scientific, Super Signal West Pico). Expression of β-actin was used as protein loading control.

Co-immunoprecipitation of TLR4 with interacting proteins was performed using the Dynabeads Protein G Immunoprecipitation Kit (ThermoFisher), according to the manufacturer's instructions with minor modifications. Briefly, after lysis of treated cells, 20 μg of total cell extracts were kept as the input control, while 90 μg of total cell extracts were incubated for 1 h at RT with 2.5 μg of anti-TLR4 antibody previously conjugated with magnetic beads. The resulting complexes were then washed, eluted, denatured, and subjected to Western blotting as described above. For DNase-treated cell extracts, DNase I (Sigma Aldrich) was added at a 1:10 dilution and incubated for 15 min at RT. Images were acquired, and densitometry of the bands was performed using Quantity One software (version 4.6.9, Bio-Rad). Densitometry values were normalized using the corresponding loading controls.

Quantitative real time PCR

Quantitative real-time PCR (qRT-PCR) was performed on a CFX96 Real-Time PCR Detection System (Bio-Rad) as previously described [54]. Total RNA was extracted using TRI Reagent (Sigma-Aldrich), and 1 μg was retrotranscribed using an iScript cDNA Synthesis Kit (Bio-Rad). Reverse-transcribed cDNAs were amplified in duplicate using SsoAdvanced Universal SYBR Green Supermix (Bio-Rad). The glyceraldehyde 3-phosphate dehydrogenase (GAPDH) gene was used as housekeeping gene to normalize for variations in cDNA levels. The relative normalized expression after stimulation as compared to control was calculated as fold change = $2^{-\Delta(\Delta CT)}$ where $\Delta CT = CT_{target} — CT_{GADPH}$ and $\Delta(\Delta CT) = \Delta CT_{stimulated} - \Delta CT_{control}$. The primer sequences are available upon request.

Cytokines measurement by ELISA

Cytokines secreted in culture supernatants after treatments were analyzed using human IL-6 DuoSet ELISA and human IL-8 DuoSet ELISA (all from R&D Systems), human TNF-α Uncoated ELISA and human IL-1β Uncoated ELISA (Thermo Fisher Scientific) according to the manufacturer's instructions. Absorbance was measured using a Spark multimode microplate reader (Tecan).

Transcription factor assay

Nuclear extracts were prepared using NE-PER Nuclear and Cytoplasmic Extraction Reagents (Thermo Fisher Scientific), according to the manufacturer's instructions. NF-κB binding activity to a DNA probe containing its binding consensus sequence was measured by Universal Transcription Factor Assay Colorimetric kit (Merck Millipore). The binding of NF-κB to the DNA probe was revealed using a specific primary antibody, with an HRP-conjugated secondary antibody used for detection with TMB substrate. The intensity of the reaction was measured at 450 nm. The following biotinylated oligonucleotides were used: sense (biotin): 5'-ATGACATAGGAAAACTGAAAGGGAGAAGTGAAAGTGGGAAATTCCTCTG-3'; antisense: 5'-CAGAGGAATTTCCCACTTTCACTTCTCCCTTTCAGTTTTCCTATGTCAT-3'.

Surface plasmon resonance analysis

The Biacore X100 (GE Healthcare) instrument was used for real-time binding interaction experiments. Recombinant TLR4 or TLR4/MD2 complex was covalently immobilized onto the surface of sensor CM5 (cat # BR100012, GE Healthcare) chips *via* amine coupling. TLR4 was diluted to a concentration of 10 μg/ml in 10 mM sodium acetate at pH 4.0, while TLR4/MD2 complex was diluted to a concentration of 20 μg/ml in the same buffer. Both proteins were injected on CM5 chips at a flow rate of 10 μl/min, upon activation of the carboxyl groups on the sensor surface with 7-min injection of a mixture of 0.2 M EDC and 0.05 M NHS. The remaining esters were blocked with 7-min injection of ethanolamine. Taking into account the ligands (TLR4 or TLR4/MD2) and analytes (IFI16, LPS-EB or IFI16/LPS-EB) molecular weights (MW) of 70 or 90 kDa, and 90, 10 or 100 kDa respectively, the appropriate ligand density (RL) on the chip was calculated according to the following equation: RL = (ligand MW/analyte MW) × Rmax × (1/Sm), where Rmax is the maximum binding signal and Sm corresponds to the binding stoichiometry. The target capture level of the TLR4 or TLR4/MD2 was of 596.0 or 1,223.9 response units (RUs), respectively. The other flow cell was used as a reference and was immediately blocked after the activation. Increasing concentrations of endotoxin-free IFI16, LPS-EB or IFI16/LPS-EB complex were flowed over the CM5 sensor chip coated with TLR4 or TLR4/MD2 at a flow rate of 30 μl/min at 25˚C with an association time of

120 s for IFI16 alone and the IFI16/LPS-EB complex, and 180 s for LPS-EB, and a dissociation phase of 180 s for IFI16 and IFI16/LPS-EB complex or 600 s for LPS-EB. A single regeneration step with 50 mM NaOH was performed following each analytic cycle. All the analytes tested were diluted in the HBS-EP+ buffer (GE Healthcare).

Recombinant IFI16 was covalently immobilized onto the surface of sensor CM5 chips via amine coupling as done for TLR4 and TLR4/MD2 complex. IFI16 was diluted to a concentration of 25 μg/ml in 10 mM sodium acetate at pH 4.0. The target capture level of IFI16 was of 1,926.6 response units (RUs). Increasing concentrations of LPS-EB, diluted in HBS-EP+ buffer, were flowed over the CM5 sensor chip coated with IFI16 at a flow rate of 30 μl/min at 25˚C with an association time of 180 s and a dissociation phase of 600 s. A single regeneration step with 50 mM NaOH was performed following each analytic cycle. The K_Ds were evaluated using the BIAcore evaluation software (GE Healthcare) and the reliability of the kinetic constants calculated by assuming a 1:1 binding model supported by the quality assessment indicators values.

Statistical analysis

All statistical analyses were performed using GraphPad Prism version 6.00 for Windows (GraphPad Software, La Jolla California USA, www.graphpad.com). The data are expressed as mean ± SD. For comparisons between two groups, means were compared using a two-tailed Student's t test. For comparisons among three groups, means were compared using one-way or two-way ANOVA followed by Dunnett's test. Differences were considered statistically significant at a P value < 0.05.

Supporting information

S1 Fig. IFI16 variant lacking HINB domain does not bind to LPS. (A) Domain organization of the IFI16ΔHINB protein. The numbers represent the amino acid positions based on NCBI Reference Sequence NP_005522. From the N- to the C-terminal (left to right), IFI16ΔHINB comprises a pyrin domain, and only one hematopoietic interferon-inducible nuclear protein with 200-amino-acid repeats (HINA) domain. S/T/P = serine/threonine/proline-rich repeats. **(B)** Coomassie brilliant blue staining of pull-down assays performed with 3 μg of recombinant IFI16ΔHINB, full-length IFI16, or HINB domain in the presence or absence of biotin-labeled LPS from *E. coli* O111:B4 (biotin-LPS-EB).
(TIF)

S2 Fig. Expression of TLR4 signaling molecules in 786-O and THP-1 cells. (A) Western blot analysis of TLR4, MD2 and MyD88 in whole-cell lysates of 786-O cells or THP-1 cells. Immunoblot with anti-β-actin antibody was used as loading control. **(B)** Cell surface expression of TLR4 and CD14 in 786-O and THP-1 cells (left and right panels, respectively), detected by flow cytometry using specific antibodies. Blue histograms represent background fluorescence; red histograms denote TLR4 (upper panels) or CD14 (lower panels) staining. The y-axis represents the number of cells, while the x-axis represents the level of fluorescence (FL-2) in a logarithmic scale. Images are representative of two independent experiments with similar results. The percentage of stained cells is reported in each panel. MFI = mean fluorescence intensity.
(TIF)

S3 Fig. Assessment of TLR4, MD2 and MyD88 knockdown upon siRNA transfection. (A) Upper panel: Western blot analysis of TLR4 and β-actin in whole-cell lysates of 786-O cells or THP-1 cells transfected with non-targeting siRNA control (siCTRL) or siRNA TLR4 (siTLR4) at 48 h after transfection. Lower panel: densitometric analysis showing the fold change

expression of the indicated proteins expressed as the mean from three independent experiments. Error bars indicate SD. **(B)** Cell surface expression of TLR4 in 786-O and THP-1 cells (upper and lower panels, respectively), detected by flow cytometry using specific antibodies at 48 h after transfection with siCTRL or siTLR4. Blue histograms represent background fluorescence; red histograms denote TLR4 staining. The y-axis represents the number of cells, while the x-axis represents the level of fluorescence (FL-2) in a logarithmic scale. Images are representative of two independent experiments with similar results. The percentage of stained cells is reported in each panel. MFI = mean fluorescence intensity. **(C, D)** Upper panels: Western blot analysis of MD2 **(C)** and MyD88 **(D)** in whole-cell lysates from 786-O cells or THP-1 cells transfected with non-targeting siRNA control (siCTRL) or specific siRNAs—siMD2 and siMyD88, respectively—at 48 h after transfection. Lower panels: densitometric analysis showing the fold change expression of the indicated proteins expressed as the mean from three independent experiments. Error bars indicate SD.
(TIF)

S4 Fig. Quantitative RT-PCR analysis of proinflammatory cytokine expression in TLR4, MD2 and MyD88 knockdown cells. (A-C) qRT-PCR analysis of IL-6, IL-8 and TNF-α mRNA expression levels in 786-O or THP-1 cells transfected for 48 h with scramble control (siCTRL), or siRNAs against TLR4 (siTLR4) **(A)**, MD2 (siMD2) **(B)** or MyD88 (siMyD88) **(C)**. Cells were then stimulated for 24 h with IFI16 (25 μg/ml), LPS from *E. coli* O111:B4 (LPS-EB, 10 ng/ml) or IFI16/LPS-EB complex (preincubated O/N at 4˚C), or left untreated (mock). Values were normalized to GAPDH mRNA and plotted as fold induction over mock-treated cells. qRT-PCR data are expressed as mean values of biological triplicates. Error bars indicate SD ($^{*}P < 0.05$, $^{**}P < 0.01$, $^{***}P < 0.001$, ns: not significant; unpaired Student's *t*-test for comparison of silenced cells *vs*. their relative control counterpart).
(TIF)

Acknowledgments

We thank Marcello Arsura for critically reviewing the manuscript.

Author Contributions

Conceptualization: Andrea Iannucci, Santo Landolfo, Marisa Gariglio, Marco De Andrea.

Data curation: Andrea Iannucci, Valeria Caneparo, Stefano Raviola, Gloria Griffante.

Formal analysis: Andrea Iannucci, Valeria Caneparo, Donato Colangelo, Riccardo Miggiano, Marco De Andrea.

Funding acquisition: Santo Landolfo, Marisa Gariglio, Marco De Andrea.

Investigation: Andrea Iannucci, Valeria Caneparo, Stefano Raviola, Isacco Debernardi, Gloria Griffante.

Methodology: Andrea Iannucci, Marisa Gariglio, Marco De Andrea.

Project administration: Santo Landolfo, Marisa Gariglio, Marco De Andrea.

Resources: Santo Landolfo, Marisa Gariglio, Marco De Andrea.

Supervision: Marisa Gariglio, Marco De Andrea.

Validation: Andrea Iannucci, Donato Colangelo, Riccardo Miggiano, Marisa Gariglio, Marco De Andrea.

Visualization: Andrea Iannucci, Marco De Andrea.

Writing – original draft: Andrea Iannucci, Marisa Gariglio, Marco De Andrea.

Writing – review & editing: Andrea Iannucci, Donato Colangelo, Riccardo Miggiano, Santo Landolfo, Marisa Gariglio, Marco De Andrea.

References

1. Gariglio M, Azzimonti B, Pagano M, Palestro G, De Andrea M, Valente G, et al. Immunohistochemical expression analysis of the human interferon-inducible gene IFI16, a member of the HIN200 family, not restricted to hematopoietic cells. J Interferon Cytokine Res. 2002; 22: 815–821. https://doi.org/10.1089/107999002320271413
2. Almine JF, O'Hare CAJ, Dunphy G, Haga IR, Naik RJ, Atrih A, et al. IFI16 and cGAS cooperate in the activation of STING during DNA sensing in human keratinocytes. Nat Commun. 2017; 8: 14392. https://doi.org/10.1038/ncomms14392
3. Choubey D, Panchanathan R. IFI16, an amplifier of DNA-damage response: Role in cellular senescence and aging-associated inflammatory diseases. Ageing Res Rev. 2016; 28: 27–36. https://doi.org/10.1016/j.arr.2016.04.002
4. Jakobsen MR, Paludan SR. IFI16: At the interphase between innate DNA sensing and genome regulation. Cytokine Growth Factor Rev. 2014; 25: 649–655. https://doi.org/10.1016/j.cytogfr.2014.06.004
5. Ouchi M, Ouchi T. Role of IFI16 in DNA damage and checkpoint. Front Biosci. 2008; 13: 236–239. https://doi.org/10.2741/2673
6. Caneparo V, Pastorelli L, Pisani LF, Bruni B, Prodam F, Boldorini R, et al. Distinct Anti-IFI16 and Anti-GP2 Antibodies in Inflammatory Bowel Disease and Their Variation with Infliximab Therapy. Inflamm Bowel Dis. 2016; 22: 2977–2987. https://doi.org/10.1097/MIB.0000000000000926
7. Vanhove W, Peeters PM, Staelens D, Schraenen A, Van der Goten J, Cleynen I, et al. Strong Upregulation of AIM2 and IFI16 Inflammasomes in the Mucosa of Patients with Active Inflammatory Bowel Disease. Inflamm Bowel Dis. 2015; 21: 2673–2682. https://doi.org/10.1097/MIB.0000000000000535
8. Costa S, Borgogna C, Mondini M, De Andrea M, Meroni PL, Berti E, et al. Redistribution of the nuclear protein IFI16 into the cytoplasm of ultraviolet B-exposed keratinocytes as a mechanism of autoantigen processing. Br J Dermatol. 2011; 164: 282–290. https://doi.org/10.1111/j.1365-2133.2010.10097.x
9. Mondini M, Vidali M, Airò P, De Andrea M, Riboldi P, Meroni PL, et al. Role of the interferon-inducible gene IFI16 in the etiopathogenesis of systemic autoimmune disorders. Ann N Y Acad Sci. 2007; 1110: 47–56. https://doi.org/10.1196/annals.1423.006
10. Mondini M, Vidali M, De Andrea M, Azzimonti B, Airò P, D'Ambrosio R, et al. A novel autoantigen to differentiate limited cutaneous systemic sclerosis from diffuse cutaneous systemic sclerosis: the interferon-inducible gene IFI16. Arthritis Rheum. 2006; 54: 3939–3944. https://doi.org/10.1002/art.22266
11. Cao T, Shao S, Li B, Jin L, Lei J, Qiao H, et al. Up-regulation of Interferon-inducible protein 16 contributes to psoriasis by modulating chemokine production in keratinocytes. Sci Rep. 2016; 6: 25381. https://doi.org/10.1038/srep25381
12. Chiliveru S, Rahbek SH, Jensen SK, Jørgensen SE, Nissen SK, Christiansen SH, et al. Inflammatory cytokines break down intrinsic immunological tolerance of human primary keratinocytes to cytosolic DNA. J Immunol. 2014; 192: 2395–2404. https://doi.org/10.4049/jimmunol.1302120
13. Tervaniemi MH, Katayama S, Skoog T, Siitonen HA, Vuola J, Nuutila K, et al. NOD-like receptor signaling and inflammasome-related pathways are highlighted in psoriatic epidermis. Sci Rep. 2016; 6: 22745. https://doi.org/10.1038/srep22745
14. Alunno A, Caneparo V, Carubbi F, Bistoni O, Caterbi S, Bartoloni E, et al. Interferon gamma-inducible protein 16 in primary Sjögren's syndrome: a novel player in disease pathogenesis? Arthritis Res Ther. 2015; 17: 208. https://doi.org/10.1186/s13075-015-0722-2
15. Antiochos B, Matyszewski M, Sohn J, Casciola-Rosen L, Rosen A. IFI16 filament formation in salivary epithelial cells shapes the anti-IFI16 immune response in Sjögren's syndrome. JCI Insight. 2018; 3. https://doi.org/10.1172/jci.insight.120179
16. Alunno A, Caneparo V, Bistoni O, Caterbi S, Terenzi R, Gariglio M, et al. Circulating Interferon-Inducible Protein IFI16 Correlates with Clinical and Serological Features in Rheumatoid Arthritis. Arthritis Care Res (Hoboken). 2016; 68: 440–445. https://doi.org/10.1002/acr.22695
17. Baer AN, Petri M, Sohn J, Rosen A, Casciola-Rosen L. Association of Antibodies to Interferon-Inducible Protein-16 With Markers of More Severe Disease in Primary Sjögren's Syndrome. Arthritis Care Res (Hoboken). 2016; 68: 254–260. https://doi.org/10.1002/acr.22632

18. Caneparo V, Cena T, De Andrea M, Dell'oste V, Stratta P, Quaglia M, et al. Anti-IFI16 antibodies and their relation to disease characteristics in systemic lupus erythematosus. Lupus. 2013; 22: 607–613. https://doi.org/10.1177/0961203313484978

19. De Andrea M, De Santis M, Caneparo V, Generali E, Sirotti S, Isailovic N, et al. Serum IFI16 and anti-IFI16 antibodies in psoriatic arthritis. Clin Exp Immunol. 2019. https://doi.org/10.1111/cei.13376

20. Uchida K, Akita Y, Matsuo K, Fujiwara S, Nakagawa A, Kazaoka Y, et al. Identification of specific auto-antigens in Sjögren's syndrome by SEREX. Immunology. 2005; 116: 53–63. https://doi.org/10.1111/j.1365-2567.2005.02197.x

21. Dell'Oste V, Gatti D, Gugliesi F, De Andrea M, Bawadekar M, Lo Cigno I, et al. Innate nuclear sensor IFI16 translocates into the cytoplasm during the early stage of in vitro human cytomegalovirus infection and is entrapped in the egressing virions during the late stage. J Virol. 2014; 88: 6970–6982. https://doi.org/10.1128/JVI.00384-14

22. Lo Cigno I, De Andrea M, Borgogna C, Albertini S, Landini MM, Peretti A, et al. The Nuclear DNA Sensor IFI16 Acts as a Restriction Factor for Human Papillomavirus Replication through Epigenetic Modifications of the Viral Promoters. J Virol. 2015; 89: 7506–7520. https://doi.org/10.1128/JVI.00013-15

23. Singh VV, Kerur N, Bottero V, Dutta S, Chakraborty S, Ansari MA, et al. Kaposi's sarcoma-associated herpesvirus latency in endothelial and B cells activates gamma interferon-inducible protein 16-mediated inflammasomes. J Virol. 2013; 87: 4417–4431. https://doi.org/10.1128/JVI.03282-12

24. Bawadekar M, De Andrea M, Lo Cigno I, Baldanzi G, Caneparo V, Graziani A, et al. The Extracellular IFI16 Protein Propagates Inflammation in Endothelial Cells Via p38 MAPK and NF-κB p65 Activation. J Interferon Cytokine Res. 2015; 35: 441–453. https://doi.org/10.1089/jir.2014.0168

25. Raetz CRH, Whitfield C. Lipopolysaccharide endotoxins. Annu Rev Biochem. 2002; 71: 635–700. https://doi.org/10.1146/annurev.biochem.71.110601.135414

26. Ryu J-K, Kim SJ, Rah S-H, Kang JI, Jung HE, Lee D, et al. Reconstruction of LPS Transfer Cascade Reveals Structural Determinants within LBP, CD14, and TLR4-MD2 for Efficient LPS Recognition and Transfer. Immunity. 2017; 46: 38–50. https://doi.org/10.1016/j.immuni.2016.11.007

27. Gioannini TL, Weiss JP. Regulation of interactions of Gram-negative bacterial endotoxins with mammalian cells. Immunol Res. 2007; 39: 249–260. https://doi.org/10.1007/s12026-007-0069-0

28. Park BS, Lee J-O. Recognition of lipopolysaccharide pattern by TLR4 complexes. Exp Mol Med. 2013; 45: e66. https://doi.org/10.1038/emm.2013.97

29. Velkov T, Roberts KD, Nation RL, Thompson PE, Li J. Pharmacology of polymyxins: new insights into an "old" class of antibiotics. Future Microbiol. 2013; 8: 711–724. https://doi.org/10.2217/fmb.13.39

30. Casella CR, Mitchell TC. Inefficient TLR4/MD-2 heterotetramerization by monophosphoryl lipid A. PLoS ONE. 2013; 8: e62622. https://doi.org/10.1371/journal.pone.0062622

31. Wähämaa H, Schierbeck H, Hreggvidsdottir HS, Palmblad K, Aveberger A-C, Andersson U, et al. High mobility group box protein 1 in complex with lipopolysaccharide or IL-1 promotes an increased inflammatory phenotype in synovial fibroblasts. Arthritis Res Ther. 2011; 13: R136. https://doi.org/10.1186/ar3450

32. Petes C, Mintsopoulos V, Finnen RL, Banfield BW, Gee K. The effects of CD14 and IL-27 on induction of endotoxin tolerance in human monocytes and macrophages. J Biol Chem. 2018; 293: 17631–17645. https://doi.org/10.1074/jbc.RA118.003501

33. Kagan JC. Lipopolysaccharide Detection across the Kingdoms of Life. Trends Immunol. 2017; 38: 696–704. https://doi.org/10.1016/j.it.2017.05.001

34. Takeda K, Akira S. TLR signaling pathways. Semin Immunol. 2004; 16: 3–9. https://doi.org/10.1016/j.smim.2003.10.003

35. Bryant CE, Spring DR, Gangloff M, Gay NJ. The molecular basis of the host response to lipopolysaccharide. Nat Rev Microbiol. 2010; 8: 8–14. https://doi.org/10.1038/nrmicro2266

36. Gao B, Wang Y, Tsan M-F. The heat sensitivity of cytokine-inducing effect of lipopolysaccharide. Journal of Leukocyte Biology. 2006; 80: 359–366. https://doi.org/10.1189/jlb.1205738

37. Plevin RE, Knoll M, McKay M, Arbabi S, Cuschieri J. The Role of Lipopolysaccharide Structure in Monocyte Activation and Cytokine Secretion. Shock. 2016; 45: 22–27. https://doi.org/10.1097/SHK.0000000000000470

38. Darveau RP, Pham T-TT, Lemley K, Reife RA, Bainbridge BW, Coats SR, et al. Porphyromonas gingivalis lipopolysaccharide contains multiple lipid A species that functionally interact with both toll-like receptors 2 and 4. Infect Immun. 2004; 72: 5041–5051. https://doi.org/10.1128/IAI.72.9.5041–5051.2004

39. Anwar MA, Panneerselvam S, Shah M, Choi S. Insights into the species-specific TLR4 signaling mechanism in response to *Rhodobacter sphaeroides* lipid A detection. Scientific Reports. 2015; 5: 7657. https://doi.org/10.1038/srep07657

40. Stoddard MB, Pinto V, Keiser PB, Zollinger W. Evaluation of a whole-blood cytokine release assay for use in measuring endotoxin activity of group B Neisseria meningitidis vaccines made from lipid A acylation mutant. Clin Vaccine Immunol. 2010; 17: 98–107. https://doi.org/10.1128/CVI.00342-09

41. Ni X, Ru H, Ma F, Zhao L, Shaw N, Feng Y, et al. New insights into the structural basis of DNA recognition by HINa and HINb domains of IFI16. J Mol Cell Biol. 2016; 8: 51–61. https://doi.org/10.1093/jmcb/mjv053

42. Unterholzner L, Keating SE, Baran M, Horan KA, Jensen SB, Sharma S, et al. IFI16 is an innate immune sensor for intracellular DNA. Nat Immunol. 2010; 11: 997–1004. https://doi.org/10.1038/ni.1932

43. Piccinini AM, Midwood KS. DAMPening inflammation by modulating TLR signalling. Mediators Inflamm. 2010;2010. https://doi.org/10.1155/2010/672395

44. Rifkin IR, Leadbetter EA, Busconi L, Viglianti G, Marshak-Rothstein A. Toll-like receptors, endogenous ligands, and systemic autoimmune disease. Immunol Rev. 2005; 204: 27–42. https://doi.org/10.1111/j.0105-2896.2005.00239.x

45. Schaefer L. Complexity of danger: the diverse nature of damage-associated molecular patterns. J Biol Chem. 2014; 289: 35237–35245. https://doi.org/10.1074/jbc.R114.619304

46. Caposio P, Gugliesi F, Zannetti C, Sponza S, Mondini M, Medico E, et al. A novel role of the interferon-inducible protein IFI16 as inducer of proinflammatory molecules in endothelial cells. J Biol Chem. 2007; 282: 33515–33529. https://doi.org/10.1074/jbc.M701846200

47. Gugliesi F, Bawadekar M, De Andrea M, Dell'Oste V, Caneparo V, Tincani A, et al. Nuclear DNA sensor IFI16 as circulating protein in autoimmune diseases is a signal of damage that impairs endothelial cells through high-affinity membrane binding. PLoS ONE. 2013; 8: e63045. https://doi.org/10.1371/journal.pone.0063045

48. Gong T, Liu L, Jiang W, Zhou R. DAMP-sensing receptors in sterile inflammation and inflammatory diseases. Nat Rev Immunol. 2019. https://doi.org/10.1038/s41577-019-0215-7

49. Chen GY, Nuñez G. Sterile inflammation: sensing and reacting to damage. Nat Rev Immunol. 2010; 10: 826–837. https://doi.org/10.1038/nri2873

50. Manco M, Putignani L, Bottazzo GF. Gut microbiota, lipopolysaccharides, and innate immunity in the pathogenesis of obesity and cardiovascular risk. Endocr Rev. 2010; 31: 817–844. https://doi.org/10.1210/er.2009-0030

51. Seki E, Schnabl B. Role of innate immunity and the microbiota in liver fibrosis: crosstalk between the liver and gut. J Physiol (Lond). 2012; 590: 447–458. https://doi.org/10.1113/jphysiol.2011.219691

52. Stoll LL, Weintraub GMD and NL. Endotoxin, TLR4 Signaling and Vascular Inflammation: Potential Therapeutic Targets in Cardiovascular Disease. In: Current Pharmaceutical Design [Internet]. 31 Oct 2006 [cited 19 Dec 2019]. Available: http://www.eurekaselect.com/58106/article

53. Hulme EC, Trevethick MA. Ligand binding assays at equilibrium: validation and interpretation. Br J Pharmacol. 2010; 161: 1219–1237. https://doi.org/10.1111/j.1476-5381.2009.00604.x

54. Albertini S, Lo Cigno I, Calati F, De Andrea M, Borgogna C, Dell'Oste V, et al. HPV18 Persistence Impairs Basal and DNA Ligand-Mediated IFN-β and IFN-λ1 Production through Transcriptional Repression of Multiple Downstream Effectors of Pattern Recognition Receptor Signaling. J Immunol. 2018; 200: 2076–2089. https://doi.org/10.4049/jimmunol.1701536